Molecular Characterization of Impaired Sialylation in Skeletal Muscle Cells

Dissertation

zur Erlangung des

Doktorgrades der Naturwissenschaften (Dr. rer. nat.)

der

Naturwissenschaftlichen Fakultät I

- Biowissenschaften -

der Martin-Luther-Universität

Halle-Wittenberg

vorgelegt

von Frau Carolin Tanja Neu

Gutachter:

1. Prof. Dr. Mike Schutkowski

2. Prof. Dr. Rüdiger Horstkorte

3. Prof. Dr. Rita Gerardy-Schahn (Medizinische Hochschule Hannover)

Datum der Verteidigung: 06.02.2026

I seem to have been only like a boy playing on the seashore, and diverting myself in now and then finding a smoother pebble or a prettier shell than ordinary, whilst the great ocean of truth lay all undiscovered before me.

- *Isaac Newton*

Table of Content

List of Figures

List of Tables

Abbreviations

Abbreviation	Full Form
AChR	Acetylcholine receptor
ADP	Adenosine diphosphate
ANOVA	Analysis of variance
APS	Ammonium persulfate
ATP	Adenosine triphosphate
BCA	Bicinchoninic acid
bp	Base pair
BSA	Bovine serum albumin
$CaCl_2$	Calcium chloride
Cacna1s	Voltage-dependent L-type calcium channel subunit α-1S
Cacna2d1	Voltage-dependent L-type calcium channel subunit α-2/δ-1
Cas9	CRISPR associated protein 9
cDNA	Complementary DNA
CK	creatine kinase
Cl.	Single cell clone
CMP	Cytidine monophosphate
CRISPR	clustered regularly interspaced short palindromic repeats
CTP	Cytidine triphosphate
Ctrl	Control
DAPI	4',6-Diamidin-2-phenylindol
DHPR	Dihydropyridine receptor
Diff	Differentiated
DM	Differentiation medium
DMEM	Dulbecco's modified eagle medium
DMSO	Dimethyl sulfoxide
DNA	Deoxyribonucleic acid
DTT	Dithiothreitol
ECM	Extracellular matrix
EDTA	Ethylenediaminetetraacetic acid
ER	Endoplasmic reticulum
FC	Fold change
Fuc	Fucose
GAG	Glycosaminoglycan
Gal	Galactose
GalNAc	N-acetylgalactosamine
GALNT	GalNAc transferase
GAPDH	Glycerinaldehyd-3-phosphate-dehydrogenase
GDP	Guanosine diphosphate
Glc	Glucose
GlcA	Glucuronic acid
GlcNAc	*N*-acetylglucosamine
GM	Growth medium
GNE	UDP-*N*-acetylglucosamine 2-epimerase/*N*-acetylmannosamine kinase

Abbreviations

Abbreviation	Full Form
GTP	Guanosine triphosphate
HCl	Hydrochloric acid
HDR	Homology directed repair
HEK	human embryonic kidney
HRP	Horseradish peroxidase
Hyl	Hydroxylysine
IF	Immunofluorescence
KCl	Potassium chloride
Kdn	Keto-deoxy-nonulonic acid
KO	Knock out
Man	Manose
ManNAc	*N*-acetylmannosamine
MB	Myoblast
$MgCl_2$	Magnesium chloride
mRNA	Messenger RNA
MT	Myotube
MW	Molecular weight
MYH	Myosin heavy chain
m/z	Mass to charge ratio
NaCl	Sodium chloride
NADPH	nicotinamide adenine dinucleotide phosphate
NCAM	Neural cell adhesion molecule 1
Neu5Ac	*N*-acetylneuraminic acid
Neu5Gc	*N*-glycolylneuraminic acid
NMJ	Neuromuscular junction
NP40	Nonidet P40
OGT	O-GlcNAc transferase
OST	Oligosaccharyltransferase
P	Phosphate
PAGE	Polyacrylamide gel electrophoresis
PAS	Periodic acid-Schiff reaction
PBS	Phosphate buffered saline
PCR	Polymerase chain reaction
PFA	Paraformaldehyd
PIC	Protease inhibitor cocktail
polySia	Poly sialic acid
Pygm	Muscle-specific glycogen phosphorylase
qRT-PCR	Reverse transcription - quantitative PCR
RLU	Relative luominescence unit
RNA	Ribonucleic acid
RNAseq	RNA sequencing
RT	Room temperature
Ryr1	Ryanodine receptor 1
Scn4a	Sodium channel protein type 4 subunit α
SDS	Sodium dodecyl sulfate
Sia	Sialic acid

Abbreviations

Abbreviation	Full Form
TBS	Tris-buffered saline
TCA	trichloroacetic acid
TEMED	tetramethylethylenediamine
TPA	Total peak area
TRIS	Tris(hydroxymethyl)aminomethane
UDP	Uridine diphosphate
UTP	Uridine triphosphate
v/v	Volume per volume
w/v	Weight per volume
WB	Western blot
WT	Wild type
Xyl	Xylose

When referring to genes or proteins, this thesis follows the guidelines prepared by the International Committee on Standardized Genetic Nomenclature for Mice and by the HUGO Gene Nomenclature Committee. Human proteins and genes are written in uppercase. Murine protein and gene symbols are written with only one capital letter. Gene symbols are always italicized.

Summary

Glycosylation is the most abundant post-translational modification and describes the decoration of proteins and lipids with glycan structures. Glycans serve a plethora of different functions by modulating protein and lipid characteristics. Sialic acids are one of the main building blocks for vertebrate glycosylation and are found at the terminal ends of glycan structures. The key enzyme in the endogenous sialic acid biosynthesis pathway is the bifunctional UDP-*N*-acetylglucosamine 2-epimerase/*N*-acetylmannosamine kinase (GNE). Mutations in the *GNE* gene are associated with a rare genetic disease called GNE myopathy that manifests in form of a slowly progressing skeletal muscle atrophy with early-adulthood onset. Until today, there is no approved therapy for the treatment of GNE myopathy and hence, a better understanding of the pathomechanism of this disorder is needed.

To study the general functions of sialic acids in a skeletal muscle background, a new cell model was generated by depleting Gne expression in the C2C12 myoblast cell line using the CRISPR/Cas9 genome-editing technique. Gne knock out (Gne^{KO}) was well tolerated by the cells and no obvious morphological difference was observed in the Gne^{KO} myoblasts compared to wild type cells. However, upon differentiation of C2C12 cells into myotubes, Gne^{KO} clones presented drastic alterations. Analysis of glycan structures of Gne^{KO} myoblasts and myotubes confirmed reduction of the sialic acid content with a concomitant remodeling of the glycome. Terminal sialic acids of N-glycans in Gne^{KO} myoblasts were replaced by an additional galactose and N-glycan branching was highly increased. Additionally, changes in proteoglycan expression were detected as well as modulation of cytoplasmic and nuclear glycosylation. Sialylation-deficiency of C2C12 Gne^{KO} cells was rescued *via* supplementation with *N*-acetylneuraminic acid but not with its metabolic precursor *N*-acetylmannosamine. Notably, increased sialylation in C2C12 wild type cells had a negative impact on cell differentiation and gene expression. Furthermore, a whole network of myopathy-related genes was found to be de-regulated in case of Gne-deficiency, pointing towards pathophysiological changes in a muscle-specific manner. Among those candidates were the skeletal muscle-specific voltage-gated sodium channel $Na_V1.4$ and voltage-gated calcium channel $Ca_V1.1$ along with the glycogen phosphorylase. Together, altered gene expression suggests a major role of sialic acids in excitation-contraction coupling and energy metabolism of skeletal muscle cells.

Zusammenfassung

Glykosylierung ist die am häufigsten vorkommende post-translationale Modifikation von Proteinen und Lipiden mittels Mono- und Polysacchariden. Diese sogenannten Glykane beeinflussen die Struktur und Funktion ihrer protein- und lipid-Träger und haben weitreichende physiologische Aufgaben. Sialinsäuren sind einer der Hauptbausteine von Glykanen und befinden sich an den terminalen Enden der Polysaccharid Ketten. Das Schlüsselenzym der Sialinsäure Biosynthese ist die bifunktionale UDP-*N*-glucosamin 2-Epimerase/*N*-acetylmannosamine Kinase (GNE). Mutationen im *GNE* Gen sind der Grund für das Auftreten einer seltenen genetischen Erkrankung, der sogenannten GNE Myopathie. GNE Myopathie ist eine langsam fortschreitende Muskel Atrophie und erste Symptome treten meistens im frühen Erwachsenenalter auf. Bis heute gibt es keine zugelassene Therapie für Betroffene, da der Pathomechanismus weitestgehend unbekannt ist. Daher ist die Grundlagenforschung unabdingbar, um ein besseres Verständnis für die spezielle Rolle der GNE in der Skelettmuskulatur zu erlangen.

Um die generelle Funktion von Sialinsäuren und der GNE in Skelettmuskeln zu erforschen wurde ein neues Zellmodell generiert. Die in der Literatur weitverbreitete Myoblasten Zelllinie C2C12 diente hierfür als Grundlage und die CRISPR/Cas9 Genom-Editierung Technologie wurde angewandt, um die Gne Expression auszuschalten (knock out, Gne^{KO}). Der Gne knock out wurde von den Zellen gut toleriert und Gne^{KO} Myoblasten zeigten keinen signifikanten Unterschied zu Wildtyp Zellen hinsichtlich ihrer Morphologie. Jedoch zeigten die Gne^{KO} Klone deutliche Unterschiede während des Differenzierungsprozesses zu Myotuben. Die Analyse von Glykanstrukturen in Gne^{KO} Klonen bestätigte die reduzierte Menge an Sialinsäuren. Sialinsäuren wurden in den N-Glykanen der Myoblasten durch Galaktose ersetzt und die Verzweigung der N-Glykane war deutlich erhöht im Vergleich zu Wildtyp Zellen. Zusätzlich wurde eine veränderte Expression von Proteoglykanen und von zytoplasmatischer und nuklearer Glykosylierung festgestellt. Der Sialinsäure-Mangel in Gne^{KO} Klonen konnte durch Supplementierung mit *N*-acetylneuraminsäure ausgeglichen werden, jedoch nicht mit dem Sialinsäure-Metabolit *N*-acetylmannosamin. Ein Überschuss an Sialinsäuren hatte jedoch eine negative Wirkung auf die Differenzierung und Genexpression von C2C12 Wildtyp Zellen. Des Weiteren wurde ein Netzwerk an Muskel-spezifischen Genen identifiziert, deren Expression in Gne^{KO} Klonen verändert war. Dabei handelte es sich unter anderem um den Spannungs-abhängigen Natriumkanal $Na_V1.4$ und dem Spannungs-abhängigen Calciumkanal $Ca_V1.1$, sowie der Glykogen Phosphorylase.

I Introduction

1 Protein glycosylation

1.1 Diversification of the proteome *via* glycosylation

The human genome comprises ~ 20,000 protein-coding genes. However, the actual human proteome is much more diverse and complex. To start with, alternative splicing of mRNAs elevates the number of potential proteins to ~ 70,000, which can then be further diversified by hundreds of different post-translational modifications (PTMs) (Aebersold et al., 2018). Protein glycosylation is one of the most diverse PTM, by which different monosaccharides are linked to a protein or lipid backbone in a sequential manner. In vertebrates, nine main monosaccharide building blocks give rise to a vast diversity of glycan structures, allowing a high degree of functional and structural modulation of proteins (**Figure 1**) (Griffin and Hsieh-Wilson, 2022).

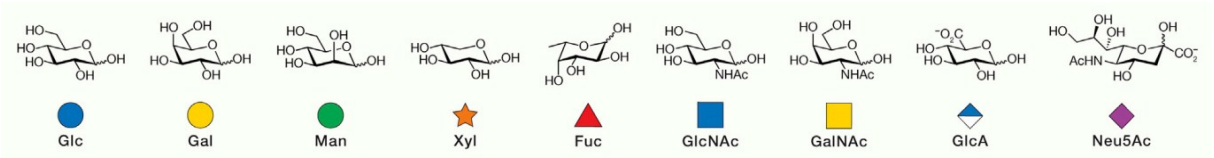

Figure 1: Main building blocks for vertebrate glycosylation.

Nine monosaccharides that are commonly found in human glycan structures. Upper row shows the chemical structures and lower row depicts the official glycan symbols according to the Symbol Nomenclature for Glycans (SNFG) (Varki et al., 2015). Glc: Glucose, Gal: Galactose, Man: Mannose, Xyl: Xylose, Fuc: Fucose, GlcNAc: *N*-acetylglucosamine, GalNAc: *N*-acetylgalactosamine, GlcA: glucoronic acid, Neu5Ac: *N*-acetylneuraminic acid. Figure adapted from (Griffin and Hsieh-Wilson, 2022).

1.2 Glycosylation pathways in mammalian cells

Glycosylation occurs in a non-templated manner and relies on the orchestrated interplay of hundreds of enzymes. While there are only few monosaccharide building blocks, it has been estimated that ~ 700 protein-coding genes are involved in the glycosylation pathway, providing enzymes, transporters, and chaperones for glycan biosynthesis and degradation (Nairn et al., 2008). Even though the general mechanisms of protein glycosylation have been unraveled decades ago, our knowledge and understanding of the diversity of glycosylation has still been growing over the past years (Hirata et al., 2018; Larsen et al., 2017; Praissman et al., 2016). Various forms of glycosylation being found in all kingdoms of life, the following sections describe general mechanisms of vertebrate glycosylation. Generally, glycosylation takes place in the endoplasmic reticulum (ER), Golgi apparatus (Golgi), nucleus, and cytoplasm of eukaryotic cells. Table 1 gives an overview of the different types and linkage-specificities of certain glycans in humans.

Table 1: Initiation steps for human glycosylation pathways.

The monosaccharide column names the first building block that is linked to the indicated amino acid residue *via* one of the specific glycosyltransferases. The listed compartment states where the specific kind of glycosylation is initiated. COLGALT: collagen *O*-Gal transferase, DPY19L: dpy-19 like *C*-Man transferase, EOGT: epidermal growth factor-domain specific *O*-GlcNAc transferase, EthNP: ethanolamine phosphate GALNT: polypeptide GalNAc transferase, Hyl: Hydroxylysine, OGT: *O*-GlcNAc transferase, OST: oligosaccharyltransferase, POFUT: protein *O*-fucosyltransferase, POGLUT: protein *O*-Glc transferase, POMT: protein *O*-Man transferase, TMTC: transmembrane *O*-Man transferase targeting cadherin, XYLT: protein *O*-Xyl transferase. Table adapted from (Schjoldager et al., 2020).

Type	Monosaccharide	Linked to	Glycosyltransferase	Compartment
N-Glycosylation	GlcNAc	Asn	OST complex	ER
O-Glycosylation	GalNAc	Ser/Thr/Tyr	GALNT1-20	Golgi
	Fuc	Ser/Thr	POFUT1-2	ER
	GlcNAc	Ser/Thr	EOGT	ER
	Man	Ser/Thr	POMT1, POMT2, TMTC1-4	ER
	Glc	Ser	POGLUT1-3	ER
	Xyl	Ser	XYLT1, XYLT2	Golgi
	Gal	Hyl	COLGALT1-2	Golgi, limited to collagens
	GlcNAc	Ser/Thr	OGT	Cytosol, nucleus
C-Mannosylation	Man	Trp	DPY19L1-4	ER
Glypiation (GPI anchor)	NA	Protein-C(O)EthNP-Man	Transamidase	ER

Neglecting enzymes that are involved in the biosynthesis of the monosaccharide building blocks, glycosyltransferases shape the glycan structures that are presented on cell surfaces, in the extracellular matrix and in the serum. Glycosyltransferases are mostly type II transmembrane glycoproteins and use activated nucleotide sugars (UDP-Glc/GlcNAc/Gal/GalNAc/Xyl/GlcA, GDP-Man/Fuc, and CMP-Neu5Ac) as substrates to initiate, elongate, branch, and cap glycan structures (Paulson and Colley, 1989; Schjoldager *et al.*, 2020). Figure 2 gives a general overview of the glycosylation pathway. Unique for N-glycosylation, initiation starts in the ER with the oligosaccharyltransferase (OST) complex that transfers a glycan structure composed of 14 monosaccharides ($Glc_3Man_9GlcNAc_2$) co- and post-translationally to an emerging polypeptide with the recognition sequence N-X-S/T, of which X is any amino acid except of proline (Kornfeld and Kornfeld, 1985; Rothman and Lodish, 1977; Wild et al., 2018). Similarly, C-mannosylation also occurs in a co-translational manner in the ER, allowing glycosylation of tryptophans within the W-X-X-W-X-X-W motif of thrombospondin repeats (Shcherbakova et al., 2017). Furthermore Fuc, Glc, and GlcNAc types of O-glycosylation are also initiated in the ER and are most commonly found on NOTCH receptor epidermal growth factor-like repeats (Holdener and Haltiwanger, 2019; Sakaidani et al., 2012; Takeuchi et al., 2018). The Golgi apparatus on the other side is where GalNAc- and

Xyl-type O-glycosylation is initiated. GalNAc-type O-glycosylation misses a consensus sequence motif and only 15 out of 20 potential polypeptide GalNAc transferases have been described as active enzymes (Bennett et al., 2012). *O*-Xyl transferases (XYLT1-2) mediate Xyl-type O-glycosylation, which is prerequisite for glycosaminoglycan (GAG) chain biosynthesis on proteoglycans. XYLT1 and XYLT2 have relatively conserved recognition motifs (a-a-a-a-G-S-G-a-(a/G)-a, with a = D/E). Distinct from the above-mentioned types of N- and O-glycosylation, *O*-GlcNAcylation is a cytosolic and nuclear type of glycosylation. The soluble *O*-GlcNAc transferase (OGT) links a single GlcNAc residue to a Ser or Thr of its client protein, serving as a master regulator of intracellular signaling, transcription, and cellular metabolism (Haltiwanger et al., 1992; Hart, 2019).

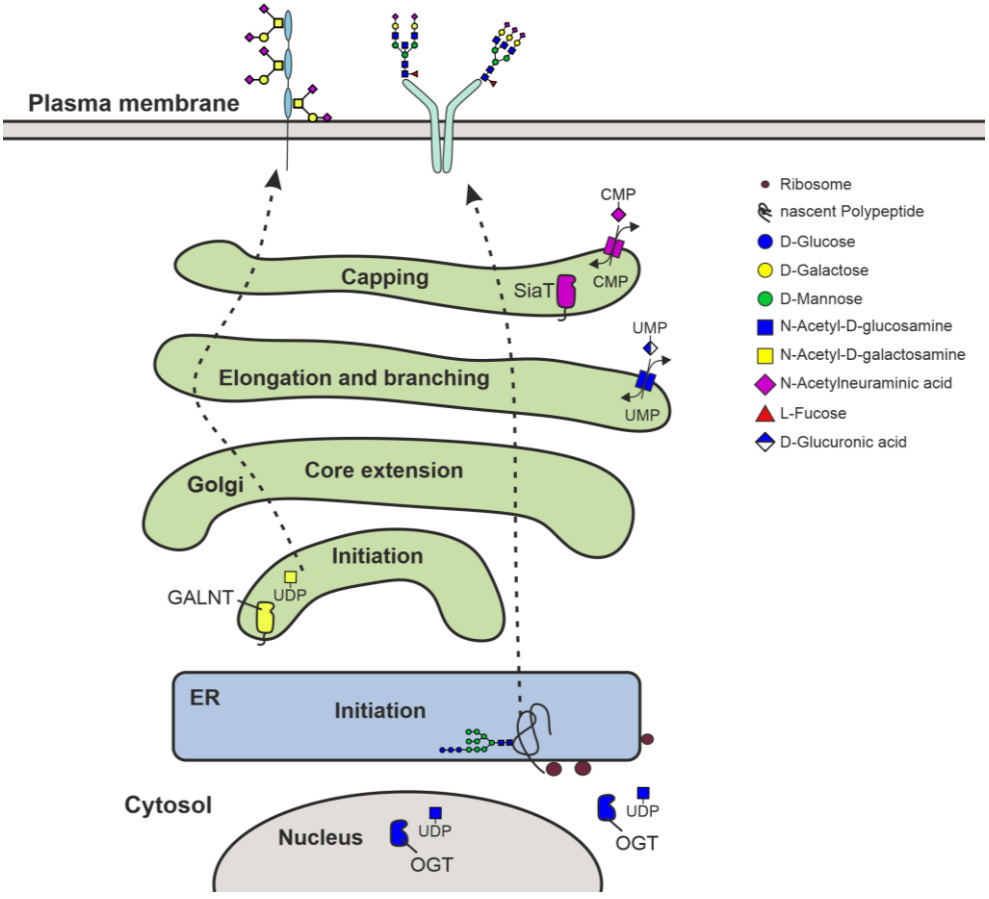

Figure 2: Glycosylation Pathway.

Glycosylation starts either in the endoplasmic reticulum (ER), Golgi apparatus, cytosol, or the nucleus. Membrane-resident glycosyltransferases in the ER and the Golgi transfer activated nucleotide sugars to the emerging glycans, while *O*-GlcNAcylation is catalyzed by the soluble OGT. Nucleotide sugars are translocated into the Golgi lumen *via* antiporter proteins. See main text for further explanations. CMP: cytidinemonophosphate, UMP: uridinemonophosphate, UDP: uridinediphosphate, OGT: *O*-GlcNAc transferase. Figure created with CorelDRAW.

1.3 Modifications of glycan structures

Once glycosylation is initiated, ER and Golgi-resident glycosyltransferases act in a sequential manner in the further processing of glycan structures. Thus, glycan structures are diversified by core extension, elongation, branching, and capping. In the end, the final composition of glycans depends on expression of sialyltranseferases, on substrate availability and competition of different glycosylation enzymes for the same substrates (Nairn *et al.*, 2008). Figure 3 shows glycan structures that are representative for the respective glycosylation pathway. More closely, processing of N-glycans results in either high-mannose, hybrid, or complex N-glycans. While high-mannose glycans consist of two GlcNAc and up to nine Man residues only, hybrid and complex N-glycans may be modified with GlcNAc, GalNAc, Gal, Fuc, and sialic acids as they travel from the ER through the Golgi to the plasma membrane (Rabouille et al., 1995; Stanley, 2011). However, glycan structures are not only limited to the monosaccharide building blocks, more-over, side-chain specific modifications may also alter glycan functions. Sulfation of glycosaminoglycans (GAGs), phosphorylation of *O*-Man and Xyl residues, as well as acetylation of sialic acids have been described to have an impact on glycan functions (Baumann et al., 2015; Honke and Taniguchi, 2002; Yoshida-Moriguchi et al., 2013).

Taken together, glycan structure determination depends on monosaccharide composition (substrate availability), anomeric state (α vs β), linkage (glycosyltransferase isoenzymes, branching), and side-chain specific modifications.

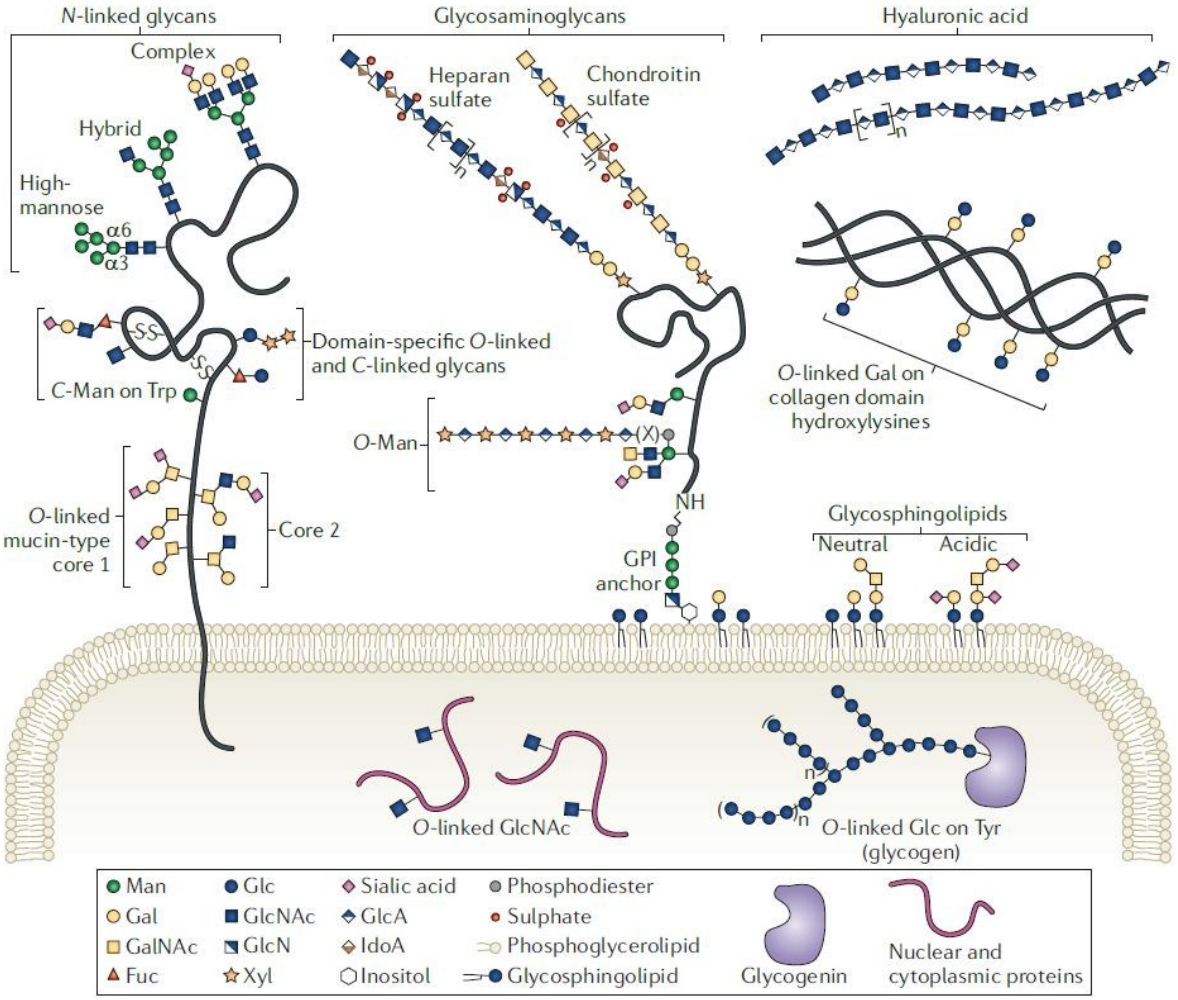

Figure 3: Diversity of commonly found glycan structures in vertebrates.

N-glycans with minimal mannosidase processing are called "high-mannose" glycans and can be transformed into hybrid glycans by the addition of a GlcNAc to the α3 arm of the acceptor Man_5 glycan. Furhter addition of galactose, *N*-acetylglucosamine, sialic acids, and fucose results in formation of complex N-glycans. Glycosaminoglycans (GAGs) are built on conserved tetrasaccharides (GlcA-Gal-Gal-Xyl-β) and differ in terms of their disaccharide repeats. The only glycan that is not linked to a protein or lipid is the extracellular matrix component hyaluronic acid. Mucin-type O-glycans are initiated by *N*-acetylgalactosamine with eight different core structures that differ in their composition. Glycogenin is a special glycosyltransferase that mediates the transfer of glucose to itself to form the glucose storage polymer glycogen. Refer to the main text for description of other special glycan forms. Man: Mannose, Gal: Galactose, GalNAc: *N*-acetylgalactosamine, Fuc: Fucose, Glc: Glucose, GlcNAc: *N*-acetylglucosamine, GlcN: Glucosamine, Xyl: Xylose, GlcA: Glucoronic acid, IdoA: Iduronic acid. Figure taken from (Moremen et al., 2012).

1.4 Linking glycan structure to cellular function

When it comes to the structural investigation of glycans, scientists face many challenges. Considering the vast heterogeneity of glycans and their specific tissue distribution, connecting structural information to biological functions is a laborious task. Generally, inhibitors of glycosyltransferases (Ortiz-Meoz et al., 2015) and modified sugar donors (Gloster et al., 2011; Rillahan et al., 2012), protein-based probes like lectins and antibodies (Bojar et al., 2022; Sterner et al., 2016), and glycan-binding reagents have been valuable tools for the characterization of certain glycan types. Above all, mass spectrometry has proven to be a

valuable method, defining structures of N-glycans and O-glycans, as well as giving insights into glycoproteomics (North et al., 2009; Wuhrer, 2013). Efforts have been made, aiming to elucidate global pathways of the glycosylation machinery in cells. Accordingly, Narimatsu *et al* established an atlas of human glycosylation pathways *via* genetic engineering of a HEK293 cell line, enabling new correlations of genetic, biosynthetic, and structural features of specific glycans in a cellular context (Narimatsu et al., 2019). A more chemical approach is the synthesis of glycans and glycoprotein mimetics of defined structures. Those probes have been especially valuable for elucidating the affinity of glycan binding proteins/ligand interactions and for the development of biopharmaceuticals (Guberman and Seeberger, 2019; Wang et al., 2013; Xu et al., 2011).

1.5 Glycoengineering

As glycosylation may have a strong impact on protein characteristics, scientists started to exploit these pathways to ameliorate biopharmaceutical properties of recombinant proteins. Supplementation of cell lines with natural monosaccharides can modulate glycosylation patterns to enhance safety, serum half-life and efficacy of those biotherapeutic proteins (Gu and Wang, 1998; Wong et al., 2010). Furthermore, cells are able to use non-natural monosaccharides in their intrinsic glycosylation pathways, which led to the development of chemoenzymatic and metabolic glycan labeling strategies (Dube and Bertozzi, 2003; Gross and Brossmer, 1988; Gross et al., 1989; Horstkorte et al., 2004; Jiang et al., 2018; Kayser et al., 1992; Saxon and Bertozzi, 2000; Wratil et al., 2016). A major target of glycoengineering approaches are the terminal sialic acids of glycan structures. For example, many types of cancer exhibit abnormal glycosylation patterns in form of increased sialylation of the cell surface, thus, prompting tumor-associated carbohydrate antigens as diagnostic and therapeutic targets (Pietrobono and Stecca, 2021). The development of bioorthogonal click chemistry enabled the synthesis of monosaccharides modulated with functional groups, like azides, that do not naturally occur in living cells and are non-toxic (Saxon and Bertozzi, 2000). One of the early approaches showed that peracetylated *N*-levulinoylmannosamine, a ManNAc analogue, which after metabolization is presented as *N*-levulinoyl sialic acid in human cancer cells, could be used as magnetic resonance contrast reagent to image tumours (Lemieux et al., 1999).

Overall, metabolic glycoengineering holds great potential for future perspectives in diagnostics, drug delivery systems, and therapeutics (Agatemor et al., 2019).

2 Sialic acids

Like no other of the monosaccharides, sialic acids attract the attention from various disciplines like neurobiology, immunology, virology, and cancer biology. Sialic acids (Sias) are a subset of α-keto acid monosaccharides with a nine-carbon backbone and cap the terminal ends of vertebrate glycoproteins and glycolipids. Different substituents on the neuraminic acid backbone enable more than 50 different structures, Neu5Ac being the most abundant one in humans (Figure 4) (Schauer and Kamerling, 2018). Sias are further characterized by the diversity of functional groups, modifications, and linkages to other monosaccharides. The complexity that arises from these structural features allows highly specific recognition of glycan-protein, cell-cell, and pathogen-host interactions. Additionally, Sias carry an electronegative charge, enabling further functions such as ion binding and ion transport (Lewis et al., 2022).

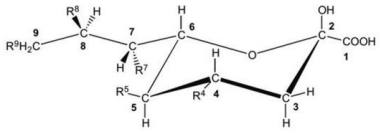

R^5	R^4	R^7	R^8	R^9
NH_2	OH	OH	OH	OH
NH—$COCH_3$	O—$COCH_3$	O—$COCH_3$	O—$COCH_3$	O—$COCH_3$
NH—$COCH_2OH$	O—$COCH_2OH$	O—$COCH_2OH$	O—CH_3	O—$COCH(OH)CH_3$
NH—$COCH_2O—COCH_3$	O—SO_3H	NH—$COCH_3$	O—SO_3H	O—CH_3
NH—$COCH_2O—CH_3$				O—SO_3H
OH				O—PO_3H_2
O—$COCH_3$				
O—CH_3				

Figure 4: Naturally occuring substituents of the sialic acid backbone.

N-acetylneuraminic acid (Neu5Ac) is the main member of a large family of nine-carbon carboxylated sugars. It is assumed that Neu5Ac is the biosynthetic precursor for all other family members. The figure lists some of the naturally occurring substitutions that have been identified. Figure taken from (Schauer and Kamerling, 2018).

2.1 Sialic acid biosynthesis

The cell intrinsic biosynthetic pathway of Sias starts with UDP-*N*-acetylglucosamine (UDP-GlcNAc), which derives from glucose metabolism *via* the hexosamine pathway (**Figure 5**). The bifunctional enzyme UDP-*N*-acetylglucosamine 2-epimerase/*N*-acetylmannosamine kinase (GNE) epimerizes UDP-GlcNAc into *N*-acetylmannosamine (ManNAc) with subsequent phosphorylation into ManNAc-6-phosphate (Hinderlich et al., 1997). Next, *N*-acetylneuraminate-9-phosphate synthase (NANS) catalyzes the condensation of phosphoenolpyruvate (PEP) with ManNAc-6-phosphate to *N*-acetylneuraminate-9-phosphate, which is then de-phosphorylated by *N*-acetylneuraminate-9-phosphatase (NANP) (Jourdian et al., 1964; Maliekal et al., 2006; Roseman et al., 1961). The resulting *N*-acetylneuraminic acid (Neu5Ac) is the major form of Sia in humans. Nevertheless, before entering the glycosylation

pathway, Neu5Ac has to be activated by *N*-acylneuraminate cytidylyltransferase (CMAS) into CMP-Neu5Ac (Munster-Kuhnel et al., 2004). While inactive in humans, Cytidine monophosphate-*N*-acetylneuraminic acid hydroxylase (CMAH) mediates the derivatization of CMP-Neu5Ac into the hydroxylated CMP-*N*-glycolyneuraminic acid (CMP-Neu5Gc) that is commonly found in other vertebrates like mice, which are commonly used as model organism in basic research. Intracellular CMP-Neu5Ac concentrations are regulated *via* a feedback mechanism, where CMP-Neu5Ac allosterically binds to a region within the epimerase domain of GNE, inhibiting its enzymatic activity (Kornfeld et al., 1964; Sommar and Ellis, 1972).

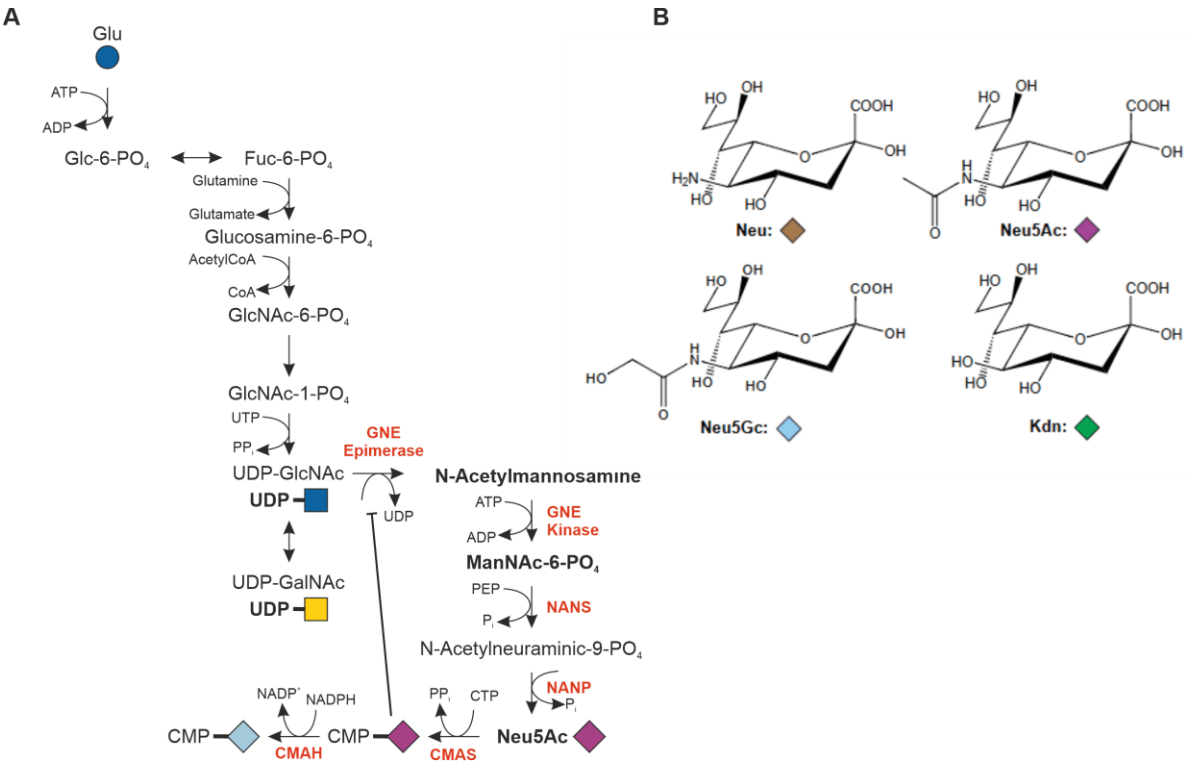

Figure 5: Sialic acid biosynthesis.

A) Metabolic flux of glucose (Glu) in the hexosamine pathway to UDP-*N*-acetylglucosamine (UDP-GlcNAc). GNE directs *N*-acetylneuraminic acid biosynthesis by epimerization of UDP-GlcNAc to *N*-acetylmannosamine (ManNAc) and phosphorylation into ManNAc-6-phosphate (ManNAc-6-PO_4). *N*-acetylneuraminate-9-phosphate synthase (NANS) condensates phosphoenolpyruvate (PEP) and ManNAc-6-PO_4 to *N*-acetylneuraminic-9-phosphate that is subsequently dephosphorylated by *N*-acylneuraminate-9-phosphatase (NANP). Activation of Neu5Ac with CTP is catalysed by *N*-acylneuraminate cytidylyltransferase (CMAS) resulting in CMP-Neu5Ac. Derivitazation of CMP-Neu5Ac into its hydroxylated form CMP-Neu5Gc is mediated by cytidine monophosphate-*N*-acetylneuraminic acid hydroxylase (CMAH) **B)** Chemical structures of different sialic acids. ATP: adenosintriphosphate, ADP: adenosindiphosphate, GlcNAc: *N*-acetylglucosamine, GalNAc: *N*-acetylgalactosamine, UDP: uridinediphosphate, CMP: cytidinemonophosphate, $P(P)_i$: phosphate, Neu: neuraminic acid, Neu5Ac: *N*-acetylneuraminic acid, Neu5Gc: *N*-glycolylneuraminic acid, Kdn: 2-keto-3-deoxynonic acid. Figure adapted from (Freeze et al., 2022).

2.2 Sialylation and Salvage pathway

Generally, CMP-Sia enters the Golgi apparatus *via* the CMP-sialic acid transporter (SLC35A1), which is an antiporter exchanging CMP from the Golgi lumen with CMP-Sia from the

cytoplasm (Eckhardt et al., 1996). In humans, a subset of 20 different sialyltransferases serve to form the glycosidic linkages of Sia to a glycoconjugate. Sialoglycans differ in terms of their linkages to the underlying monosaccharide; Table 2 A summarizes the four different families of sialyltransferases.

Table 2: Sialyltransferase and neuraminidase families.

The table lists the sialyltransferase families that are involved in the sialylation process of glycoproteins and neuraminidase isoenzymes that are involved in the sialic acid salvage pathway and turnover. Gal: Galactose, GalNAc: *N*-acetylgalactosamine, Sia: sialic acid.

A

	Family	Linkage
Sialoglycan Synthesis	ST3Gal	α-2,3-Gal
	ST6Gal	α-2,6-Gal
	ST6GalNAc	α-2,6-GalNAc
	ST8Sia	α-2,8-Sia

B

	Name	Localization	Substrate
Sialoglycan Catabolism	NEU1	lysosome, plasma membrane	oligosaccharides, glycopeptides
	NEU2	cytosol	oligosaccharides, glycoproteins, gangliosides
	NEU3	plasma membrane	gangliosides
	NEU4	ER, lysosome, mitochondria	oligosaccharides, glycoproteins, gangliosides

The catabolic salvage pathway of Sias enables cells to dynamically regulate cell surface sialylation and to reuse Sias in the biosynthetic pathway. In mammals, four different neuraminidases (NEU1-4) are known to hydrolyze Sia residues in glycoconjugates, allowing the catabolic release of Sia. NEU1-4 differ in terms of their subcellular localization, substrate specificity and tissue distribution (Table 2 B) (Du et al., 2024). Free Sia is transported into the cytosol where it can be processed by the Neu5Ac aldolase into ManNAc and pyruvate (Morin et al., 2004; Schauer and Wember, 1996).

2.3 UDP-*N*-acetylglucosamine 2-epimerase/*N*-acetylmannosamine kinase (GNE)

GNE is often referred to as the key enzyme in the sialic acid biosynthetic pathway. Its bifunctionality was first discovered in 1997, while the UDP-GlcNAc 2-epimerase and ManNAc kinase have been known as individual enzymes before (Comb and Roseman, 1958; Ghosh and Roseman, 1961; Hinderlich *et al.*, 1997). Characterization of the enzymatic activity led to the initial suggestion, that the GNE forms hexamers and tetramers, while also a dimeric state was observed, depending on substrate availability (Hinderlich *et al.*, 1997). *Gne* knock out causes the complete loss of endogenous sialic acid production, which leads to early embryonic lethality

in mice (Schwarzkopf et al., 2002). Cultured cells on the other side can compensate this loss, supporting the physiological importance of sialic acids during development (Keppler et al., 1999). Interestingly, heterozygous *Gne* knock out mice only displayed a 25 % reduction of sialoglycans compared to their wild type littermates with no obvious phenotype (Gagiannis et al., 2007). The *Gne* gene is expressed ubiquitously in all tissues, but highest expression was observed in the liver, presumably due to the high demand of serum glycoprotein secretion (Horstkorte et al., 1999). GNE is a primarily cytosolic enzyme and different post-translational modifications have been investigated in terms of their effects on GNE activity. For instance, phosphorylation of GNE by protein kinase C (PKC) led to enhanced activation of the UDP-GlcNAc 2-epimerase domain (Horstkorte et al., 2000). Furthermore, hGNE1 harbours five potential *O*-GlcNAcylation sites and western blot analysis of immunoprecipitated Gne from rat liver proofed the existence of this PTM *in vivo* (Hinderlich et al., 2015).

3 GNE myopathy

Mutations within the *GNE* gene were finally identified to be the cause of the rare genetic disease "hereditary inclusion body myopathy" (HIBM), which from then on, was termed "GNE myopathy" (GNEM) (Eisenberg et al., 2001). Features of GNEM will be discussed in more detail in the following sections.

3.1 Clinical phenotype

GNE myopathy is a slowly progressing neuromuscular disorder with an early-adulthood onset. Hundreds of different mutations in the UDP-GlcNAc 2-epimerase as well as in the ManNAc kinase domain, have been reported (Celeste et al., 2014). The disorder is inherited in an autosomal recessive manner; hence, the pathology only develops if both alleles carry a mutation. The clinical phenotype is characterized by a progressive muscle weakness and atrophy, exclusively affecting the skeletal muscle tissue of patients. As there is no cure or therapy available, most patients become wheelchair bound within 10-20 years after disease onset (Argov and Yarom, 1984). Examination of affected muscle tissue *via* needle electromyography shows myopathic changes in form of spontaneous activity (Liu et al., 2022). Noteworthy, even though some patients were described to show signs of inflammatory infiltrates at early stages of the disease, inflammation is not a common feature of GNE myopathy (Krause et al., 2003).

3.2 Histological features

A main characteristic of GNEM biopsies is the presence of rimmed vacuoles that contain Congo red-positive deposits that were identified as beta-amyloid, lysosomal proteins, ubiquitin, and

tau proteins. GNE protein itself was detected in the cytoplasm and myonuclei as well as in the rimmed vacuoles by immunohistochemistry. When it comes to the analysis of the sialylation status of GNEM patients, different conclusions are drawn, depending on the study. Staining of biopsies with different lectins that recognize sialic acids suggest a reduced abundance of sialoglycans (Saito et al., 2004; Voermans et al., 2010). Antibody staining of various muscle glycoproteins generally shows some alterations in GNEM patients compared to healthy individuals but without uniform conclusions (Broccolini et al., 2005; Huizing et al., 2004). Furthermore, a case report of two GNEM patients shows the accumulation of glycogen in muscle biopsies of the affected tissue, adding a new feature to the histopathological spectrum of GNEM (Granger et al., 2022).

3.3 Pathomechanism and disease models

The exact pathomechanism of GNE myopathy remains largely unknown. The multitude of disease models, ranging from studies on the recombinant protein to patient-derived muscle cells, makes it difficult to compare the different findings. However, valuable insights and hypotheses have been gathered over the past three decades of GNEM research. Studies on recombinantly expressed GNE variants showed that enzymatic activity is impaired to varying degrees, depending on the mutation (Noguchi et al., 2004; Penner et al., 2006). Furthermore, while there were no alterations of sialic acid levels observed in the serum of patients, skeletal muscle tissue showed reduced sialylation (Noguchi *et al.*, 2004; Saito *et al.*, 2004). Additionally, Gne protein and mRNA levels were found to be upregulated in response to muscle injury in a mouse model, suggesting an important role of sialic acids during muscle regeneration (Nakamura et al., 2010). A major hallmark of GNE myopathy is the occurrence of rimmed vacuoles and protein aggregates. A study performed in the skeletal muscle cell line C2C12, and to some extend on patient biopsies, proposed that hyposialylated myotubes favour the endocytosis of amyloid β-peptides, triggering apoptotic signalling pathways in those cells. Interestingly, amyloid β-peptide internalization seemed to be clathrin and heparansulfate proteoglycan dependent (Bosch-Morato et al., 2016). Another aspect was illuminated by Patzel *et al*, who confirmed a non-specific increase of glycosphingolipids in GNEM patients (Patzel et al., 2014). A recent lipidomic analysis that compared the sera of 32 GNEM patients with the sera of 22 healthy individuals revealed a metabolic signature of GNE myopathy, showing alterations in the abundancies of carnitines and lysophosphatidylcholines, as well as certain metabolites from the tricarboxylic acid cycle (Manis et al., 2024).

Based on the *Gne*$^{-/-}$ mouse that is embryonic lethal, two different knock-in mouse models are found in the literature. The mouse model created by Malicdan and co-workers is a knock-in

mouse carrying the human GNE D176V variant (*Gne*$^{-/-}$h*GNE*D176V-Tg), which represents one of the most common variants found in Japan. According to their findings, the *Gne*$^{-/-}$h*GNE*D176V-Tg mice exhibit hyposialylation and develop a phenotype that resembles human disease progression, with significantly reduced muscle power after 30 weeks of age (Malicdan et al., 2008; Malicdan et al., 2007). Mechanistically, skeletal muscle tissue derived from this mouse model indicated an increase in intracellular reactive oxygen species (ROS) levels that led to an increase in *S*-nitrosylation of certain proteins like glycogen phosphorylase, titin, and α-actin (Cho et al., 2017). A second knock-in mouse model with the *Gne*$^{M712T/M712T}$ genotype had a high mortality rate in the first generation due to renal failure. The following offspring generations had no consistent phenotype, presenting either muscle or kidney defects with severe, mild, or no obvious symptoms (Sela et al., 2013).

3.4 Therapeutic strategies

As hyposialylation of skeletal muscle tissue seems to be the most obvious driver of disease manifestation and progression, the major strategy of therapeutic intervention is to target the sialic acid content in GNEM patients. Thus, many trials evaluated safety and efficacy of different sialic acid metabolite supplements. While cell and mouse models showed promising effects on sialylation in response to *N*-acetylmannosamine (ManNAc) and sialic acid treatment, clinical utility of those compounds is still under investigation (Malicdan et al., 2012; Morozzi et al., 2019; Park et al., 2023; Sparks et al., 2007; Yonekawa et al., 2014). A phase 3 double-blind, placebo-controlled study on aceneuramic acid extended-release (Ace-ER) failed to indicate any benefits in terms of improving muscle strength and functions in GNEM patients (Lochmuller et al., 2019). Interestingly, a similar phase 3 trial was conducted in Japan with a more promising outcome (Mori-Yoshimura et al., 2023).

Besides oral supplementation efforts, development of a gene replacement therapy based on viral delivery is also being investigated. A single dose of a recombinant Adeno Associated Virus (rAAV) based *GNE* gene therapy was more efficient in increasing the *N*-glycolyneuraminic acid (Neu5Gc) content in a *Cmah*$^{-/-}$*Gne*$^{-/-}$h*GNE*D176V-Tg mouse model compared to oral Neu5Gc supplementation (Crowe et al., 2022). However, assessment of the therapeutic benefit of this approach is yet to be determined, as there was no consistent phenotype of the *Gne*$^{-/-}$h*GNE*D176V-Tg mouse model, impeding reliable conclusions (Mitrani-Rosenbaum et al., 2022).

4 Skeletal muscle architecture and physiology

As GNE myopathy solely affects the skeletal muscle tissue, one could assume that sialic acids play a specialized role in the striated musculature. In fact, the negative charge of sialic acids were described to contribute to the membrane potential of myofibers, thereby regulating excitation-contraction events (Bennett et al., 1997). Generally, skeletal muscles use chemical energy to generate force and body movement, which comes with the expanses of high energy requirements. Proper muscle function relies on the complex interplay of myriad components and the vast diversity of genetic muscular disorders reflects the tightly organized regulatory mechanisms that are needed for motility.

4.1 Organization of the muscle fiber

Skeletal muscle tissue comprises a specialized architecture, where individual muscle fibers (multinucleated cells) are bundled in so-called fascicles that in turn form the muscle (Figure 6). Each myofiber contains several myofibrils that are constituted by contractile proteins and are organized in sarcomeres (Figure 7). For effective signal transduction, the sarcolemma (plasma membrane) forms deep invaginations into the myofibers, known as the transverse tubules (T-tubules) that are in close proximity with the sarcoplasmic reticulum. Another characteristic of the skeletal muscles is their capacity to regenerate. A pool of satellite cells, unipotent muscle precursor cells, resides between basal lamina and sarcolemma of adult skeletal muscle tissue. In case of an injury, satellite cells become activated and start to proliferate. A subset of this proliferating pool differentiates into mature fibers, replacing the damaged ones, while another subpopulation goes back to its quiescent state to maintain the pool of satellite cells. During this process of myogenesis, N-glycans and expression of certain glycoproteins and lectins seem to play an important role, directly linking glycosylation to muscle regeneration (Blazev et al., 2021).

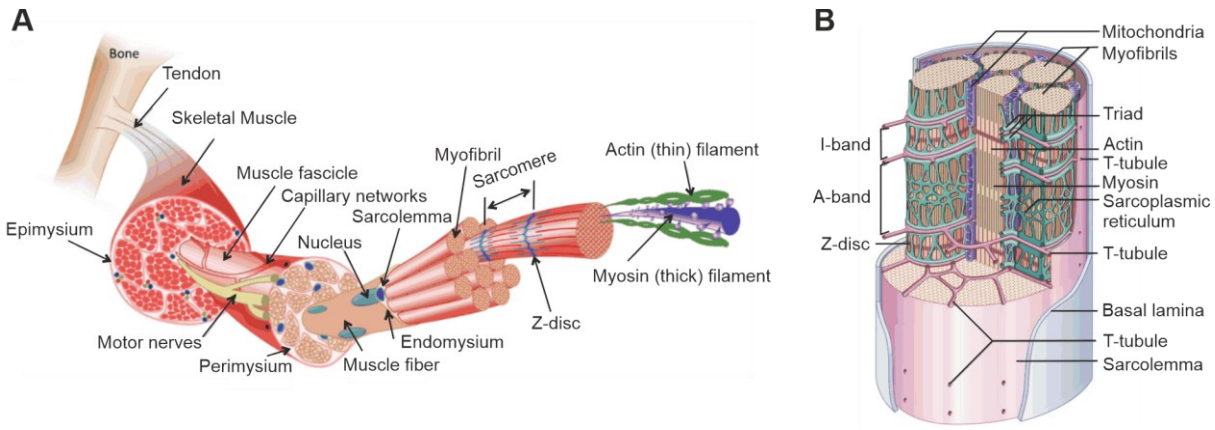

Figure 6: Cellular organization of skeletal muscle tissue.

A) Skeletal muscle consists of bundled muscle fascicles that are surrounded by a network of capillaries and motor neurons. Each fascicle spans several myofibers that are large, individual, multinucleated cells. Myofibrils are the functional units of the myofibers, constituting the sarcomeres that build the contractile apparatus of muscle cells. Major components of the sarcomeres are thin filaments (α-actin) and thick filaments (myosin). **B)** Schematic drawing of a myofiber, showing the transverse tubule (T-tubule) system of the sarcolemma and the sarcoplasmic reticulae network, spanning the myofibrils. Figure adapted from (Samandari et al., 2022).

4.2 Neuromuscular junction

Innervation of skeletal muscle by motor neurons allows the transmission of electric impulses from the neuron to the muscle. The neuromuscular junction (NMJ) is the synapse between the motor neuron terminal and the sarcolemma of a myofiber. The neurotransmitter acetylcholine (ACh) is stored in vesicles in the presynaptic terminal and upon arrival of an action potential, the vesicles fuse with the membrane and ACh is released into the synaptic cleft. Acetylcholine receptors (AChR), located at the postsynaptic sarcolemma, undergo a conformational change upon binding of ACh, leading to the opening of the channel forming pore. Noteworthy, proper folding and receptor function relies on N-glycosylation of select subunits of the AChR (Gehle et al., 1997). Opening of AChR allows the influx of positively charged ions (mainly Na^{2+} and K^{+}) that alter the membrane potential. When the depolarization reaches a certain threshold-value, voltage-gated sodium channels ($Na_V1.4$) start to open and generate an action potential that is propagated from the motor endplate to the rest of the sarcolemma, leading to contraction of the muscle. It is well established in the literature that sialylation has a major impact on $Na_V1.4$ channel gaiting and function, pointing to another important role of sialic acids in muscle physiology (Bennett *et al.*, 1997; James and Agnew, 1987).

4.3 Excitation contraction coupling

To induce muscle contraction, the action potential arriving at the sarcolemma has to be converted into a signal that reaches the sarcomeres in the interior of the myofibers. The T-tubules play a major role in the propagation of the action potential from the outside to the inside of the muscle cells. The triad junction is the interaction point of the T-tubules with the

membrane of the sarcoplasmic reticulae that forms a network around the myofibrils. Dihydropyridine receptor (DHPR) is a voltage-gated Ca^{2+} channel residing in the T-tubules, adjacent to the terminal cisternae of the sarcoplasmic reticulum (SR). Upon depolarization of the sarcolemma, DHPRs are activated and undergo a conformational change, which in turn allows the interaction with the ryanodine receptor (RyR) in the SR (Block et al., 1988). This interaction triggers the release of large amounts of Ca^{2+} from the SR that can then bind to troponin C, initiating a cascade that leads to muscle contraction. While the role of sialylation on $Na_V1.4$ function has been thoroughly investigated, not much is known about the impact of glycosylation on DHPR activity.

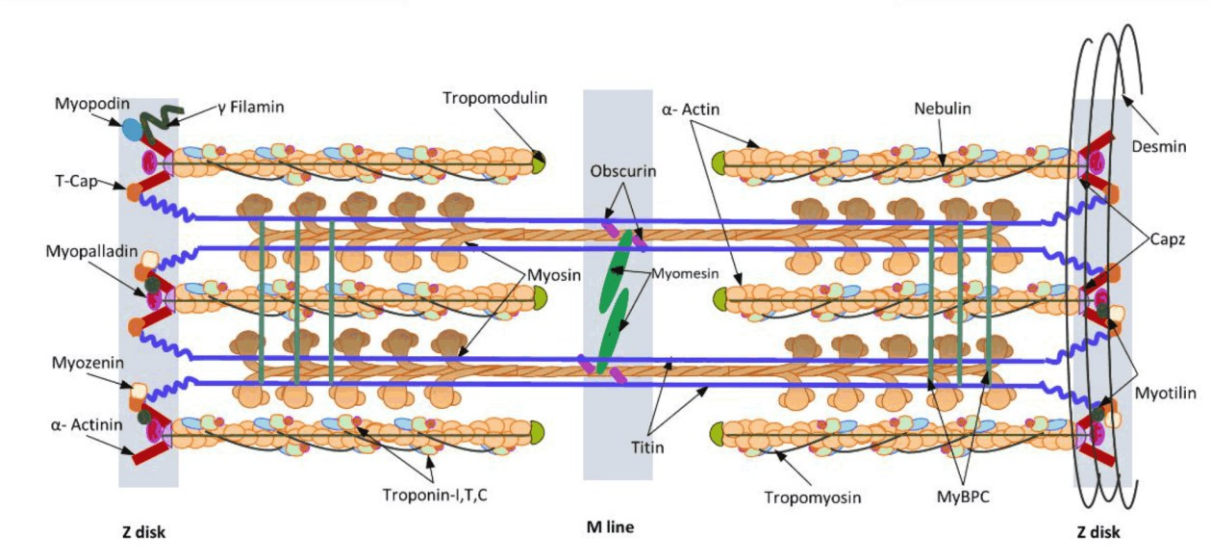

Figure 7: Sarcomere organization.

Each sarcomere unit is bordered by a dark-appearing narrow line called Z-disk. The Z-disks connect the thin filaments (α-actin) in a lateral axis, while the thick filaments (myosin) are connected at the M-line. Troponin complexes occupy myosin head binding sites on the actin filaments and are released upon Ca^{2+} binding. Titin and nebulin are two very large proteins, ensuring structural integrity by maintaining the length of the thick and thin filaments, respectively. Figure adapted from (Mukund and Subramaniam, 2020).

To enable muscle relaxation, the excess Ca^{2+} has to be removed from the cytosol back into the SR, which is an energy-consuming process, mediated by the ATP-dependent Ca^{2+} ATPase (SERCA) pumps (Periasamy and Kalyanasundaram, 2007).

4.4 Extracellular matrix (ECM)

Due to the contractile nature of the skeletal muscle tissue, the connective tissue surrounding the muscles has to withstand frequent mechanical stress. The extracellular matrix (ECM) comprises fibroblasts, macrophages and a network of capillaries and nerves that have to tolerate the ongoing contraction-relaxation cycles. Similarly, the ECM serves as biomechanical support through the linkage of the cytoskeleton to the ECM (Humphrey et al., 2014). Besides the

cellular components, ECM also contains various proteins, mainly collagens, non-collagenous glycoproteins, and proteoglycans of which collagens make up the biggest proportion (Figure 8). Indisputably, glycosylation is fundamental for correct ECM composition, for example, aberrant expression of the major heparan sulfate proteoglycan perlecan is linked to the Schwartz-Jampel syndrome, an autosomal recessive skeletal dysplasia (Arikawa-Hirasawa et al., 2002).

In response to muscle injury, ECM expansion is a crucial step towards muscle recovery (Chapman et al., 2017). However, uncontrolled expansion of the ECM, called fibrosis, leads to the replacement of normal tissue architecture and in skeletal muscle, is most often associated with muscular dystrophies (Mann et al., 2011). Mechanistically, mutations in genes encoding for structural proteins that link the cytoskeleton to the basal lamina, often results in the dislocation of whole protein complexes. Hence, the sarcolemma loses stability, leading to membrane disruption during contractile activity (Blake et al., 2002).

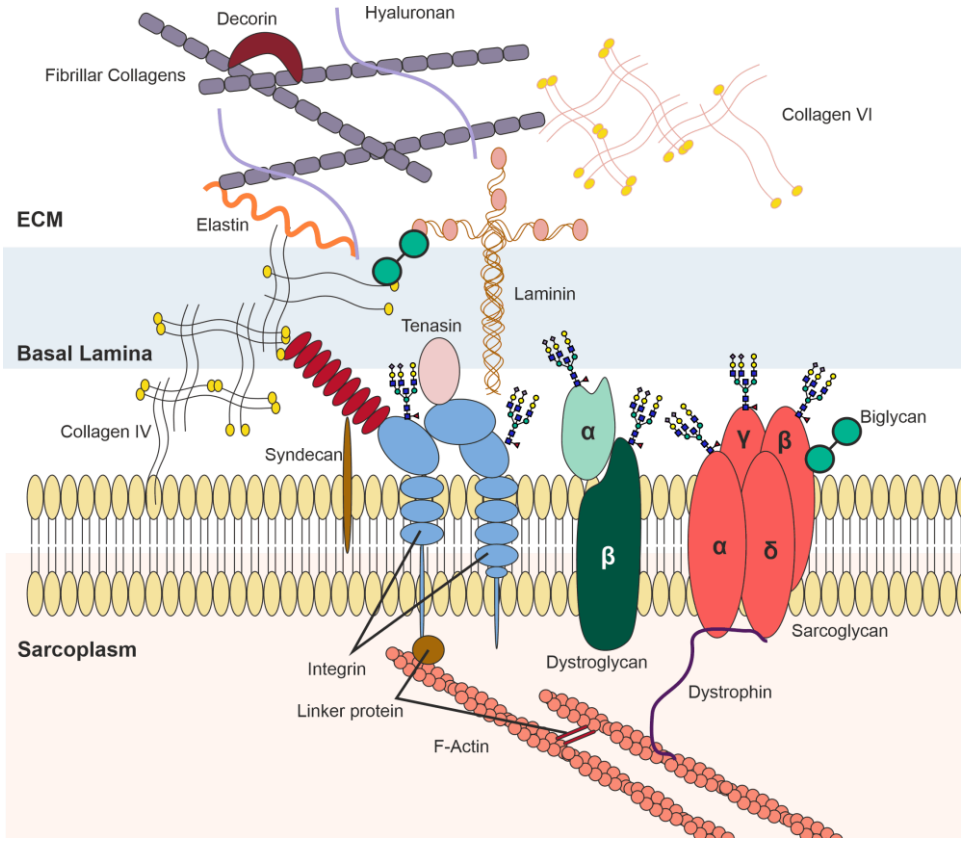

Figure 8: Extracellular matrix and basal lamina.

Simplified schematic drawing, representing major components of the extracellular matrix and basal lamina of myofibers. ECM: extracellular matrix. Figure created in CorelDRAW.

4.5 Skeletal muscle glucose metabolism

Skeletal muscle has a high energy demand, mainly because of the ATP requirements during the cross-bridge cycle that enables contraction of the sarcomeres. Anaerobic (glycolysis) and aerobic (oxidative phosphorylation) glucose metabolism are the two major pathways for generating energy in form of ATP in the myofibers. Upon insulin stimulation, the glucose transporter GLUT4 translocates to the sarcolemma, facilitating glucose uptake into the cells. To keep blood sugar levels in a tolerable range, excess glucose can be stored in form of glycogen in skeletal muscle and in the liver. Glycogen is a branched polymer and contains up to 55,000 glucose residues, that are either needed for the cells own demands (skeletal muscle) or can be distributed to distant organs and tissues (liver). In order to use glucose from glycogen, two enzymes are needed, glycogen phosphorylase and glycogen debranching enzyme. While glycogen phosphorylase acts on linear glycogen chains to release glucose-1-phosphate, glycogen debranching enzyme is needed to untie the branch points for complete glycogen degradation. Additionally, muscle creatine kinase (CKM) can transfer high-energy phosphates (P_i) from phosphocreatine stores to ADP, providing ATP for immediate energy demands (Meyer et al., 1984).

4.6 Neuromuscular disorders

When looking at the specialized architecture of myofibers and the function it is linked to, it becomes obvious that only a complex interplay of all proteins involved can ensure proper muscle function. This fact is highlighted by the vast amount of different neuromuscular disorders that arise due to genetic mutations. An updated gene table of neuromuscular disorders is published each year in the journal of Neuromuscular Disorders, categorizing the diseases into 17 groups, with one of them being devoted to mitochondrial myopathies. The 2025 version of this list comprises 686 genes and 1216 diseases, in which GNE myopathy (listed as Nonaka myopathy) is classified as distal myopathy (Benarroch et al., 2024b). As there are so many different causes for neuromuscular disorders, understanding of the respective pathomechanisms is limited. Collectively, many of the listed genes encode for proteins that provide structural stability to the myofiber and sarcolemmal integrity or are involved in protein turnover, intracellular trafficking, calcium signaling, and electrical excitability.

5 Aims of the Study

Sialylation of glycoproteins has various physiological roles like increasing protein solubility and immune signaling. Perturbations in the endogenous glycosylation machinery may result in varying degrees of pathophysiological disorders that are collectively referred to as congenital disorders of glycosylation (CDGs). As such, mutations within the *GNE* gene that encodes for the key enzyme of the sialic acid biosynthesis pathway, lead to the development of a muscular disorder with early-adulthood onset. GNE myopathy is a rare autosomal recessive disease with a prevalence of 1-9/1,000,000. Despite many approaches to study the pathomechanism of GNE myopathy, no significant breakthrough has been achieved concerning our understanding of this neuromuscular disorder. Hence, there is no cure available for the patients and more efforts are needed to develop robust therapeutic strategies.

Thus, the aims of this study can be split in two parts. First, a *Gne* knock out model was to be established to investigate the effects of hyposialylation on a cellular level. Second, consequences of *Gne* disruption should be studied with a focus on the special physiology of skeletal muscle cells. In summary, the aims were:

- To use CRISPR/Cas9 technology to knock out *Gne* in C2C12 myoblasts
- To assess how glycosylation is altered in C2C12 *Gne* knock out myoblasts and myotubes
- To rescue sialylation in C2C12 *Gne* knock out cells by exogenous supplementation with *N*-acetylmannosamine and *N*-acetylneuraminic acid
- To analyze the expression of de-regulated genes in C2C12 *Gne* knock out clones

II Methods & Material

1 Material

1.1 Chemicals

Table 3: List of used chemicals

Chemical	Company
2-Propanol	Carl Roth
3-[(3-cholamidopropyl)dimethylammonio]-1-propanesulfonate (CHAPS)	Roche
Acetic acid	Sigma Aldrich
Acetonitrile (MeCN)	Romil
Acrylamid	Carl Roth
Agarose	Carl Roth
Albumin Bovine Fraction V (BSA)	Carl Roth
Alcian blue 8GX	Sigma Aldrich
Ammonium hydrogen carbonate (AMBIC)	Sigma Aldrich
Ammonium Persulfate (APS)	Carl Roth
Bromphenol blue	SERVA
Calcium Chloride (CaCl2)	Merck
Chloroform (CHCl3)	Sigma Aldrich
Copper sulfate (CuSO4)	Sigma Aldrich
Dimethyl sulfoxide (DMSO)	Sigma Aldrich
Dithiothreitol (DTT)	Carl Roth
DMEM	Gibco (#41965-039)
Ethanol	Sigma Aldrich
Ethidium bromide	AppliChem
Ethylenediamine tetraaectic acid disodium salt dehydrate (EDTA)	Carl Roth
Fetal Bovine Serum (FBS)	Gibco (#10206270)
Formic acid (FA)	Sigma Aldrich
Glycerol	Carl Roth
Glycine	Carl Roth
Guanidine hydrochloride (GuHCl)	Sigma Aldrich
hydrochloric acid (HCl)	Carl Roth
Immobilon Forte Western HRP-Substrate	Millipore
Insulin	Sigma Aldrich (#I6634-50MG)
Iodoacetic acid (IAA)	Sigma Aldrich
L-Glutamine	Gibco (#25030081)
Magnesium chloride	Merck
Methanol (MeOH)	Romil
N,N,N',N'-Tetramethyl-ethylenediamine (TEMED)	Carl Roth
N-acetylmannosamine (ManNAc)	New Zealand Pharmaceuticals
N-acetylneuraminic acid (Neu5Ac)	Molekula Group
non-fat dry milk	Carl Roth
Nonidet P40 (NP40)	Fluka Analytical
PageRulerTM Plus Prestained Protein Ladder	Thermo Fisher
Paraformaldehyde (PFA)	Carl Roth

Chemical	Company
Periodic acid	Carl Roth
Phenylmethanesulfonyl fluoride (PMSF)	Boehringer Mannheim
PNGase F	New England Biolabs
Ponceau S	Carl Roth
Potassium borohydride (KBH4)	Sigma Aldrich
Potassium chloride (KCl)	Sigma Aldrich
Propanol (PrOH)	Romil
Protease Inhibitor Cocktail (PIC)	Sigma Aldrich
Puromycin	Thermo Fisher
Resorcinol	Carl Roth
Schiff's reagent	Carl Roth
Sodium chloride (NaCl)	Carl Roth
Sodium dodecyl sulphate (SDS)	Carl Roth
Sodium hydrogen phosphate (Na2HPO4)	Carl Roth
Sodium hydroxide (NaOH)	Carl Roth
Sulfosalicylic acid (SSA)	Carl Roth
Trichloroacetic acid (TCA)	Carl Roth
Trifluoroacetic acid (TFA)	Sigma Aldrich
tris(hydroxymethyl)aminomethane (TRIS)	Carl Roth
Triton X-100	Carl Roth
Trizol Reagent	Carl Roth
Trypsin	Sigma Aldrich
Trypsin/EDTA	Gibco (#R001100)
Tween 20	Carl Roth

1.2 Kits and Composite Reagents

Table 4: List of used kits and composite reagents.

Reagent	Company
CellTiter-Glo 2.0 Cell Viability Assay	Promega (#G9241)
GeneRulerTM 100 bp Plus DNA Ladder	Thermo Fisher (#SM0241)
oligo dT Primer 12-18	Thermo Fisher (#18418012)
Phusion High-Fidelity PCR Master Mix	Thermo Fisher (#F531)
PierceTM BCA Protein Assay Kit	Thermo Fisher (#23225)
PNGase F	New England Biolabs (#P0704S)
qPCR Sybr Master Mix	Jena Bioscience (PCR-372L)
RiboLock Rnase Inhibitor	Thermo Fisher (#EO0382)
Super Script II Reverse Transcriptase	Thermo Fisher (#18064014)

1.3 Consumables

Table 5: List of used consumables.

Consumable	Company
10 cm Cell culture plate	greiner bio-one
12 Well Cell culture plate	greiner bio-one
6 Well Cell culture plate	greiner bio-one
96 Well cell culture plate	greiner bio-one
96 Well plate, white opaque	Thermo Fisher
96 Well, thin-wall, Hard-Shell PCR Plate	Bio-Rad
Amersham Protran nitrocellulose membrane 0.45 µm	TH. Geyer
Cell Scraper	greiner bio-one
CELLSTAR Cell culture flask 250 mL	greiner bio-one
CELLSTAR Cell culture flask 550 mL	greiner bio-one
CELLSTAR Test Tube 15 mL	greiner bio-one
CELLSTAR Test Tube 50 mL	greiner bio-one
Coverslips 15 mm	epredia
CryoTube vials	Thermo Fisher
Micro Tubes, 1.5 mL	Sarstedt
Microscope glass slides	Hecht Assistent
PCR Tubes 0.2 mL	Brand
Pipet Tips, 0.5 to 20 µL	Sarstedt
Pipet Tips, 10 to 200 µL	Sarstedt
Pipet Tips, 100 to 1000 µL	Sarstedt
Platesealer EASYSEALtm, transparent foil	greiner bio-one
Slide-A-Lyzer Dialysis cassette	Thermo Fisher
SPE classic C18 cartridges	Thermo Fisher
SPE HLB plus C18 cartridges	Thermo Fisher
Whatman filter paper 3 MM	GE Healthcare

1.4 Buffers and solutions

Table 6: List of buffers and solutions.

Buffer/Solution	Component	Concentration
1 x PBS pH 7.4	NaCl	137 mM
	KCl	2.7 mM
	Na_2HPO_4	10 mM
	KH_2PO_4	1.8 mM
1 x TBS buffer pH 7.6	NaCl	137 mM
	TRIS	7.7 mM
1 x TBS-T buffer pH 7.6	NaCl	137 mM
	TRIS	7.7 mM
	Tween-20	0.1 % (v/v)
5 % Milk/TBS-T	TBS-T	
	Non-fat dry milk powder	5 % (w/v)

Buffer/Solution	Component	Concentration
5 % BSA/TBS-T	TBS-T	
	BSA	5 % (w/v)
5 x SDS sample buffer pH 6.8	SDS	12.5 % (v/v)
	TRIS	0.3 M
	Glycerol	50 % (v/v)
	DTT	50 mM
	Bromphenol blue	1 mM
NP-40 lysis buffer pH 8.5	TRIS-HCl	50 mM
	NaCl	150 mM
	NP-40	1 % (v/v)
RIPA lysis buffer pH 7.5	TRIS-HCl	25 mM
	NaCl	150 mM
	NP-40	1 % (v/v)
	EDTA	1 mM
Ponceau-S solution	Ponceau-S	0.2 % (w/v)
	TCA	3 % (v/v)
	SSA	3 % (w/v)
1 x Running buffer pH 8.5	TRIS	25 mM
	Glycine	192 mM
	SDS	0.1 % (v/v)
1 x Blotting buffer pH 8.5	TRIS	20 mM
	Glycine	150 mM
	Ethanol	10 % (v/v)
Resolvin gel buffer pH 8.8	Acrylamide	8-15 %
	TRIS	377 mM
	SDS	0.05 % (v/v)
	APS	0.08 % (v/v)
	TEMED	0.08 % (v/v)
Stacking gel buffer pH 6.8	Acrylamide	4 %
	TRIS	124 mM
	SDS	0.05 % (v/v)
	APS	0.04 % (v/v)
	TEMED	0.1 % (v/v)
1 x TAE buffer	Tris acetate	40 mM
	EDTA	1 mM
10 x DNA loading buffer	Glycerol	50 % (v/v)
	EDTA	50 mM
	Xylene cyanol	0.05 % (w/v)
	Bromphenol blue	0.05 % (w/v)
Glycomic Lysis buffer pH 7.4	TRIS	25 mM
	NaCl	150 mM
	EDTA	5 mM
	CHAPS	1 % (w/v)
Dialysis buffer	Ammonium hydrogen carbonate	50 mM

Buffer/Solution	Component	Concentration
TRIS/GuHCl buffer pH 8.5	TRIS	0.6 M
	GuHCl	4 M
	degased under a gentle stream of nitrogen	
TRIS buffer pH 8.5	TRIS	0.6 M
	degased under a gentle stream of nitrogen	

1.5 Cells

Table 7: List of cells used in this work.

Cells	Background	Source
HEK-293	human embryonic kidney	DSMZ: ACC 305
HEK-293 GNE knock out clone	human embryonic kidney	Peters et. al 2023
C2C12	murine myoblasts	DSMZ: ACC 565
C2C12 Gne knock out clone #24	murine myoblasts	this work
C2C12 Gne knock out clone #26	murine myoblasts	this work
Sol8	murine myoblasts	kind gift from Prof. Dr. Stella Mitrani-Rosenbaum
Sol8 Gne knock out clone	murine myoblasts	Ilouz et. al 2022

1.6 Cell culture media

Table 8: List of used medium for all cell lines

Medium	Component	Amount
Growth medium	DMEM	
	FBS	10 % (v/v)
	L-Glutamine	1 % (v/v)
Differentitation medium	DMEM	
	FBS	2 % (v/v)
	L-Glutamine	1 % (v/v)
	Insulin	10 nM

1.7 Instruments

Table 9: List of used instruments

Instrument	Name	Company
Mass Spectrometer	4800 MALDI-TOF-TOF	Applied Biosystems, Darmstadt, Germany
Analytical Lab Balance	MC1	Sartorius, Göttingen, Germany
Blot and SDS-PAGE System	Mini-Protean® Tetra Cell	Bio-Rad, Hercules, USA
Cell counter	CellDrop BF	DeNovix, Wilmington, USA
Centrifuge	5427R	Eppendorf, Hamburg, Germany
Centrifuge	5425	Eppendorf, Hamburg, Germany
Centrifuge	Color Sprout Plus Mini	Biozym, Hessisch Oldendorf, Germany
Centrifuge	Universal 320R	Hettich, Tuttlingen, Germany
Flow Cytometer	Accuri C6	BD, New Jersey, USA
Gel Electrophoresis system	Owl™EasyCast™ B1A	Thermo Fisher Scientific, Waltham, USA
Heating Block	TS pro	CellMedia, Zeitz, Germany
Heating Block	Thermo Mixer F1.5	Eppendorf, Hamburg, Germany
Imaging System	ChemiDoc MP	Bio-Rad, Hercules, USA
Incubator	Hera Cell	Heraeus, Hanau, Germany
Laminar Flow Cabinet	Aura 2000 M.A.C.	BioAir, Siziano, Italy
Magnetic Stirrer	FB14001	Thermo Fisher Scientific, Waltham, USA
Microscope	Axio Observer	Zeiss, Oberkochen, Germany
Microscope	Axiovert 100	Zeiss, Oberkochen, Germany
Molecular Imager	Gel Doc™ XR System	Bio-Rad, Hercules, USA
Orbital Shaker	Polymax 2040	Heidoph, Schwabach, Germany
PCR System	T100 Thermal Cycler	Bio-Rad, Hercules, USA
pH-Electrode	Orion Lab Star PH111	Thermo Fisher Scientific, Waltham, USA
Pipette	Transferpette®	Brand, Wertheim, Germany
Plate Reader	CLARIOStar^{Plus}	BMG Labtech, Ortenberg, Germany
Power Supply	Power Pac 300	Bio-Rad, Hercules, USA
Real-Time PCR System	CFX Connect™	Bio-Rad, Hercules, USA
Sealing Device	Easy Packer Impulse Sealer	Wilke & Witzel, Hamburg, Germany
Spectrophotometer	DS-11 FX+	DeNovix, Wilmington, USA
Vacuum Concentrator	Concentrator Plus	Eppendorf, Hamburg, Germany
Vacuum Pump	Vacusafe	Integra, Biebertal, Germany
Vortexer	MS2 Minishaker	IKA, Staufen, Germany
Water Bath	1002	GFL, Burgwedel, Germany

1.8 Antibodies

Table 10: Primary antibodies and lectins used for western blot and immunofluorescence (IF)

Antibody	Host species	Dilution	Company
polySia (735)	mouse	1:1,000	gift from Prof. Dr. Rita Gerardy-Schahn
Ncam (5B8)	mouse	-	in-house
NCAM (123C3)	mouse	1:1,000	Santa Cruz Biotechnology (sc-7326)
Gne (H10)	mouse	1:1,000	Santa Cruz Biotechnology (sc-376057)

Antibody	Host species	Dilution	Company
b-Tubulin (BT7R)	mouse	1:5,000	Thermo Fisher (MA5-16308)
Myh	mouse	1:1,000	Santa Cruz Biotechnology (sc-376157)
Myh (IF)	mouse	1:100	Santa Cruz Biotechnology (sc-376157)
O-GlcNAc (CTD110.6)	mouse	1:1,000	Cell Signaling Technology (#9875)
NAGK	rabbit	1:1,000	Bioss (#bs-7916R)
Pygm (OTI5D1)	rabbit	1:1,000	Invitrogen (MA5-27442)
Cacna1s [1A]	mouse	1:1,000	Abcam (ab2862)
Cacna2d1 [EPR23267-8]	rabbit	1:1,000	Abcam (ab253190)
Hoechst H33258 (IF)		1:1,000	Sigma-Aldrich (#94403)
Lectin PHA-L, Alexa Fluor 488			Thermo Fisher (L11270)

Table 11: Secondary antibodies used for western blot and immunofluorescence (IF)

Antibody	Dilution	Company
HRP-Goat anti-Mouse IgG	1:10,000	Abcam (#ab6789)
HRP-Goat anti-Rabbit IgG	1:20,000	Abcam (#ab6721)
Goat anti-Mouse IgG (H+L) Alexa Fluor™ Plus 647 (IF)	1:1,000	Thermo Fisher (#A32728)

1.9 Primers

Table 12: List of sgRNAs used for Gne knock out in C2C12 myoblasts.

Name	Target Sequence (5' - 3')	Exon
sgRNA-1	TCCCACCTGATTGACGACTA	2
sgRNA-2	CGGAACACCCGTGATCAACC	3
sgRNA-3	CCTAGCGCTCGTGAAGCTAC	5

Table 13: List of primers used for qPCR

Name	Sequence (5' - 3')	Expected size [bp]	Annealing T
Gapdh fwd	CCTGGAGAAACCTGCCAAGTATG	133	62°C
Gapdh rev	AGAGTGGGAGTTGCTGTTGAAGTC		
St8sia2 fwd	GTGTGGAGTGGGTCAATGCT	342	60°C
St8sia2 rev	TCAATGCCCCCTGTTCATGT		
St8sia4 fwd	GCTGGGACAACCAGGACTTT	318	60°C
St8sia4 rev	ACGTCACGTTCCGCATCTAA		
Scn4a fwd	TTCTCGGAGCCTGAGGACATCA	155	62°C
Scn4a rev	GTGAAACACTCCTCAGGTAGCTC		
Pygm fwd	CCCTACCCACTTTGGAACCC	131	60°C
Pygm rev	GTGCACTTGGTTAGACCCCA		
Ryr1 fwd	TTTCCTGGACCGAGTGTATGGC	157	64°C
Ryr1 rev	CAGACAGAGGTAGCGGTTCAGT		
Cacna1s fwd	CCTGGCTATTGCTGTGGACAAC	154	62°C
Cacna1s rev	CTGCTCCAGTTTCTTGGTCACC		

Table 14: Primers used for PCR.

Name	Sequence (5' - 3')	Expected size [bp]	Annealing T
Gne-202 fwd	ATGGAGAAGAACGGG	2169	65°C
Gne-202 rev	CTAGTGGATCCTGCGCGTT		

1.10 Plasmids

Table 15: List of used plasmids.

Name	Purpose	Source
GLCNE CRISPR/Cas9 KO Plasmid	Gne knock out	Santa Cruz Biotechnology #sc-424509
GLCNE HDR Plasmid	Gne knock out	Santa Cruz Biotechnology #sc-424509-HDR

1.11 Software

Table 16: List of used software.

Software	Company/Source
BD Accuri C6 Analysis Software, version 1.0.264.21	BD Biosciences
CorelDRAW 2021	Corel Corporation
Endnote	Clarivate Analytics
GlycoWorkbench	Freeware
ImageJ (Fiji)	Wayne Rasband, NIH
Microsoft Office	Microsoft Corporation
OriginPro 2019	OriginLab
SnapGene Viewer	Dotmatics
ZEN Microscopy Software	Zeiss

2 Methods

2.1 Cell biology methods

2.1.1 Cell culture

HEK-293, C2C12, and Sol8 cells were cultivated in DMEM medium supplemented with 10 % fetal bovine serum (FBS) and 1 % L-glutamine. All cell lines were grown at 37°C in a humidified incubator with 20 % O_2 and 5 % CO_2. Cell lines were passaged when cells reached ~80 % confluency (HEK-293) or ~50 % confluency (C2C12 and Sol8), respectively. Briefly, after aspirating the culture medium, cells were washed with 1 x PBS and detached using a 2 x trypsin/EDTA solution. After detachment from the culture flask, cells were re-suspended in fresh culture medium and transferred to a new flask. Cell numbers were determined using the CellDrop BF cell counter. For a 48 h period, C2C12 and Sol8 cells were seeded at a density of 4,000 cells/cm^2.

For storage, cells were frozen in normal culture medium supplemented with 5 % DMSO in CryoTube™ vials at -80 °C in a CellCamper® container. After a minimum of 24 h cells were transferred to -150°C for long time storage.

2.1.2 Differentiation of C2C12 and Sol8 cells

For differentiation of myoblasts into myotubes, C2C12 and Sol8 cells were seeded in a fresh culture dish. After 24 h, when cells reached a confluency of ~90 %, growth medium was replaced by differentiation medium (DMEM + 2 % FBS + 1 % L-glutamine). Cells were differentiated for seven days and the differentiation medium was refreshed every other day. Where indicated, dishes were coated with 0.1 % gelatine/PBS for 24 h at 37°C prior to cell seeding.

2.1.3 Supplementation of cells with *N*-acetylmannosamine and *N*-acetylneuraminic acid

A 1 M *N*-acetylmannosamine stock and a 0.2 M *N*-acetylneuraminic acid stock were prepared by dissolving the respective compound in dH_2O with subsequent sterile filtration, using a 0.2 µM filter device. For supplementation studies in HEK-293, C2C12 myoblasts, and Sol8 myoblasts, cells were seeded in normal growth medium for 24 h. Then, medium was replaced by medium containing the respective concentration of *N*-acetylmannosamine or *N*-acetylneuraminic acid and cells were cultured for additional 24 h. For supplementation of differentiated C2C12 myotubes, cells were first differentiated and on day six of differentiation, differentiation medium was supplemented with the respective compound for the last 24 h. For long-term treatment, differentiation medium was supplemented with the respective compound from day zero to day seven of the differentiation protocol.

2.1.4 CRISPR/Cas9

Commercial CRISPR/Cas9 Gne knock out and HDR plasmids were purchased from Santa Cruz Biotechnology (sc-424509-HDR). Briefly, 25,000 C2C12 wild type cells were seeded in full growth medium in a 6-well dish 24 h prior to transfection. Co-transfection of the CRISPR-KO and HDR-plasmids were done using UltraCruz® Transfection Reagent (sc-395739). Positive clones were selected *via* puromycin treatment (1.5 µg/mL) and single cell suspension was seeded into 96-well plates to obtain single cell clones.

2.2 Molecular methods

2.2.1 Western Blotting

For protein isolation, cells were washed two times with ice-cold PBS and harvested from the culture dish using a cell scraper. Cells were pelleted in 1 mL PBS at 12,000 x g for 1 min at 4°C. Cell pellets were lysed in RIPA buffer or NP-40 lysis buffer, freshly supplemented with 1x protease inhibitor cocktail and 1 mM PMSF. Following 30 min incubation on ice, total protein was isolated by centrifugation at 14,000 × g at 4 °C for 10 min and quantified using the Pierce™ BCA Protein Assay Kit. Equal amounts of protein were mixed with 5 × SDS-protein buffer (containing 50 mM DTT) and boiled for 5 min at 95°C. Proteins were separated using SDS-polyacrylamide gel electrophoresis (SDS-PAGE) and transferred onto a nitrocellulose membrane by wet-blotting. Whole protein was stained with Ponceau S as loading control. Membranes were subsequently blocked with 5 % skimmed milk in TBS-T for 1 h at room temperature prior to incubation with primary antibody over night at 4 °C with agitation. On the next day, membranes were washed three times with TBS-T and subsequently incubated with secondary antibody for 1 h at room temperature. After three repeated washing steps with TBS-T, Immobilon® Forte Western HRP Substrate was used for detection using the ChemiDoc MP imaging system from Bio-Rad Laboratories. Signal quantification was performed using ImageJ Software.

2.2.2 Release of N-glycans using peptide:N-glycosidase F (PNGase F)

To remove the N-glycans from the protein backbones, protein lysates were subjected to PNGase F digestion according to the manufacturer's instructions. Briefly, 9 µL lysate were mixed with 1 µL 10 x Glycoprotein Denaturing Buffer and boiled for 10 min at 100°C. After letting the samples cool down to room temperature, 2 µL Glycobuffer 2, 2 µL NP-40, and 6 µL dH_2O were added and mixed before adding 1 µL PNGase F. Lysates were digested for 1 h at 37°C and subsequently mixed with 5 µL 5 x SDS sample buffer for SDS-PAGE and western blot analysis.

2.2.3 Immunofluorescence Staining

Cells were grown on coverslips coated with 0.1 % gelatine in a 12-well plate. After aspiration of culture medium, cells were washed twice with pre-warmed PBS and fixed with pre-warmed 4 % PFA for 10 min at room temperature. Following two washing steps with PBS, cells were permeabilized with 0.5 % Triton X-100/PBS for 10 min at room temperature, washed two times with PBS and blocked with 1 % BSA/PBS for 30 min. Primary antibody was diluted 1:100 in 1 % BSA/PBS and incubated over night at 4°C. Cells that served as negative control (secondary antibody only) were incubated with 1 % BSA/PBS only. The next day, cover slips were washed again three times with PBS and incubated with Goat anti-Mouse IgG (H+L) Alexa Fluor™ Plus 647 and DAPI diluted 1:1,000 in PBS for 1.5-2 h at room temperature, protected from light. Excess staining solution was removed by another three PBS washing steps and cover slips were mounted on glass slides with mowiol mounting medium.

2.2.4 RNA-Isolation

Total RNA was isolated by phenol/chloroform extraction. For this, cell pellets from a 6-well plate were lysed in 1 mL Trizol reagent and transferred to a 1.5 mL tube. The samples were mixed with 200 µL chloroform, shaken vigorously for 15 seconds, and incubated at room temperature for 3 min. For phase separation, the samples were centrifuged for 15 min at 12,000 x g at 4°C. The aqueous phase containing the RNA was transferred to a new tube with 500 µL of isopropanol, mixed, and incubated at room temperature for 10 min. The samples were then centrifuged for 20 min at 12,000 x g at 4°C to precipitate the RNA. The RNA pellet was washed with 1 mL of 70 % ethanol and centrifuged at 8,000 x g at 4°C for 5 min. The ethanol was removed and the pellet was air-dried for 10 min before being re-suspended in 20-50 µL RNase-free H_2O. RNA concentration was determined using the DS-11 FX+ spectrophotometer.

2.2.5 cDNA synthesis

For reverse transcription of RNA into cDNA, the SuperScript™ II reverse transcriptase kit with oligo $(dT)_{12-18}$ as primers was used, according to the manufacturer's instruction. Briefly, 2 µg RNA was mixed with 1 µL oligo dT and 1 µL dNTP-Mix and brought to a final volume of 12 µL with RNAse-free H_2O. The mixture was heated at 65°C for 5 min and then placed on ice for 2 min. Subsequently, 4 µL 5 x FS buffer, 2 µL 0.1 M DTT, 1 µL RiboLock, and 1 µL SuperSript™ II reverse transcriptase were added and samples were incubated at 42°C for 50 min. To stop the reaction, samples were incubated at 70 °C for 15 min.

2.2.6 Quantitative reverse transcription PCR (qRT-PCR)

For mRNA expression quantification, the qRT-PCR technique was used. For qRT-PCR reaction, 2 x qPCR GreenMaster mix was used according to the manufacturer's instruction. To perform the qRT-PCR, components as stated in Table 17 A were mixed and run on the CFX Connect™ real-time PCR system (Bio-Rad) as described in Table 17 B. Measurements were performed in triplicates in a 96-well plate and *Gapdh* was used as a housekeeping gene for normalization of the expression values. Relative expression values were calculated using the $2^{-\Delta Ct}$ method. To validate the specificity of the used primers, melt curves were generated. –For that, temperature was increased in 1°C steps from 55°C to 95°C and melt curve was recorded.

Table 17: qRT-PCR protocol.

A) Reaction composition and **B)** thermocycler conditions.

A

Component	Amount
2 x qPCR GreenMaster mix	10 µL
forward primer	0.5 µM
reverse primer	0.5 µM
cDNA	1 µL
PCR-grade H2O	8 µL

B

Temperature [°C]	Time	# cycles
95	3 min	1
95	10 s	40
60-64[1]	10 s	40
72	40 s	40
+ melting curve analysis		1

[1] depending on T_m of the respective primer, see ***Table 13***.

2.2.7 PCR and cDNA sequencing

For PCR analysis of the *Gne*-202 transcript in C2C12 cells, a reaction was set up as described in Table 18. PCR products were analysed on a 1 % agarose gel.

For sequencing of PCR products, 360 ng of DNA were mixed with 3 µL 20 µM *Gne*-202 forward primer and sent to Microsynth for sequencing.

Table 18: PCR protocol.

A) Reaction composition and **B)** thermocycler conditions.

A

Component	Amount
2 x Phusion Master Mix	25 µL
forward primer	0.5 µM
reverse primer	0.5 µM
cDNA	1 µL
PCR-grade H2O	21.5 µL

B

Temperature [°C]	Time	# cycles
98	30 s	1
98	10 s	30
65	20 s	30
72	40 s	30
72	10 min	1
4	∞	

2.2.8 N-Glycan branching (PHA-L lectin staining)

100,000 cells were seeded in a 6-well plate and cultivated for 48 h prior to lectin staining. Cells were washed with PBS and detached using 2 x trypsin/EDTA solution for 3 min. Cells were re-suspended in fresh medium and pelleted by centrifugation for 3 min at 500 x g at 4°C. For removal of medium remnants, cells were washed again with PBS. The cell pellets were re-suspended in 100 µL staining solution (20 µg/mL PHA-L in PBS) and incubated for 1 h at 4°C. Excess staining solution was removed by additional three washing steps with PBS before cells were re-suspended in 300 µL PBS for flow cytometry analysis. PHA-L positive cells were detected in the FL-1 channel using the 488 nm excitation laser. Unstained cells served as negative control.

2.2.9 Glycomic analysis of N-glycans

For N-glycan structural analysis, all cells were treated as described previously (Jang-Lee et al., 2006). Briefly, cell pellets (harvested from two 15 cm plates) were subjected to sonication in lysis buffer in the presence of detergent (CHAPS), reduced in 4 M guanidine-HCl, carboxymethylated, and digested with trypsin. The digested glycoproteins were then purified by C18-Sep-Pak (Waters Corp., Hertfordshire, UK). N-glycans were released by peptide N-glycosidase F digestion. Released N-glycans were permethylated using the sodium hydroxide procedure and purified by C18-Sep-Pak. Released N-glycans were incubated in 200 µl of 50 mM sodium acetate (37 °C, pH 5.5). One hundred and seventy milliunits of the enzyme were added to the sample for 24 h. The results shown are representative of two independent cell glycan preparations.

To analyze the structure of released glycans, matrix-assisted laser desorption ionization-time of flight MS (MALDI-TOF MS) and MALDI-TOF/TOF MS/MS (data not shown) were performed. MS and MS/MS data were acquired using a 4800 MALDI-TOF/TOF (Applied Biosystems) mass spectrometer. Permethylated samples were dissolved in 10 µl of methanol, and 1 µl of dissolved sample was premixed with 1 µl of matrix (20 mg/ml 3,4-diaminobenzophenone in 75% (v/v) aqueous MeCN), spotted onto a target plate, and dried under vacuum.

The MS data were processed using Data Explorer 4.9 Software (Applied Biosystems). The processed spectra were subjected to manual assignment and annotation with the aid of a glycobioinformatics tool, GlycoWorkBench. The proposed assignments for the selected peaks were based on ^{12}C isotopic composition together with knowledge of the biosynthetic pathways. The proposed structures were then confirmed by data obtained from MS/MS experiments.

2.2.10 Polar metabolite extraction

Cells were grown in 6-well plates according to the indicated conditions. Cells were washed twice with 2 mL/well of 75 mM ammonium carbonate solution (pH adjusted to 7.3 (±0.1) with acetic acid). After removing the washing solution, the plates were snap-frozen by contact of the underside of the plate with liquid nitrogen and stored at -80 °C until extraction.

Polar metabolites were extracted using a −20 °C cold extraction buffer of 40:40:20 *v*/*v* acetonitrile, methanol, and ultra-pure water. While keeping the plates on ice, each well was incubated for 5 min with 1.4 mL of extraction buffer at 4 °C. Next, the extracts were centrifuged at 13,000 rpm for 3 min at 4 °C to pellet and remove cell debris. Lastly, the samples were dried in a vacuum centrifuge for 5 h at room temperature and stored at −80 °C until analysis.

Analysis of (nucleotide) sugar metabolites by mass spectrometry was provided by Prof. Dr. Dirk Lefeber at the Translational Metabolic Laboratory, Department of Laboratory Medicine at the Radboud University Medical Center in Nijmegen, The Netherlands.

2.2.11 Periodic acid/Schiff's Reaction (PAS) and Alcian blue staining

Cells were differentiated in a 12-well plate, coated with 0.1 % gelatine, for 7 days. Cells were washed twice with pre-warmed PBS and fixed with 4 % PFA for 10 min at room temperature. After washing again with PBS, cells were incubated for 15 min in a filtered alcian blue staining solution (1 % w/v alcian blue in 3 % acetic acid), followed by 5 min incubation with 1 % periodic acid. Then, cells were stained with Schiff's reagent for 15 min, followed by counterstaining with hematoxylin solution for 2 min. All steps were performed at room temperature and cells were rinsed with tap water after each step.

2.2.12 ATP-Glo® Assay

To quantify intracellular ATP levels, the CellTiter-Glo® 2.0 assay from Promega was used according to the manufacturer's instructions. Briefly, 8,000 cells were seeded in a 96-well plate and cultured for either 48 h (myoblasts) or differentiated for 7 days (myotbues). ATP-Glo reagent was added directly into the wells in a 1:1 ratio with culture medium. Cells were lysed for two min on an orbital shaker and incubated for 10 min at room temperature before measuring the luminescence signal in a plate reader (ClarioSTAR).

2.2.13 Resorcinol/Periodate Assay

Total amounts of sialic acids were quantified using the periodate-resorcinol assay. Briefly, cells were washed three times with ice-cold PBS and lysed in 250 µl PBS via freeze–thaw cycles in

liquid nitrogen. All samples and the standard curve were oxidized with 5 µl of 0.4 M periodic acid for >10 min on ice. Then, 500 µl of the following solution were added to each sample and mixed by vortexing: 0.6% resorcinol, 0.25 mM $CuSO_4$, 36% H_20, 44% concentrated HCl. Samples were incubated at 100 °C for exactly 15 min and allowed to cool down to room temperature afterwards, before adding 500 µl of *tert*-butanol. To remove any particular remnants, the samples were briefly centrifuged. OD_{630} was measured in triplicate in a 96-well plate and sialic acid levels were calculated from the standard curve and normalized to the total protein amount of each sample.

2.3 Statistical analysis

Data analyses were performed using OriginPro 2019 software and differences were considered significant when $p < 0.05$. Unpaired student's t-test and one-way ANOVA were used as appropriate. Visualization of graphs was finalized with CorwlDRAW 2021. Figures show the average mean ± standard deviation. Statistical significance was indicated by * $p < 0.05$, ** $p < 0.01$, *** $p < 0.001$.

III Results

1 The impact of Gne-depletion in a C2C12 cell model

1.1 Generation of a Gne knock out (Gne^{KO}) myoblast cell line

Various models have been used in basic research approaches to study the pathophysiological mechanisms of GNE Myopathy and hypo-sialylation. Among others, patient-derived stem cells and biopsies are good models, however, patient material is rare and requires expensive and time-consuming handling. Thus, the well-described murine myoblast cell line C2C12 was chosen as parental cell line for the establishment of a Gne knock out, as it is known for its easy, low-cost handling. Wild type cells were transfected with a pool of three different single-guide RNAs (sgRNAs), targeting different exons in the *Gne* gene (Figure 9 A). Successfully transfected cells were selected with puromycin and diluted to single cell level. Two single cell clones (Cl. 24 and Cl. 26) were selected for this work and all following experiments.

Analysis of *Gne*-202 expression, the dominant *Gne* transcript in C2C12 cells, *via* PCR showed drastically reduced *Gne* expression in clone #24 and a truncated gene product in clone #26 (Figure 9 B). Computational translation of the cDNA sequence of clone #26 into an amino acid sequence is distinct from the wild type sequence, starting at the target site of sgRNA-1 (Figure 9 C). cDNA sequencing of Gne^{KO} clone #24 and clone #26 suggest that clone #26 is a homozygous clone, expressing one single *Gne* transcript, while clone #24 is heterozygous, expressing more than one transcript variant (Figure 9 D).

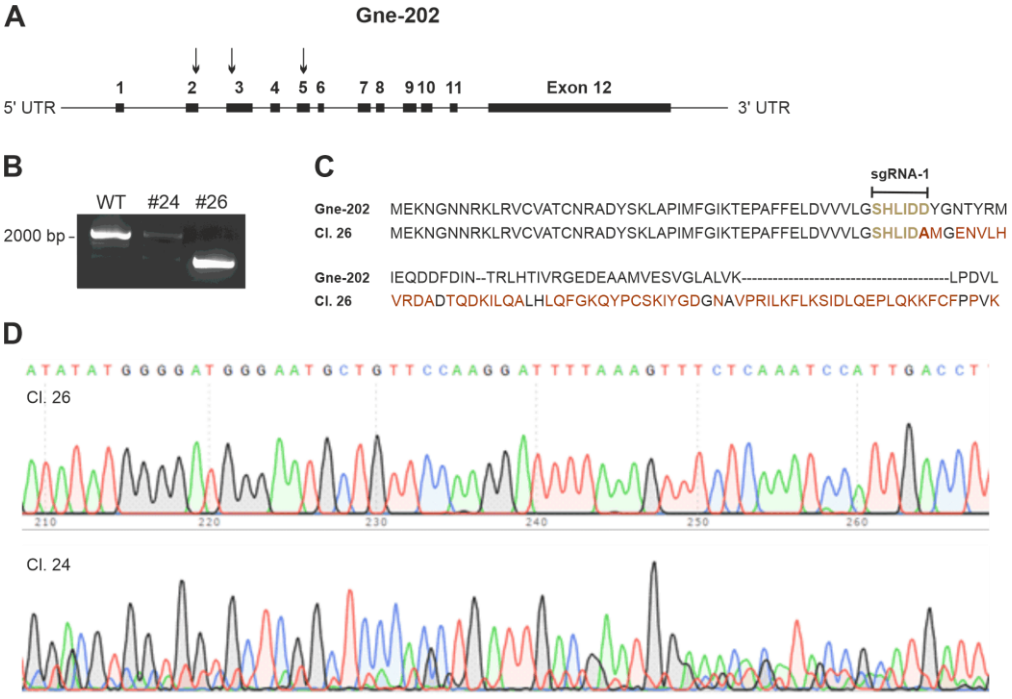

Figure 9: CRISPR/Cas9-mediated knock out of Gne in C2C12 myoblasts.

CRISPR-Cas9 technology was used to induce a DNA double strand brake at the sgRNA target sites in the *Gne* gene. **A)** Gene structure of the *Gne*-202 transcript, which is the dominant transcript, expressed in C2C12 myoblasts. Arrows indicate the binding sites of the three different sgRNAs used for transfection. **B)** PCR from cDNA of C2C12 wild type and Gne^{KO} clones #24 and #26. Wild type cells show the expected product size of 2169 bp while clone #26 shows a truncated gene product. **C)** Amino acid sequence of the translated gene of wild type *Gne*-202 and clone #26. Clone #26 shows alterations starting at the target site of sgRNA-1. **D)** Excerpt of the sequencing results from clone #26 and clone #24. Clone #26 shows a homogenous DNA sequence suggesting a homozygous clone while clone #24 shows an overlay of several sequences pointing towards a heterozygous genotype. UTR: untranslated region. Bp: base pairs. sgRNA: single-guide RNA. WT: wild type. cDNA: copy DNA.

Furthermore, western blot analysis proofed the absence of the Gne protein in clone #24 and #26 (Figure 10 A). Sialic acid detection by western blot is generally not feasible, due to missing antibodies that recognize specific glycan structures. However, one specific form of sialylation can be detected by a monoclonal antibody, recognizing poly sialic acid (polySia). PolySia is found on very few protein substrates, of which the neural cell adhesion molecule 1 (Ncam) is the best studied one. Therefore, polySia and Ncam expression were analysed in C2C12 wild type and Gne^{KO} clones. In accordance to its known role in the sialic acid biosynthesis pathway, there was no polySia signal detectable in the Gne^{KO} clones #24 and #26 (Figure 10 A). Protein expression of Ncam, the major polySia carrier in cells, was analysed as internal control (Figure 10 A). Additionally, expression of the two sialyltransferases that are known to mediate the α-2,8-linkages of poly-sialic acid, were significantly down-regulated on mRNA level in the Gne^{KO} myoblasts (Figure 10 B).

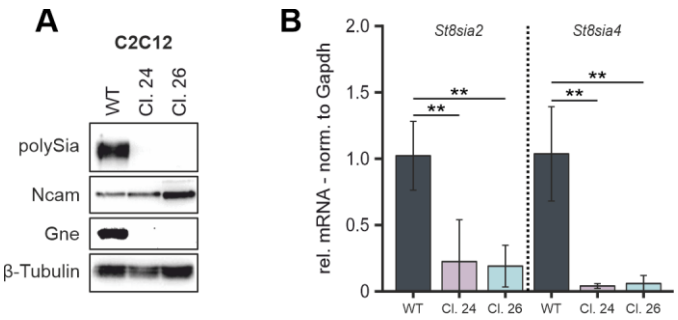

Figure 10: Gne^{KO} validation in C2C12 myoblasts.

A) Western Blot analysis showing the absence of the Gne protein in C2C12 single cell clones #24 and #26. The knock-out of Gne results in the absence of poly sialylation as determined by a specific antibody. **B)** qPCR analysis of polysialyltransferases *St8sia2* and *St8sia4* showing significant down-regulation in clone #24 and clone #26 compared to wild type expression. β-Tubulin and Ncam were used as loading control. polySia: poly sialic acid. Ncam: neural cell adhesion molecule 1. Bar graphs represent the mean of three independent experiments ± standard deviation. Asterisk indicate the *p*-value of the sample compared to the wild type controll. Statistical analysis: One-way ANOVA. * $p < 0.05$, ** $p < 0.01$, *** $p < 0.001$. Figure adapted from (Neu et al., 2024).

1.2 Gne-deficiency influences C2C12 differentiation

C2C12 myoblasts resemble a myoprogenitor or muscle stem cell-like phenotype with the ability to differentiate into mature multi-nucleated myotubes. This process of differentiation can be induced by low serum concentrations in the culture medium and results in migration and fusion of the myoblasts with an increase in myosin heavy chain 1 (Myh) expression, a well described differentiation marker (Figure 11). However, the differentiation process is disrupted in Gne^{KO} clone #24 and clone #26 as there was no fusion and no expression of Myh (Figure 11 A, B). This differentiation-deficient phenotype could partly be rescued by addition of 10 nM insulin to the differentiation medium and by coating the culture dishes with 0.1 % gelatine (Figure 11 C, D, E). Still, Gne^{KO} clones differed from wild type morphology. Clone #24 formed extremely large myotubes with cell debris floating on top of the cells. Furthermore, Myh localized into clumped structures rather than the filamentous structures observed in wild type cells (Figure 11 D). Morphology of clone #26 resembled more the wild type myotubes but with significantly reduced expression of Myh (Figure 11 C, D, E).

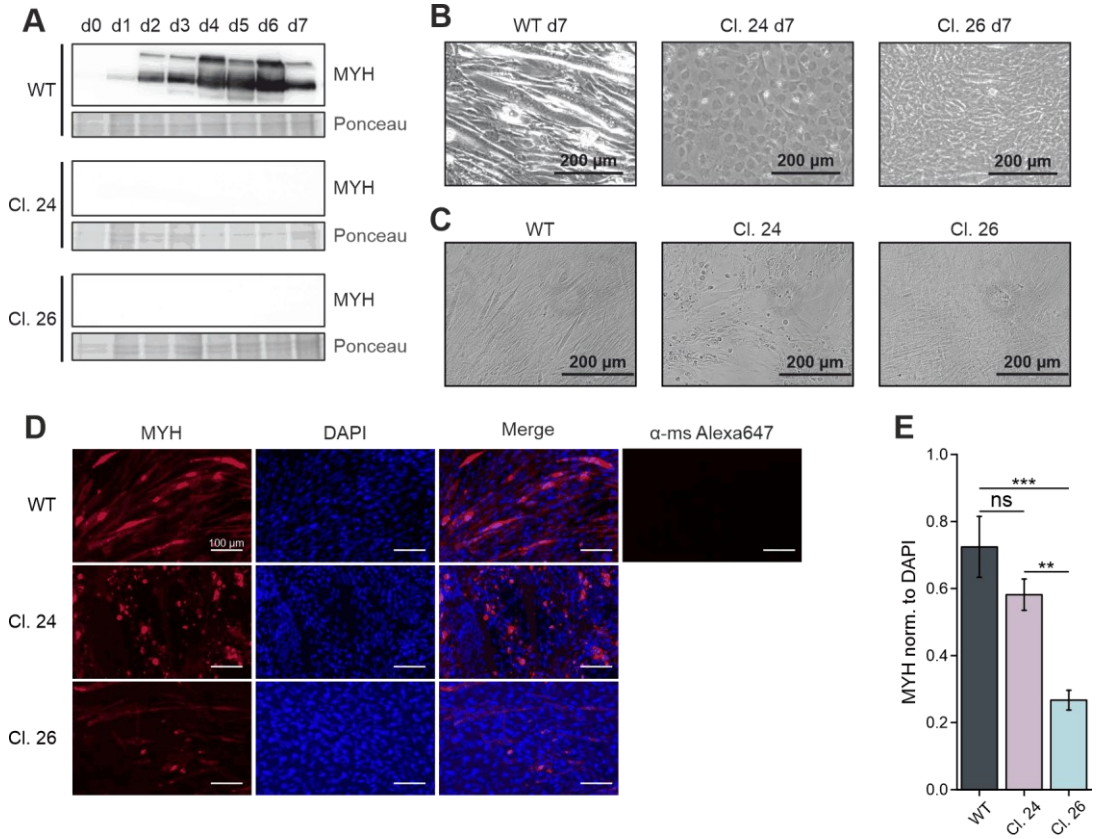

Figure 11: Differerntiation phenotype in C2C12 wild type and Gne^{KO} cells.

Myoblastst were seeded and grown to ~90 % confluence. Growth medium (GM) was changed to differentiation medium (DM) on day zero (d0) and refreshed every other day. Cells were harvested and subjected to cell lysis at each day indicated. **A)** Western blot analyis of Myh expression during the seven day time course of the differentiation protocoll. **B)** Micrographs of differentiated C2C12 wild type and Gne^{KO} clone #24 and clone #26 **C)** Micrographs of differentiated C2C12 wild type and Gne^{KO} cells clone #24 and clone #26 on 0.1 % gelatine-coated plates and DM containing 10 nM insulin. **D)** Immunofluorescent staining of Myh on d7 of differentiation in C2C12 WT and Gne^{KO} clones. **E)** Quantification of the Myh signal norm. to DAPI. Myh: myosin heavy chain I. d: day. α-ms Alexa647: negative controll, secondary antibody only. Micrographs and immunofluorescent staings show representative pictures. Scale Bar in **B)** and **C)** 200 µm, in **D)** 100 µm. Bar graph in **E)** shows the mean of three independent micrographs ± standard deviation. Asterisks indicate the *p*-value of the sample compared to the wild type controll. Statistical analysis: One-way ANOVA. ns = non significant, * $p < 0.05$, ** $p < 0.01$, *** $p < 0.001$. Figure adapted from (Neu *et al.*, 2024).

1.3 Structural Analysis of N-Glycans in C2C12 WT and GneKO Myoblasts

The glycome of a cell comprises the entity of all glycan structures, protein and lipid-bound glycans, as well as free, intracellular glycans. Gne is known to be the key enzyme in the sialic acid biosynthesis pathway, supplying the cell with sialic acids for the incorporation into glycan structures. It was already shown that Gne^{KO} clones have a lack of poly sialic acid (Figure 10 A), but how sialylation in general is influenced has not been analysed. Thus, the next step was to determine whether missing sialic acids have an influence on the overall glycan structures of muscle-derived cells. Along with that, the question arose on how much sialylation is derived from the intrinsic biosynthetic pathway, compared to the salvage pathway.

For that, N-glycan structures were analysed in the C2C12 wild type and Gne^{KO} clone #24 myoblasts by MALDI/TOF-TOF mass spectrometry. As seen in Figure 12, terminal sialic acids were mainly replaced by additional galactose residues, resulting in an increase of galactose-α-1,3-galactose epitopes in clone #24. The overall sialoglycan content is decreased by about 46 %. The high-intensity sialoglycan peaks with the mass to charge (m/z) ratio of 3602 and 3964 were probably serum-derived glycans from the fetal bovine serum that was used in the cell culture medium.

Generally, both cell lines contained high mannose glycans, some bisected glycans and complex N-glycans (Figure 12). Higher mass glycans also contained chains of repeating units of galactose and *N*-acetylglucosamine (polyLacNAcs). Analysis of high-mass glycans revealed a high degree of branching in form of branched LacNAcs, referred to as I-branches. I-branched glycans are the result of the linkage of *N*-acetylglucosamine to galactose residues on polyLacNAc structures, mediated by β1,6-*N*-acetylglucosaminyltransferase (GCNT2). Remodelling of the N-glycan core structures was not observed.

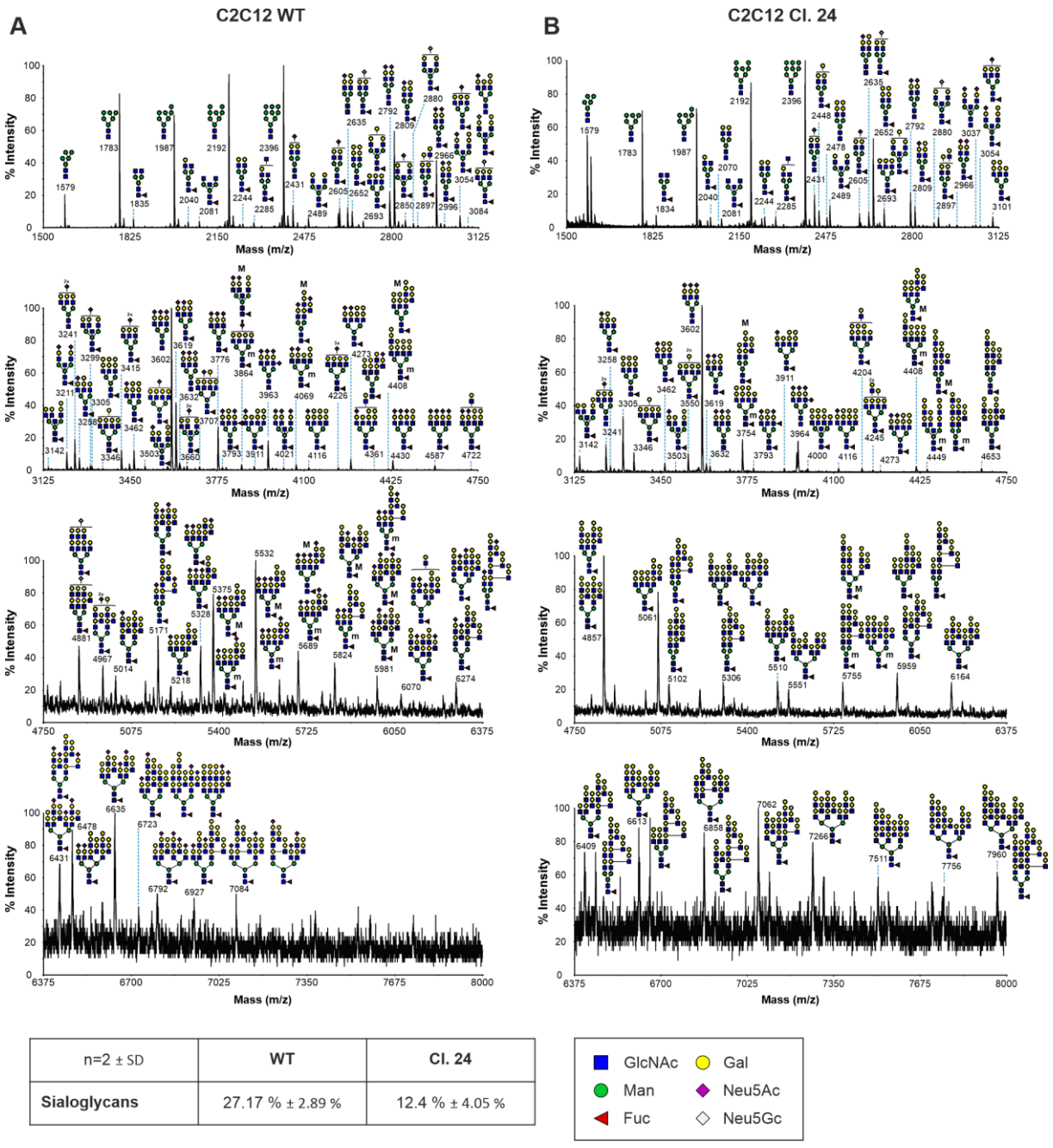

n=2 ± SD	WT	Cl. 24
Sialoglycans	27.17 % ± 2.89 %	12.4 % ± 4.05 %

Figure 12: N-Glycan analysis of C2C12 WT and Gne^{KO} clone #24 myoblasts.

MALDI-TOF-TOF MS spectra of N-glycans obtained from panel **A)** C2C12 wild type myoblasts and panel **B)** Gne^{KO} clone #24. Putative cartoon structures assigned were based on composition, tandem mass spectrometry, the literature and knowledge of N-glycan biosynthetic pathways. All spectra were graphed as % relative intensity. All molecular ions are $[M+Na]^+$. Experiments were repeated on two biological replicates and the spectra shown are representative. Isotopic glycan structures with "M" and "m" indicating major (M) and minor (m) abundancies, respectively. Quantification of sialoglycans in two independent experiments indicate that 27.17 ± 2.89 % of the detected N-glycans are sialylated in wild type cells, while there are 12.4 ± 4,05 % sialoglycans in Gne^{KO} cells. GlcNAc: *N*-acetylglucosamine, Man: Mannose, Fuc: Fucose, Gal: Galactose, Neu5Ac: *N*-acetylneuraminic acid, Neu5Gc: *N*-glycolylneuraminic acid.

1.4 Metabolic fate of UDP-*N*-acetylglucosamine in C2C12 Gne^{KO} clones

Uridine diphosphate *N*-acetylglucosamine (UDP-GlcNAc) is not only the substrate for the sialic acid biosynthesis pathway but is also one of the fundamental building blocks of different glycan structures (Figure 13 A). UDP-GlcNAc can be used for N-glycan branching, glycosaminoglycan synthesis, for cytoplasmic and nuclear *O*-GlcNAcylation, and is also found in O-glycans. In the Gne^{KO} clones, UDP-GlcNAc cannot be used for sialic acid biosynthesis and thus has to follow another route. To decipher the metabolic fate of UDP-GlcNAc, several approaches were used. First, for the analysis of N-Glycan branching, the lectin phytohaemagglutinin-L (PHA-L), which recognizes β1,6-branched N-glycans, was used to evaluate its binding. There was a strong increase in binding observed in Gne^{KO} myoblasts compared to the wild type cells *via* flow cytometry analysis (Figure 13 B).

Additionally, UDP-GlcNAc can be used by the O-GlcNAc transferase (OST) to transfer a single *N*-acetylglucosamine (GlcNAc) to the hydroxyl group of a serine or threonine side chain *via* a β-glycosidic bond on intracellular proteins. This modification can be analysed by a monoclonal antibody (CTD110.6, Figure 13 A) using western blot analysis. There was no significant increase in *O*-GlcNAcylation observed in the Gne^{KO} clones compared to wild type cells in the myoblast state (Figure 13 C). However, *O*-GlcNAcylation was more prominent, even though not significant, in the differentiated Gne^{KO} clones compared to wild type myotubes (Figure 13 D).

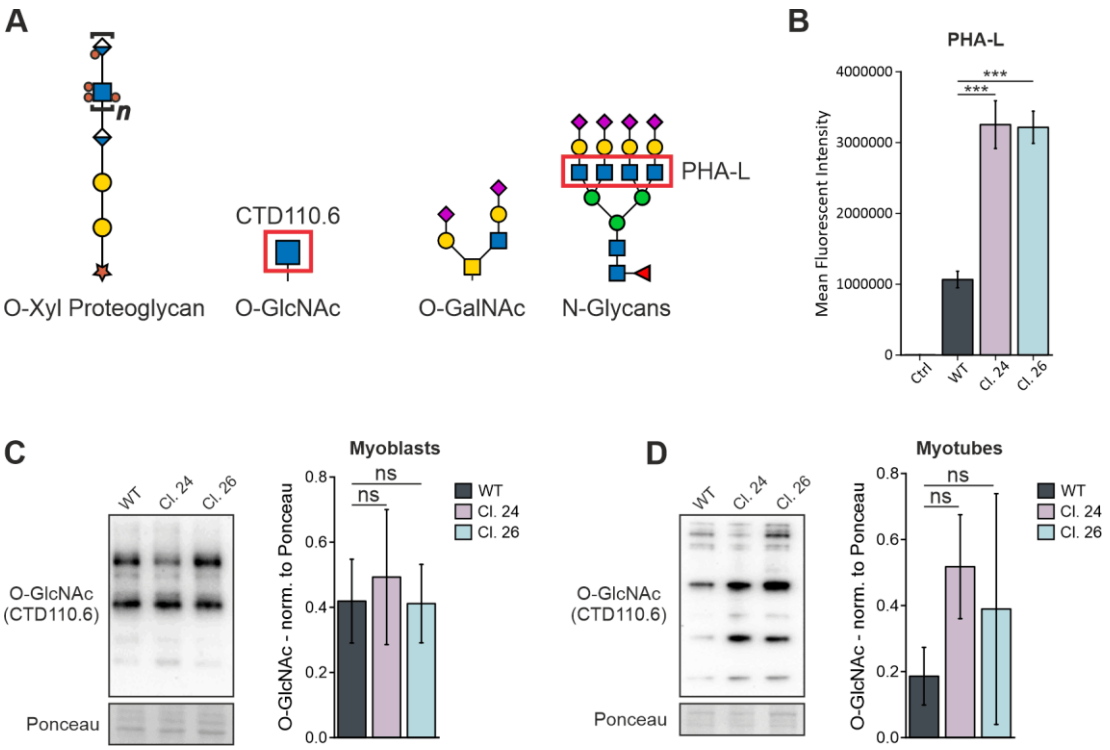

Figure 13: Analysis of N-glycan branching and *O*-GlcNacylation in C2C12 wild type and Gne^{KO} cells.

A) Schematic illustration of the most common glycan structures that feature GlcNAc in their structures. *O*-Xyl Proteoglycans are found in the extracellular matrix with extensive sulfated GlcNAc-GlcA repeats. *O*-GlcNAc is found in the cytoplasm and nucleoplasm of cells and is constituted of a single GlcNAc residue linked to a Ser/Thr in the protein sequence. *O*-GalNAc is a prominent example for mucin-type O-glycans that may also include GlcNAc. N-Glycans are always build on two initial GlcNAc residues. Additional GlcNAc will lead to N-glycan branching or extension of poly LacNAc/LacdiNAc structures. **B)** Binding of PHA-L lectin on C2C12 wild type and Gne^{KO} myoblasts analysed by flow cytometry. Ctrl = non-stained control cells. **C)** Western Blot analysis of *O*-GlcNAcylation in C2C12 myoblasts and **D)** in myotubes. GlcNAc: *N*-acetylglucosamine, GalNAc: *N*-acetylgalactosamine, PHA-L: phytohaemagglutinin-L. LacNAc: Galβ1-4GlcNAc, LacdiNAc: GalNAcβ1-4GlcNAc. Bar graphs show the mean of three independent experiments ± standard deviation. Asterisks indicate the *p*-value of the sample compared to the wild type controll. Statistical analysis: One-way ANOVA. ns = non significant, * $p < 0.05$, ** $p < 0.01$, *** $p < 0.001$

The third potential fate of UDP-GlcNAc is incorporation into proteoglycan/glycosaminoglycan structures, which are found in the extracellular matrix and on the cell surface. Proteoglycan expression was visualized by alcian blue staining of sulphated glycosaminoglycans and acidic mucins (O-glycans), in combination with a periodic acid – Schiff's reaction (PAS) which counterstains carbohydrates, glycoproteins, and glycolipids in the cells. Clone #24 shows a distinct staining pattern compared to wild type and clone #26 with less abundant PAS positive structures (Figure 14, coloured in purple). On the other side, alcian blue-positive structures are most prominent in clone #24 and to a lesser degree in clone #26 (Figure 14, white arrows). Furthermore, clone #24 forms abnormally large myotubes, which has been observed before (Figure 11). The phenotype described for Gne^{KO} clone #24 is less pronounced in clone #26,

which exhibits structures resembling more the wild type cells, but with less intense PAS staining and slightly increase alcian blue staining.

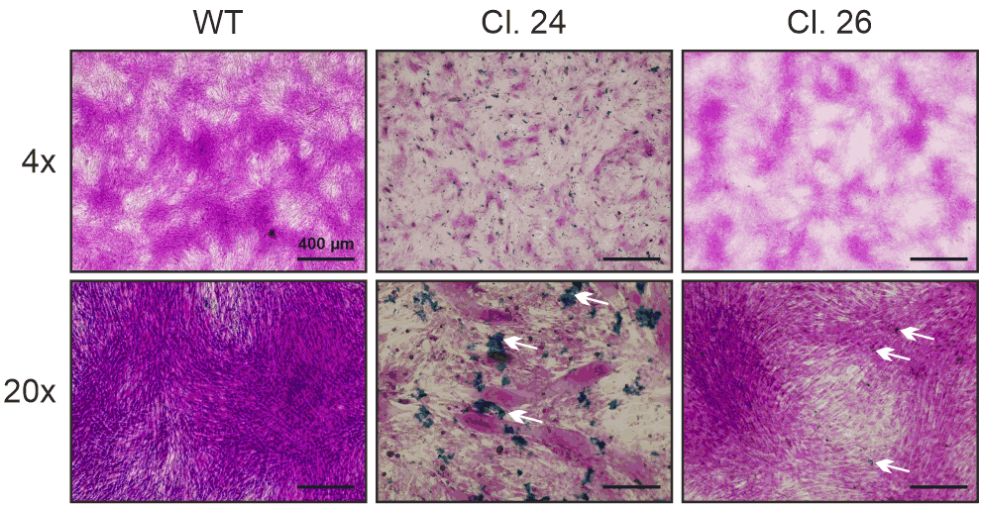

Figure 14: PAS staining in differentiated C2C12 cells.

Differentiated C2C12 wild type and Gne^{KO} cells, grown on 0.1 % gelatine-coated dishes and DM containing 10 nM insulin were fixed with 4 % paraformaldehyde and subjected to alcian blue/PAS staining. Alcian blue stains acidic mucins and sulphated glycosaminoglycans (blue/cyan) and periodic acid/Schiff's reagent stain carbohydrates, glycoproteins, and glycolipids (purple). White arrows indicate alcian blue-positive aggregates in the extracellular matrix of Gne^{KO} clone #24 and clone #26. Pictures are representative of three independent experiments. DM = differentiation medium. Upper panel: 4x magnification. Lower panel: 20x magnification. Scale Bar = 400 µm.

In conclusion, while there is no increase in *O*-GlcNAcylation observed in C2C12 Gne^{KO} myoblasts, enhanced reactivity of PHA-L indicates that UDP-GlcNAc is used preferentially for N-glycan branching. Differentiated Gne^{KO} cells however, show an increase in *O*-GlcNAcylation and additionally also in alcian blue staining, hinting towards a remodelling of the extracellular matrix and altered intracellular signalling.

2 Rescue of sialylation in Gne^{KO} cells

2.1 Disrupted sialylation can be rescued by *N*-acetylmannosamine in a HEK-293 GNE-knock out model

Cells can use exogenously applied *N*-acetylneuraminic acid (Neu5Ac) precursors or metabolites, such as *N*-acetylmannosamine (ManNAc) or derivatives, in their intrinsic glycosylation pathway. This knowledge is widely exploited for glycoengineering efforts, aiming at therapeutic and diagnostic strategies (Agatemor *et al.*, 2019). Until today, there is no therapy for GNEM patients, despite insistent approaches to enhance sialylation in patients *via* oral ManNAc or Neu5Ac administration (Lochmuller *et al.*, 2019). As a proof of principle, HEK-293 wild type and GNE^{KO} cells were supplemented with either 0.5 mM or 5 mM ManNAc for 24 h. The cells were subsequently analysed for their poly sialylation (polySia) levels. While 0.5 mM ManNAc had no effect, 5 mM ManNAc efficiently restored the polySia signal to wild type levels (Figure 15 A). It is not exactly known how ManNAc is phosphorylated in the absence of the GNE kinase domain. Noteworthy, another enzyme, *N*-acetylglucosamine kinase (NAGK), was shown to phosphorylate exogenous ManNAc and was thus supposed to substitute GNE kinase activity in case of GNE-deficiency (Gorenflos Lopez et al., 2023). In line with that hypothesis, NAGK expression was analysed in HEK-293 GNE^{KO} cells, and found to be upregulated compared to wild type cells (Figure 15 B).

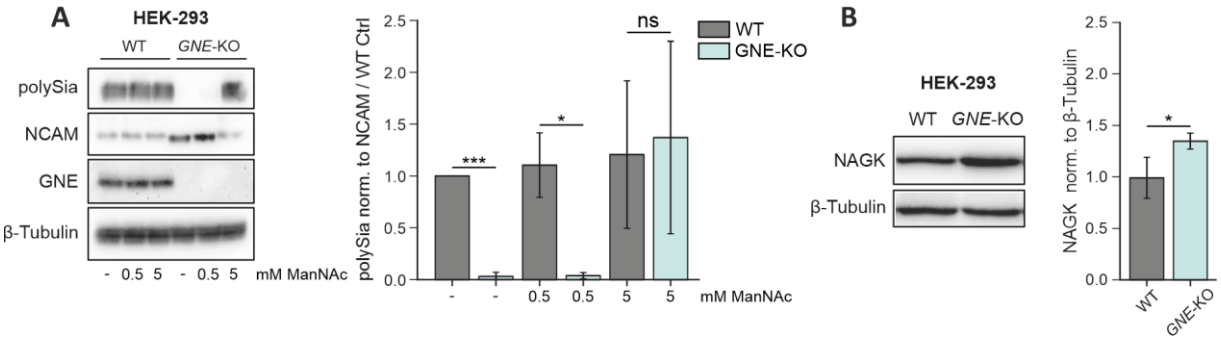

Figure 15: Supplementation of HEK-293 GNE-knock out cells with *N*-acetylmannosamine.

A) Representative western blot showing the expression of polySia, its carrier protein NCAM, GNE, and β-tubulin in HEK-293 wild type and GNE-knock out cells in relation to supplementation with different concentrations of ManNAc. **B)** Representative western blot showing the expression of GlcNAc kinase (NAGK) and β-tubulin in HEK-293 wild type and GNE-knock out cells. β-tubulin is used as a loading control in **A** and **B**. ManNAc: *N*-acetylmannosamine. Bar graphs show the mean of three independent experiments ± standard deviation. Asterisks indicate the p-value of the sample compared to the wild type controll. Statistical analysis: A) One-way ANOVA. B) Unpaired t-test. ns = non significant, * $p < 0.05$, ** $p < 0.01$, *** $p < 0.001$. Figure adapted from (Neu *et al.*, 2024)

2.2 *N*-acetylmannosamine and *N*-acetylneuraminic acid supplementation does not restore poly sialylation in C2C12 Gne^{KO} cells

HEK-293 cells are a well characterized cell line, often used for basic biochemical research. However, HEK-293 GNE^{KO} cells are not suitable to investigate the pathomechanism of GNE myopathy, as the cells do not have the skeletal muscle background. Thus, to evaluate the potential benefit of ManNAc supplementation on muscle cells, the above-mentioned experiments were repeated in the C2C12 Gne^{KO} model.

In contrast to the results from the HEK-293 GNE^{KO} model, C2C12 Gne^{KO} myoblasts cultured in the presence with 0.5 mM and 5 mM ManNAc, respectively, impaired poly sialylation could not be rescued (Figure 16 A). Considering that ManNAc is an early metabolite of the sialic acid pathway, still requiring many downstream enzymes, direct administration of Neu5Ac in the same concentrations (0.5 mM and 5 mM) was tested (Figure 16 B). Like the ManNAc treatment, Neu5Ac failed to rescue poly sialylation in C2C12 Gne^{KO} myoblasts after 24h (Figure 16 B). The supplementation experiments were repeated in terminal differentiated C2C12 wild type and Gne^{KO} cells with the same outcome as in the myoblasts, showing no detectable polySia signal in the western blot analysis (Figure 16 C, D).

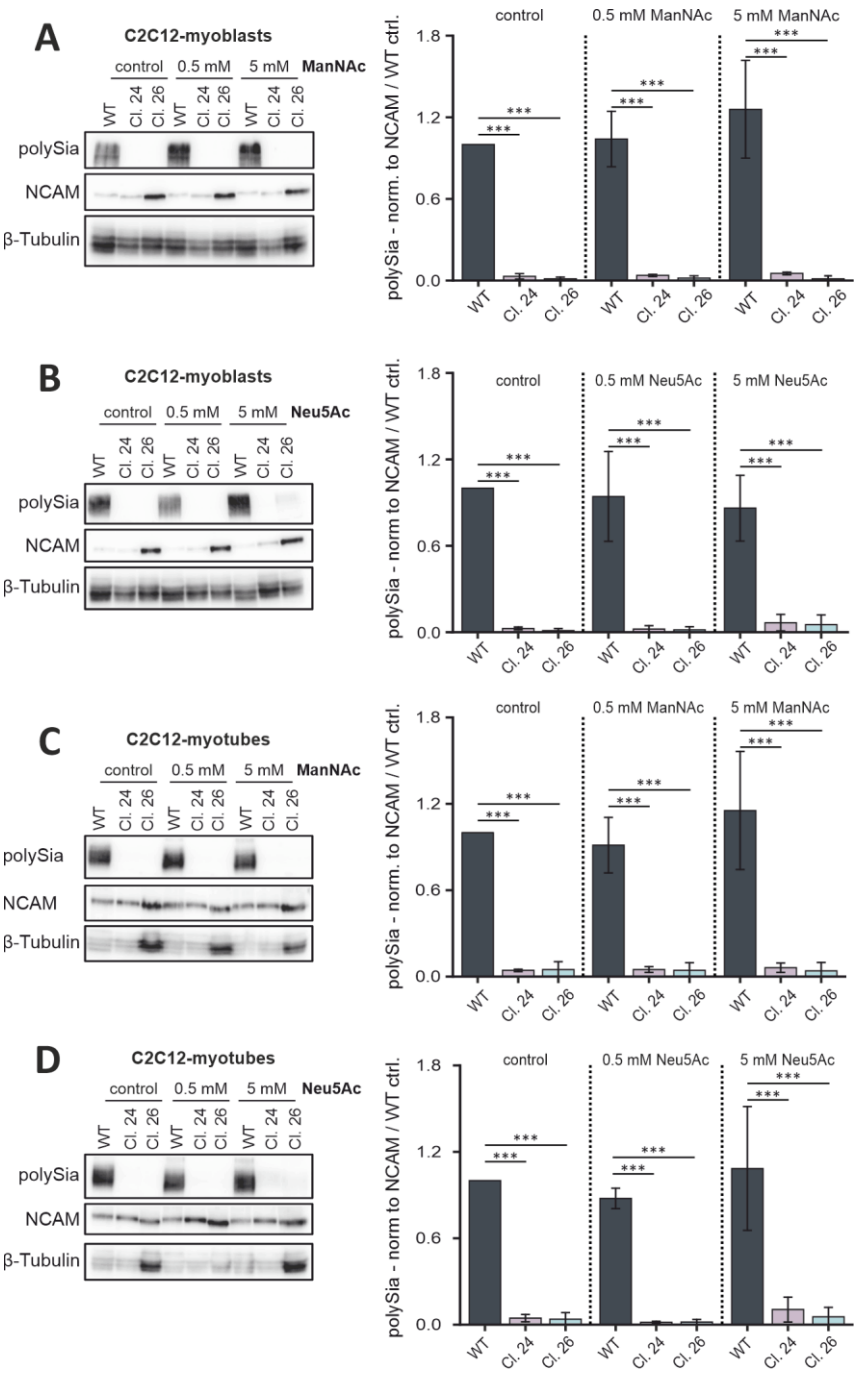

Figure 16: Supplementation of C2C12 cells with ManNAc and Neu5Ac for 24 h.

A) Representative western blots showing the expression of polySia, Ncam, and β-tubulin after 24 h treatment of C2C12 myoblasts with different concentrations of ManNAc. **B)** Representative western blots showing the expression of polySia, Ncam, and β-tubulin after 24 h treatment of C2C12 myoblasts with different concentrations of Neu5Ac. **C)** Representative western blots showing the expression of polySia, Ncam, and β-tubulin after 24 h treatment of C2C12 myotubes with different concentrations of ManNAc. **D)** Representative western blots showing the expression of polySia, Ncam, and β-tubulin after 24 h treatment of C2C12 myotubes with different concentrations of Neu5Ac. The bar graphs next to the western blots in each subpanel show the polySia level normalized to the Ncam level in the C2C12 wild type control. ManNAc: *N*-acetylmannosamine, Neu5Ac: *N*-acetylneuraminic acid. Bar graphs show the mean of three independent experiments ± standard deviation. Asterisks indicate the *p*-value of the sample compared to the indicated controll. Statistical analysis: One-way ANOVA. ns = non significant, * $p < 0.05$, ** $p < 0.01$, *** $p < 0.001$. Figure adapted from (Neu *et al.*, 2024).

2.3 Validation of supplementation studies in an independent Sol8 cell line

To exclude any cell line-specific effects, another myoblast cell line, Sol8, was used as additional control. Sol8 wild type myoblasts and a Gne^{KO} clone were treated with either 0.5 mM or 5 mM ManNAc or Neu5Ac for 24 h, respectively. Poly sialylation was not affected by the treatment in Sol8 Gne^{KO} cells, in accordance with what was observed in C2C12 Gne^{KO} cells (Figure 17 A, B). As an additional internal control, protein lysates were subjected to endoneuraminidase-N (EndoN) digestion, an enzyme that specifically degrades α-2,8-linked sialic acids polymers with a minimal length of 7-9 residues (Figure 17 A).

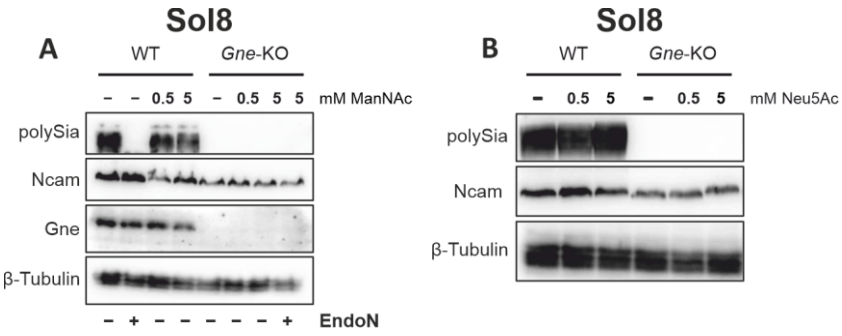

Figure 17: *N*-acetylmannosamine and *N*-acetylneuraminic acid supplementation in Sol8 wild type and Gne^{KO} cells.

A) Sol8 myoblasts were supllemented with 0.5 mM and 5 mM ManNAc for 24 h, respectively. Western blot analysis of polySia, Ncam, Gne, and β-tubulin in Sol8 wild type (WT) and Gne^{KO} cells. **B)** Sol8 myoblasts were supllemented with 0.5 mM and 5 mM Neu5Ac for 24 h, respectively. Western blot analysis of polySia, Ncam, Gne, and β-tubulin in Sol8 wild type (WT) and Gne^{KO} cells. Western blots are representative for three independent experiments. β-tubulin was used as loading controll. EndoN: endoneuraminidase-N. ManNAc: *N*-acetylmannosamine, Neu5Ac: *N*-acetylneuraminic acid. Figure adapted from (Neu *et al.*, 2024).

2.4 *N*-acetylmannosamine supplementation does not increase sialylation in C2C12 Gne^{KO} cells

Since poly sialylation is only one specific form of sialylation and not representative of the sialic acid status of a cell, quantification of all free and glycan bound sialic acids was performed by using the periodate/resorcinol colorimetric assay. Similar to what was observed in the structural analysis of the N-glycans, overall sialic acid content in Gne^{KO} clone #24 and clone #26 was reduced by about 65 % compared to wild type myoblasts and by about 75 % compared to wild type myotubes (Figure 18 A, B). However, ManNAc was not able to enhance the sialic acid content in any of the tested conditions, ± 5 mM ManNAc for 24 h in myoblasts and myotubes, respectively (Figure 18 A, B). Noteworthy, the amount of sialic acid per µg protein was higher in C2C12 wild type myotubes than in the undifferentiated myoblast cells (Figure 18 C).

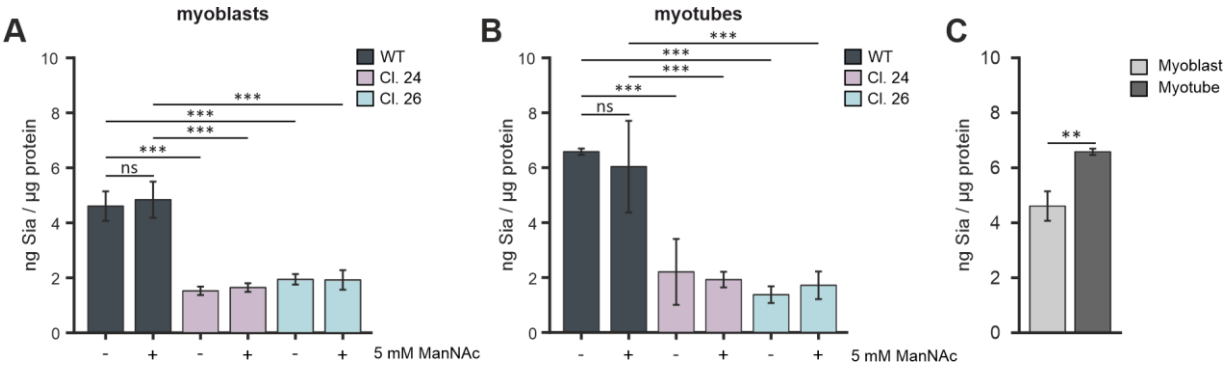

Figure 18: Sialic acid quantification via resorcinol assay.

A) Colorimetric quantification of free and bound sialic acid in C2C12 wild type and Gne^{KO} myoblasts. Where indicated, growth medium has been supplemented with 5 mM ManNAc for 24 h. **B)** Colorimetric quantification of free and bound sialic acid in C2C12 wild type and Gne^{KO} differentiated cells. Where indicated, differentiation medium has been supplemented with 5 mM ManNAc for 24 h. **C)** Comparison of sialic acid content in C2C12 wild type myoblasts and myotubes. ManNAc: *N*-acetylmannosamine. Bar graphs show the mean of three independent experiments ± standard deviation. Asterisks indicate the *p*-value of the sample compared to the wild type controll condition. Statistical analysis: **A)** and **B)** One-way ANOVA. **C)** Unpaired t-test. ns = non-significant, * $p < 0.05$, ** $p < 0.01$, *** $p < 0.001$. Figure adapted from (Neu *et al.*, 2024).

2.5 Prolonged *N*-acetylmannosamine and *N*-acetylneuraminic acid supplementation in C2C12 Gne^{KO} cells

So far, the duration of the ManNAc and Neu5Ac treatments was limited to 24 h, which may not be enough time for the effective metabolic turnover in muscle cells. Consequently, experiments were repeated with a prolonged incubation time. For that, 5 mM ManNAc and 5 mM Neu5Ac, respectively, were added to the differentiation medium and refreshed every 48 h for the duration of the differentiation protocol for seven days. ManNAc supplementation had no effect on cell morphology (Figure 19 A), poly sialylation (Figure 19 B, D), Myh expression (Figure 19 B, C), nor intracellular sialic acid concentration (Figure 19 E). Neu5Ac supplementation on the other hand had a negative effect on myotube formation in wild type cells as analysed by cell morphology and Myh protein expression (Figure 19 A, B, C). Poly sialylation tended to be increased in wild type and Gne^{KO} clones, however without statistical significance (Figure 19 B, D). Furthermore, clone #26 showed rescue of Myh expression upon Neu5Ac treatment, which did not account for clone #24 (Figure 19 B, C). Extensive Neu5Ac supplementation was able to rescue the sialic acid content in the Gne^{KO} clones (Figure 19 E). Additionally, Gne protein expression in C2C12 wild type cells also tended to be stronger in Neu5Ac treated cells compared to the control cells (Figure 19 B, F). Note that those experiments were carried out without the addition of insulin in the differentiation medium and on non-coated cell culture dishes.

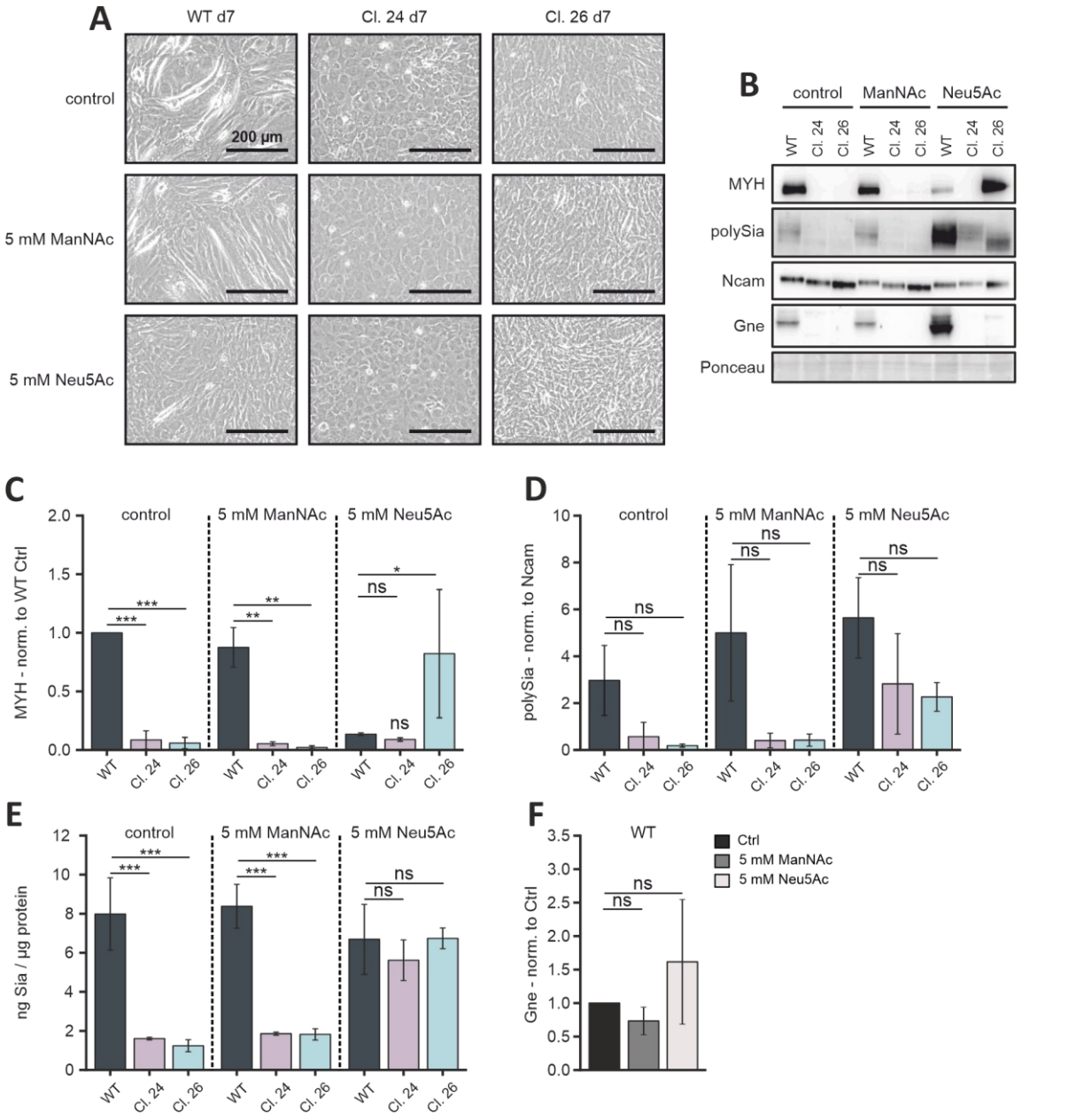

Figure 19: Long-term ManNAc and Neu5Ac treatment of C2C12 wild type and Gne^{KO} cells.

C2C12 wild type and Gne^{KO} cells were grown in differentiation medium (DM) on non-coated dishes and without insulin for seven days. Where indicated, DM was supplemented with either 5 mM ManNAc or 5 mM Neu5Ac, respectively, for the whole duration of the differentiation process. **A)** Micrographs showing cell morphology after seven days of differentiation under controll (upper panel), 5 mM ManNAc (middle panel), and 5 mM Neu5Ac (lower panel) supplementation, respectively. **B)** Western Blots showing Myh, polySia, Ncam, and Gne expression after seven days of differentiation. **C)** Myh protein expression under indicated treatments. **D)** polySia expression under indicated treatments. **E)** Resorcinol/Periodate assay for quantification of sialic acids after seven days of differentiation. **F)** Gne protein expression in C2C12 wild type cells after seven days of differentiation and respective treatments. Myh: myosin heavy chain I, polySia: poly sialic acid, Ncam: neural cell adhesion molecule 1, ManNAc: *N*-acetylmannosamine, Neu5Ac, *N*-acetylneuraminic acid. Bar graphs show the mean of three independent expeiments ± standard deviation. Asterisks indicate the *p*-value of the sample compared to the respective condition. Statistical analysis: One-way ANOVA. ns = non-significant, * $p < 0.05$, ** $p < 0.01$, *** $p < 0.001$. Scale bar in **A)** = 200 µm. Figure adapted from (Neu *et al.*, 2024).

2.6 Metabolomic analysis of *N*-acetylneuraminic acid metabolites in C2C12 wild type and Gne^{KO} cells

Western Blot analysis of poly sialylation and periodate/resorcinol assay are rather coarse methods for the detection of sialic acids. Considering the fact that ManNAc is not metabolized into Neu5Ac in C2C12 Gne^{KO} cells, a more detailed analysis of three of the metabolites of the sialic acid pathway (*N*-acetylmannosamine-6-phosphate, *N*-acetylneuraminic acid, and cytidine-5'-monophospho-*N*-acetylneuraminic acid) were quantified by mass spectrometry. Figure 20 D gives an overview of the metabolic pathway starting with UDP-GlcNAc as a substrate for the Gne enzyme. *N*-acetylmannosamine-6-phosphate (ManNAc-6P) is the product of Gne and is further turned into Neu5Ac-9-phosphate (Neu5Ac-9P) with subsequent de-phosphorylation into Neu5Ac. Prior to the entry of Neu5Ac into the Golgi apparatus, Neu5Ac has to be activated into CMP-Neu5Ac, which happens in the nucleus of cells.

As quantified by the normalized peak area, ManANc-6P is less abundant in differentiated C2C12 wild type myotubes than in myoblasts (Figure 20 A). However, while there is no increase in ManNAc-6P after additional ManNAc supplementation in the myoblasts, myotubes respond to the supplementation. Addition of Neu5Ac to the growth medium of wild type cells affects ManNAc-6P levels negatively by depleting the intracellular pool. ManNAc-6P levels were generally low in C2C12 Gne^{KO} cells, myoblasts as well as in differentiated cells (Figure 20 A). In contrast to wild type cells, Gne^{KO} clones responded to the ManNAc supplementation in an undifferentiated as well as differentiated state, however to a very low degree. While previous experiments did not show any significant increase in sialylation after 24 h Neu5Ac treatment, intracellular Neu5Ac levels increased in Gne^{KO} clones #24 and #26 to wild type levels (Figure 20 B). Wild type cells responded to the Neu5Ac treatment by a ~30-fold increase in Neu5Ac levels. ManNAc on the other side did not show any effect on Neu5Ac levels in the Gne^{KO} clones, neither in the myoblasts nor in the differentiated cells. Noteworthy, in the differentiated wild type cells, Neu5Ac levels were about 20 times higher in the ManNAc treated samples and in the myoblasts about 10 times higher, compared to the untreated cells (Figure 20 B). However, Neu5Ac treatment did not increase CMP-Neu5Ac in wild type cells, but to a certain degree (almost reaching untreated-wild type levels) in the Gne^{KO} clones (Figure 20 C). ManNAc supplementation exclusively had an effect on differentiated wild type cells, increasing the activated CMP-Neu5Ac amounts by about 3-fold (Figure 20 C).

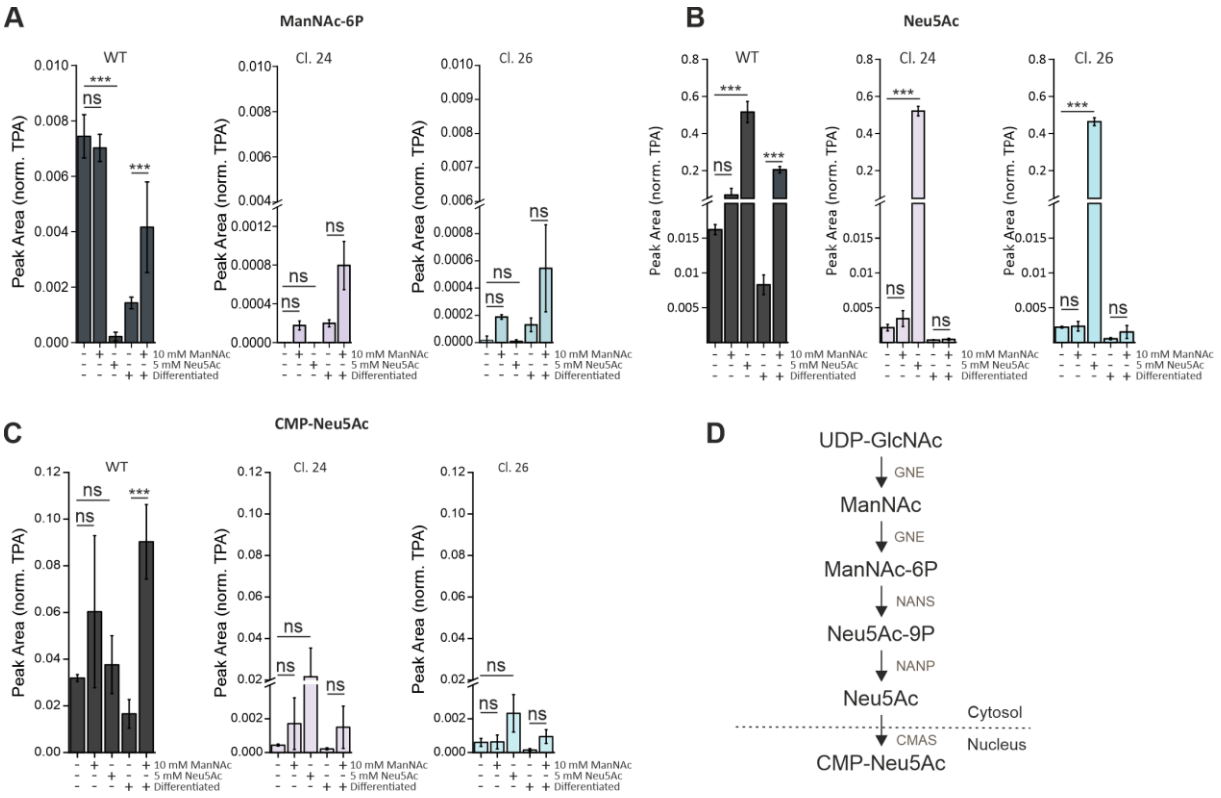

Figure 20: Metabolomic analysis of intermediate Neu5Ac metabolites.

C2C12 wild type (WT) and Gne^{KO} clones #24 and #26 were subjected to metabolite extraction and quantification of intracellular levels of **A)** *N*-Acetylmannosamine-6-Phosphate (ManNAc-6P), **B)** *N*-acetlyneuraminic acid (Neu5Ac), and **C)** Cytidin-5'-Monophospho-*N*-acetylneuraminic acid (CMP-Neu5AC) were analysed by mass spectrometry. **D)** Overview of the biosynthetic pathway of Neu5Ac starting with UDP-GlcNAc and its activation into CMP-Neu5Ac. TPA = total peak area, UDP-GlcNAc = uridine diphosphate *N*-acetylglucosamine, GNE = UDP-*N*-acetylglucosamine 2-epimerase/*N*-acetylmannosamine kinase, NANS = sialic acid synthase, NANP = *N*-acylneuraminate-9-phosphatase, CMAS = *N*-acylneuraminate cytidylyltransferase. Bar graphs show the mean of three independent experiments ± standard deviation. Statistical analysis: One-way ANOVA. ns = non-significant $p > 0.05$, * $p < 0.05$, ** $p < 0.01$, *** $p < 0.001$.

3 Analysis of muscle-specific gene signature in Gne^{KO} muscle cells

3.1 Computational analysis of gene expression in Sol8 wild type and Gne^{KO} cells

Congenital myopathies are a heterogeneous group of muscle disease with > 450 known causative genes (Benarroch et al., 2024a; Dowling et al., 2021). Many of those genes can be categorized into subgroups of the cellular process or the cellular structure they affect. Prominent examples are genes that are associated with the dystrophin glycoprotein complex (DGC) or the sarcomere filaments. How mutations in the Gne gene, which is not a skeletal muscle specific gene, leads to muscle atrophy is not understood so far. For a better understanding of the complex interplay of muscle-specific genes and genes associated with congenital myopathies, a public available RNAseq data set of Sol8 wild type and Sol8 Gne^{KO} cells was analysed with focus of a subset of muscle disease-associated genes (Ilouz et al., 2022). The expression of manually selected genes are depicted in Figure 21 in form of a heatmap. By looking at the expression

data, four columns can be distinguished, representing the wild type myoblasts, differentiated wild type, Gne^{KO} myoblasts, and Gne^{KO} differentiated cells, respectively. The differentiated wild type cells show the strongest expression of muscle-specific genes in accordance with their myotube-phenotype. Gne^{KO} cells on the other side show a lack of differentiation and generally low expression of important muscle genes. Genes of special interest are highlighted in red and were selected due to their strong down-regulation compared to the differentiated wild type cells. Among those are the muscle-specific glycogen phosphorylase (*Pygm*), sodium channel protein type 4 subunit α (*Scn4a*), ryanodine receptor 1 (*Ryr1*), and voltage-dependent L-type calcium channel subunit α-1S (*Cacna1s*).

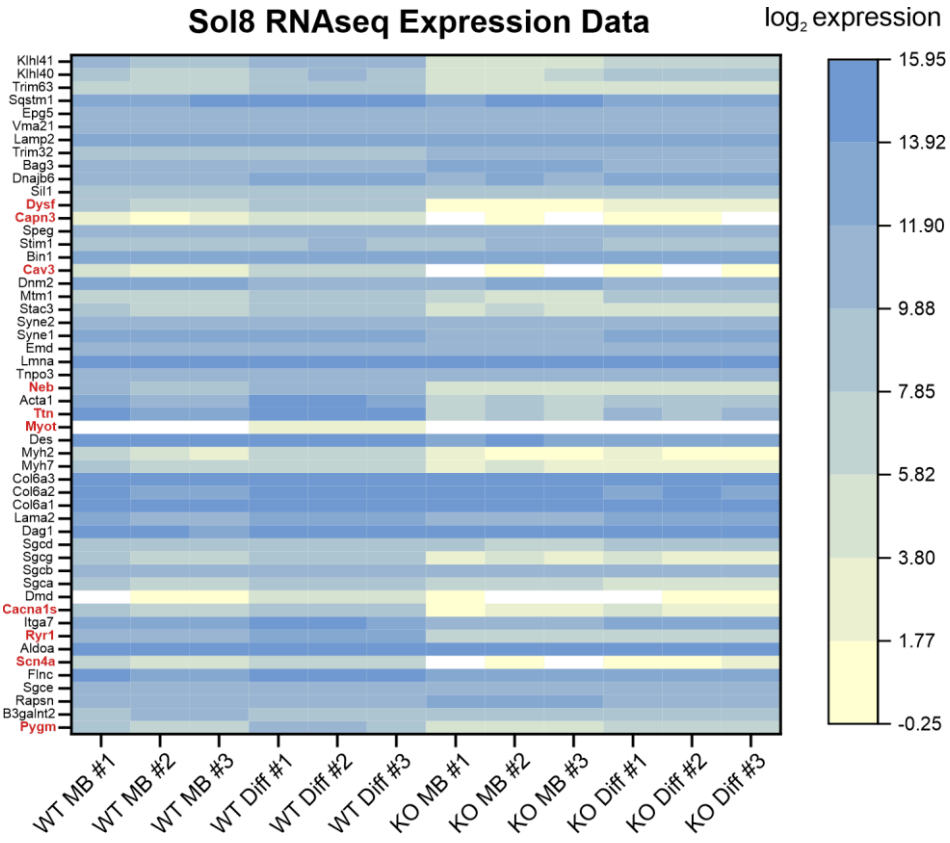

Figure 21: Heatmap showing the expression levels of genes associated with congenital myopathies from RNAseq data of Sol8 wild type and Gne^{KO} cells.

Computational analysis of a manually selected subset of genes from a published data set of Sol8 wild type and Gne^{KO} RNAseq analysis. Gene expression is plottet as $\log_2$ RPKM. Genes of special interest are highlighted in red. WT: Sol8 wild type, KO: Sol8 Gne^{KO}, MB: myoblast, Diff: differentiated. Each collumn shows the expression of one biological experiment (#1-#3). Expression data were manually drawn from the data set published in Ilouz et al, 2022 (Ilouz *et al.*, 2022).

3.2 Validation of RNAseq candidate genes in Sol8 cells

As Sol8 cells are an immortalized cell line that does not reflect the physiology of mature skeletal muscle tissue, the RNAseq data was compared to a data set from a GNEM patient biopsy. The transcriptomic analysis compared muscle specific gene expression in affected tissue from an

atrophying muscle to healthy tissue within the same patient (Chakravorty et al., 2019). According to the transcriptomic data, there was significant lower expression of *PYGM*, *RYR1*, and *SCN4A* in the disease-associated tissue (Figure 22 A), in accordance of what was observed in the RNAseq data set of the Sol8 cells. For further validation of the computational analysis of the RNAseq data sets, expression of *Scn4a* (Figure 22 B), *Ryr1* (Figure 22 C), and *Pygm* (Figure 22 D) was analysed by qPCR in Sol8 wild type and Gne^{KO} cells. The expression patterns reflect the RNAseq data and the strongest expression of each gene was observed in differentiated wild type cells, respectively. Expression of *Scn4a*, *Ryr1*, and *Pygm* was close to zero in Gne^{KO} myoblasts, with slight, but non-significant, increase in differentiated Sol8 Gne^{KO} cells.

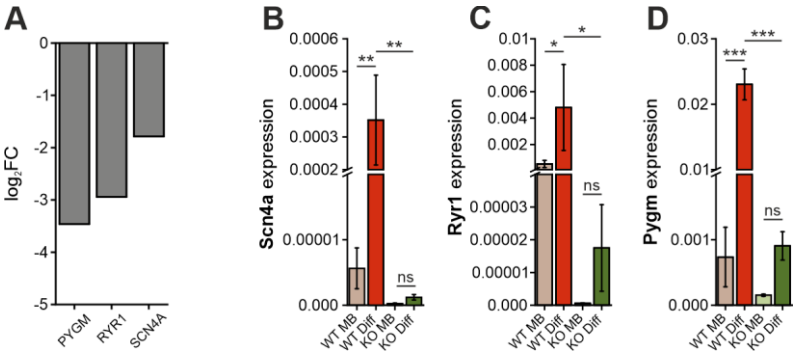

Figure 22: Gene expression analysis of down-regulated genes in Sol8 wilt type (WT) and Gne^{KO} (KO) cells.

A) log_2FC mRNA expression values from a RNAseq dataset of a GNEM patient showing down-regulation of glycogen phosphorylase (*PYGM*), ryanodine receptor (*RYR1*), and sodium channel protein type 4 subunit α (*SCN4A*). Data drawn from the supplementary information from (Chakravorty *et al.*, 2019). qPCR analysis of Sol8 wild type (WT) and Gne^{KO} (KO) cells of **B)** mRNA expression of the sodium channel protein type 4 subunit α (*Scn4a*). **C)** mRNA expression of the ryanodine receptor 1 (*Ryr1*). **D)** mRNA expression of the muscle-specific glycogen phosphorylase (*Pygm*). All values represent the ΔC_t value norm. to Gapdh expression. MB: myoblast, Diff: differentiated. Bar graphs show the mean of three independent experiments ± standard deviation. Statistical analysis: One-way ANOVA. ns = non-significant $p > 0.05$, * $p < 0.05$, ** $p < 0.01$, *** $p < 0.001$.

3.3 Expression of muscle-specific genes in C2C12 wild type and Gne^{KO} cells

For an independent confirmation of the observed de-regulation of *Scn4a*, *Pygm*, *Ryr1*, and *Cacna1s* in Gne^{KO} cells, qPCR analysis was used to determine the expression of those genes in C2C12 wild type and Gne^{KO} clones. *Scn4a* shows a generally low expression in differentiated C2C12 wild type myotubes and is hardly detectable in wild type and Gne^{KO} myoblasts (Figure 23 A). Furthermore, expression of *Scn4a* in differentiated Gne^{KO} cells is significantly reduced compared to wild type cells. Previous experiments showed a beneficial effect on Gne^{KO} myoblast differentiation, when the differentiation medium was supplemented with 5 mM Neu5Ac. Hence, expression of *Scn4a* was analysed in cells, supplemented with Neu5Ac to evaluate, whether sialylation is able to rescue aberrant gene expression. Noteworthy, expression of *Scn4a* was significantly reduced in wild type cells, when treated with Neu5Ac during the

differentiation process (Figure 23 A), similar to what was observed for Myh protein expression (Figure 19 B, C). In the Gne^{KO} clones on the other side, Neu5Ac treatment increased Scn4a expression, however not to wild type control levels (Figure 23 A). Similar results were obtained for *Pygm* expression analysis with the exception, that Neu5Ac treatment restored *Pygm* expression in Gne^{KO} clone #24 to untreated wild type levels (Figure 23 B). Expression of *Pygm* in untreated differentiated Gne^{KO} clones #24 and #26 were significantly reduced compared to wild type cells. *Ryr1* gene expression was significantly reduced in Gne^{KO} myoblasts compared to wild type myoblasts (Figure 23 C). In differentiated cells, *Ryr1* was similarly expressed in clone #24 but reduced in clone #26. Neu5Ac treatment had no significant effect on *Ryr1* gene expression. *Cacna1s* expression was only analysed in differentiated C2C12 cells (Figure 23 D). Clone #24 showed lower *Cacna1s* expression, however not significant compared to wild type cells. *Cacna1s* expression in clone #26 was significant lower compared to wild type cells and both clones showed slight increase of gene expression in response to Neu5Ac treatment. In summary, all four investigated genes, *Scn4a*, *Pygm*, *Ryr1*, and *Cacna1s* were reduced in clone #26 and clone #24, with exception of *Ryr1* expression in clone #24, which was close to wild type levels.

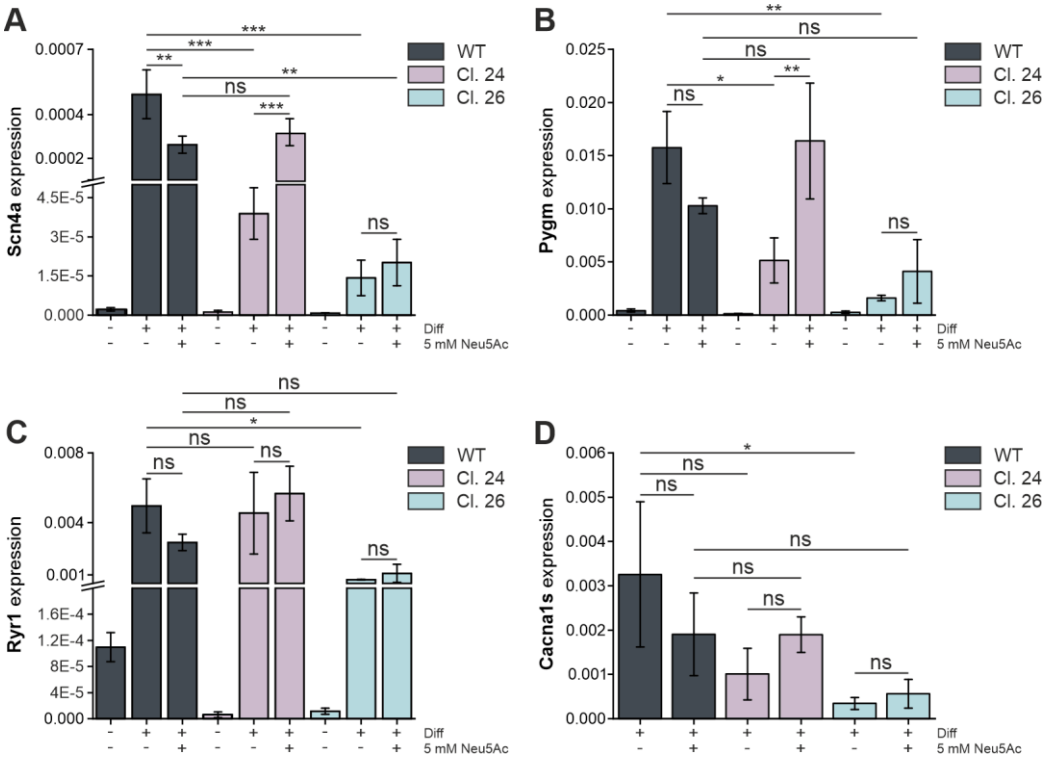

Figure 23: Expression analysis of muscle-specific genes in C2C12 wild type and Gne^{KO} cells.

qPCR analysis was used to examine gene expression in C2C12 wild type (WT) and Gne^{KO} (Cl. 24 and Cl. 26) myoblasts and differentiated cells, cultured on 0.1 % gelatine-coated dishes in differentiation medium containing 10 nM insulin (DM). Where indicated, DM was supplemented with 5 mM Neu5Ac for the duration of the entire differentiation protocoll. **A)** mRNA expression of the sodium channel protein type 4 subunit α (*Scn4a*). **B)** mRNA expression of the muscle-specific glycogen phosphorylase (*Pygm*). **C)** mRNA expression of the ryanodine receptor 1 (*Ryr1*). **D)** mRNA expression of voltage-dependent L-type calcium channel subunit alpha-1S (*Cacna1s*). All values represent the ΔC_t value norm. to *Gapdh* expression. Diff: differentiated, Neu5Ac: *N*-Acetylneuraminic acid. All graphs represent the mean of three independent experiments ± standard deviation. Asterisks indicate the *p*-value of the sample compared to the respective condition. Statistical analysis: One-way ANOVA. ns = non-significant $p > 0.05$, * $p < 0.05$, ** $p < 0.01$, *** $p < 0.001$.

3.4 Alterations in metabolic pathways and energy levels in C2C12 Gne^{KO} clones

It has been reported, that glycogen accumulates in biopsies of GNEM patients (Granger *et al.*, 2022). With that in mind and regarding the reduced expression of the muscle-specific glycogen phosphorylase (*Pygm*) in C2C12 Gne^{KO} clones, Pygm protein was analysed by western blot (Figure 24 A). Even though the results were not significant, there is a strong tendency of reduced Pygm protein expression in differentiated Gne^{KO} clones #24 and #26 compared to wild type expression. Pygm is needed for the degradation of glycogen into glucose-1-phosphate, which can then be further metabolised in the cell, rendering ATP. Thus, ATP levels were quantified using the ATP-Glo® Assay. Gne^{KO} myoblasts showed uniform 50-40 % reduction of ATP levels compared to wild type myoblasts (Figure 24 B). In the differentiated cells however, only clone #24 showed a reduction of 30 % in ATP levels, while clone #26 was similar to wild type levels (Figure 24 C).

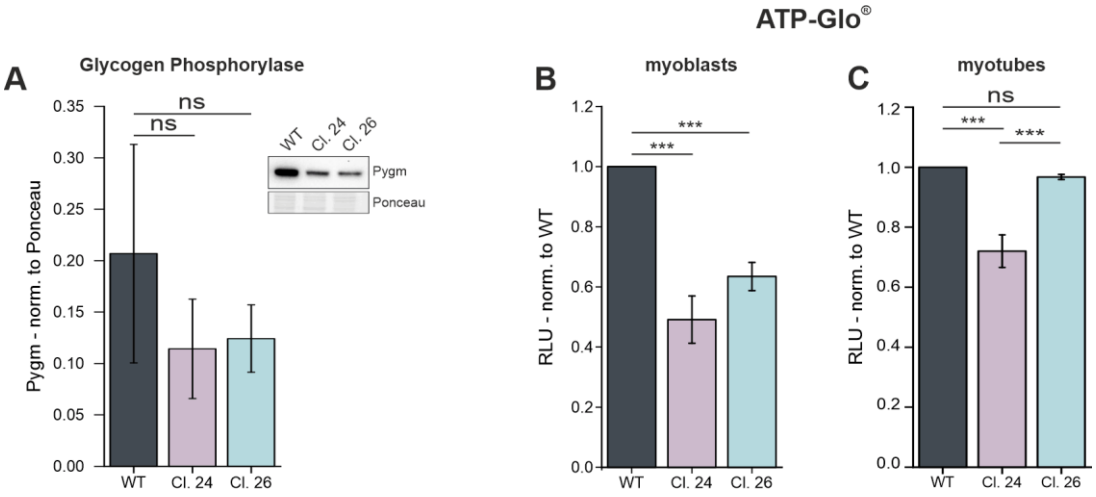

Figure 24: Reduced glycogen phosphorylase protein expression and decreased ATP production in C2C12 Gne^{KO} cells.

A) Western Blot analysis of muscle-specific glycogen phosphorylase (Pygm) protein expression in differentiated C2C12 wild type (WT) and Gne^{KO} clones #24 and #26. ATP-Glo® assay for the quantitative analysis of intracellular ATP levels in C2C12 wild type (WT) and Gne^{KO} (Cl. 24 and Cl. 26) **B)** myoblasts and **C)** differentiated myotubes, normalized to wild type cells. RLU: relative louminescent units. Cells were differentiated on 0.1 % gelatine-coated dishes in differentiation medium with 10 nM insulin. Bar graphs show the mean of three independent experiments ± standard deviation. Asterisks indicate the *p*-value of the sample compared to the respective condition. Statistical analysis: One-way ANOVA, ns = non-significant $p > 0.05$, * $p < 0.05$, ** $p < 0.01$, *** $p < 0.001$.

3.5 Voltage-dependent L-type calcium channel subunits are differentially expressed in C2C12 Gne^{KO} cells

Excitation-contraction coupling in skeletal muscle is initiated by the depolarization of the sarcolemma. Voltage-dependent L-type calcium channels play a crucial role in sensing the depolarization signal and passing it on to the ryanodine receptor in the sarcoplasmatic reticulum membrane, leading to Ca^{2+} efflux into the cytoplasm. Previous experiments showed the reduced expression of the voltage-dependent L-type calcium channel subunit alpha-1S (*Cacna1s*) in Gne^{KO} cells (Figure 23 D). Protein expression of Cacna1s in the differentiated Gne^{KO} clone #24 was reduced by ~50 % compared to wild type cells and not detectable in clone #26 (Figure 25 A, B). PNGase F is an enzyme that specifically cleaves all the N-glycans from a protein backbone and is commonly used for analysis of protein glycosylation. Even though Cacna1s has three potential N-glycosylation sites, PNGase F digestion of the protein lysate led to the disappearance of any western blot signal (Figure 25 A). While Cacna1s is the pore-forming subunit of the channel, voltage-dependent L-type calcium channel subunit alpha-2/delta-1 (Cacna2d1) regulates the activation/inactivation kinetics of the channel and is also known to be glycosylated. Protein analysis revealed a slight size shift in clone #24 and clone #26 to a lower molecular weight of the glycosylated protein compared to the wild type control, due to the missing sialic acids (Figure 25 A). Additionally, clone #26 showed reduced protein expression

of Cacna2d1, but not clone #24 (Figure 25 C). Unlike Cacna1s, Cacna2d1 was susceptible to PNGase F digestion and showed a shift from about ~140 kDa to the theoretical molecular weight of ~124 kDa.

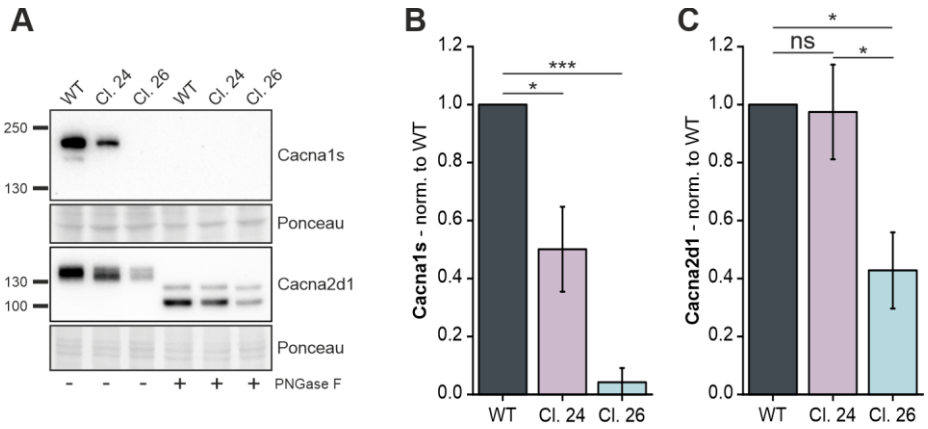

Figure 25: Reduced expression of two voltage-dependent L-type calcium channel subunits in C2C12 Gne^{KO} differentiated cells.

A) Western Blot showing the protein expression of the voltage-dependent L-type calcium channel subunits alpha-1s (Cacna1s) and alpha-2/delta-1 (Cacna2d1). **B)** Quantitative analysis of Cacna1s protein expression normalized to ponceau and wild type (WT) expression. **C)** Quantitative analysis of Cacna2d1 protein expression normalized to ponceau and wild type (WT) expression. Cells were differentiated on 0.1 % gelatine-coated dishes in differentiation medium with 10 nM insulin. Bar graphs show the mean of three independent experiments ± standard deviation. Asterisks indicate the *p*-value of the sample compared to the respective condition. Statistical analysis: One-way ANOVA. Ns = non-significant, $p > 0.05$, * $p < 0.05$, ** $p < 0.01$, *** $p < 0.001$.

IV Discussion

1 Disruption of the endogenous sialic acid biosynthesis pathway in skeletal muscle cells

1.1 C2C12 cells as chosen cell model

One of the hallmarks of GNE myopathy is that the disease only affects skeletal muscle tissue. Thus, to investigate the potentially special role of GNE and sialic acids in muscle tissue, this work aimed to knock out GNE in a suitable muscle cell line. Different cell lines are described in the literature for basic research on skeletal muscle tissue. One of the best studied ones is the immortalized murine myoblast cell line C2C12 that was used for all main experiments in this work. C2C12 myoblasts proliferate rapidly under high-serum conditions and can be subjected to differentiation into multi-nucleated myotubes under low-serum conditions. In contrast, Sol8 murine myoblasts are less often found in the literature, as they are not as committed to differentiation as the C2C12 cells. Nevertheless, Sol8 cells served as additional control for some of the conducted experiments in this study. As both cell lines, C2C12 and Sol8, are of murine origin, it is debatable whether all the findings can be translated to human skeletal muscle cells, especially in terms of certain glycosylation patterns. However, wherever possible, comparisons to other models of human origin are drawn. Moreover, using a well-defined cell line rather than primary cells or patient-derived cells, allows a higher degree of standardization to investigate global mechanisms, as glycosylation profiles exhibit high inter-individual differences between (healthy) subjects. Thus, working with cell lines facilitates the search for matching controls.

1.2 Single cell heterogeneity

As CRISPR/Cas9 technology was used to knock out *Gne* in C2C12 cells, controls had to be chosen very carefully. In this study, the non-transfected wild type (parental) cell line was generally used for comparison. As the wild type is composed of a heterogeneous population, selection of single cell clones poses the bias of non-specific effects. Hence, using a "negative clone" that underwent the same procedure as the knock out clones, but that still expresses Gne, might have led to uncertain conclusions. To rule out those off-target effects in the Gne knock out cells, two single cell clones, clone #24 and clone #26, were selected to confirm uniform Gne-specific findings and variations, respectively. An independent Sol8 Gne knock out clone was used as additional control, where indicated (Ilouz *et al.*, 2022). Throughout the study, clone #24 and clone #26 exhibited more or less obvious differences that partially can be explained by the selection method. For instance, Gne^{KO} clone #26 showed a stronger expression of Ncam,

already indicating differences on cell surface protein expression between clone #24 and clone #26 (Figure 10).

1.3 Role of (poly-) sialylation and NCAM in myoblasts

Concomitantly, both Gne^{KO} clones lacked poly sialic acid, confirming the key role of Gne in the sialic acid biosynthesis pathway (Figure 10). Poly sialylation is a special form of sialylation, occurring only on few proteins like NCAM. The α-2,8-linkage between the sialic acid residues is thereby mediated by the ST8Sia-family of sialyltransferases of which *St8sia2* and *St8sia4* are known to polysialylate NCAM in a synergistic manner (Angata et al., 2002). In a physiological setting, polysialylated (polySia) NCAM is expressed during neural development, enabling neurite outgrowth and synaptogenesis (Angata and Fukuda, 2003). This is explained by modulation of the adhesive properties of NCAM *via* polysialylation, facilitating cellular movement (Rutishauser and Landmesser, 1996). Interestingly, both of the sialyltransferases were equally expressed in C2C12 wild type myoblasts, though at low copy numbers, and significantly reduced in the two Gne^{KO} clones (Figure 10). How transcription of the individual sialyltransferase isoenzymes is regulated in detail, is not fully understood so far, but it would be interesting to see whether gene expression can be rescued by increased substrate availability (CMP-Neu5Ac). How expression of other sialyltransferases is affected in Gne^{KO} cells has not been investigated in this work and could be a prospective subject for future studies.

Besides its role in the central nervous system, Ncam was shown to play a crucial role during muscle cell differentiation, with expression of a muscle-specific domain, carrying mucin type O-glycans (Suzuki et al., 2003). Another study could show that expression levels of Ncam in primary satellite cells determined the myogenic potential of these cells (Capkovic et al., 2008). Taken together, unequal Ncam expression might explain the differences in the differentiation phenotypes between C2C12 Gne^{KO} clones #24 and #26, as the latter one showed stronger Ncam expression (Figure 10, Figure 11).

2 Role of Gne and sialic acids during muscle cell differentiation

Skeletal muscle is one of the most regenerative tissue systems and holds the capacity to replace damaged myofibers. To do so, muscle stem cells that are called satellite cells are needed. Those satellite cells reside in a specific niche that is marked by its microenvironment between the sarcolemma and the laminin-rich basal lamina. Importantly, the satellite cell niche in adult skeletal muscle differs markedly from the niche of the myoprogenitor cells during embryonic development. Along with that, myoprogenitor and adult satellite cells are differentially regulated by their respective niches (Hicks and Pyle, 2023).

The differentiation process of (adult) muscle cells has been intensively studied in different models and remodelling of the glycome and sialylation were shown to play important roles for myotube formation (Chen et al., 2021; Janot et al., 2009). In accordance to the literature, C2C12 Gne^{KO} clones #24 and #26 showed abnormal differentiation patterns (Figure 11), as it was described previously for Sol8 Gne^{KO} cells and GNEM patient-derived stem cells (Ilouz *et al.*, 2022; Schmitt et al., 2022). First, wild type and Gne^{KO} clones were differentiated in low-serum DMEM medium (containing 2 % FBS) and showed no sign of myoblast fusion or expression of myosin heavy chain (Myh). Interestingly, this phenotype changed upon addition of 10 nM insulin into the differentiation medium, which induced cell fusion and myotube formation (Figure 11). However, especially Gne knock out clone #24 showed strong alterations in cell morphology, hinting towards de-regulated cell fusion, which led to the formation of abnormally large myotubes. Insulin has been described to have positive effects on myogenesis in cultured myoblasts *via* the Akt/P70S6K/MAPK pathway (Conejo et al., 2002; Conejo et al., 2001). However, the mechanism on how insulin rescues myoblasts fusion in Gne^{KO} cells is yet to be determined.

Considering that GNE myopathy is a genetic disease with a late-onset, it is tempting to speculate whether the cause for the disease lies within the satellite cells and impaired muscle regeneration. Little is known about satellite cells in GNEM patients regarding their number and activity. Moreover, there is evidence that the master regulator of satellite cell quiescence Pax7, also regulates *Gne* expression (Lilja et al., 2017). Even though there is no Pax7 binding site annotated in the promoter regions of *Gne*, Pax7 was shown to interact with methyltransferases, regulating chromatin accessibility and thus, gene transcription in an indirect manner (McKinnell et al., 2008). A study that investigated transcriptional changes in the early activation of satellite cells after injury found that *Gne* is one of the genes that is down-regulated 5 h after satellite cell activation (Machado et al., 2017). Further experiments are needed to evaluate the relationship between Pax7 and *Gne*, as Pax7 in turn is regulated *via* external stimuli that depend on glycoproteins and proteoglycans in the satellite cell niche.

3 Alterations in the glycome of Gne knock out muscle cells

As GNE is the key enzyme for sialic acid biosynthesis, the main cause for GNE myopathy is thought to be due to a reduction in sialylation. Hence, one of the aims of this study was to investigate how Gne knock out influences the overall glycan structures of muscle cells. As glycosylation is a highly complex post-translational modification and includes a plethora of

enzymes and substrates, this work can only give a snapshot of select structural aspects in this respective cellular model.

3.1 N-Glycans

Glycomic analysis of N-glycan structures in C2C12 wild type and Gne knock out clone #24 revealed a decrease in sialoglycan abundancy, as it was expected (Figure 12). Furthermore, an increase in terminal galactose-α-1,3-galactose epitopes was observed, which is a structure that does not exist in human tissue, due to the inactivation of the α-1,3-galactosyltransferase (Huai et al., 2016). Thus, direct conclusions on how hyposialylation effects human N-glycan structures cannot be drawn from these experiments. However, another glycomic study, using differentiated muscle cells that were established from patient biopsies, compared glycan structures to matched controls. There, it was shown that the most distinctive variation between GNEM-derived muscle cells and healthy subjects were in the composition and sialylation of glycolipids, rather than in N- and O-glycans (Sela et al., 2020). These results are further supported by the findings of Paccalet and co-workers, who found reduced GM3 ganglioside levels in the Gne mouse model with the $Gne^{M712T/M712T}$ genotype (Paccalet et al., 2010). This reduction in GM3 also seemed to be muscle-specific, as no alterations were observed in the kidney. Interestingly, GM3-deficient mice have been reported to be viable, but presented a higher insulin-sensitivity, while GM3 was also found to be differentially regulated during C2C12 differentiation (Go et al., 2017; Yamashita et al., 2003). Taken together, glycomic analysis of ganglioside composition of C2C12 Gne^{KO} cells could add more information to the already existing models. However, despite the indisputable value mass spectrometry-based methods have for structural analysis of glycans, the technique also has some limitations. Handling and preparation of samples and quality of sample material can have a vast impact on the result outcome. Especially high-mass glycans are often neglected in the literature because of their relatively low abundance. Hence, subtle changes in specific low abundance glycans might be missed in the analysis of whole-cell glycomic analysis.

To assess N-glycan branching, PHA-L lectin staining of C2C12 myoblasts was performed. N-glycans are usually found in either bi-, tri-, or tetra-antennary conformation, with or without a bisecting GlcNAc. As already observed in the glycomic data of the N-glycans, C2C12 myoblasts generally exhibited complex glycan structures with many I-branched glycans (Figure 12). Nevertheless, the strong increase in PHA-L reactivity in Gne^{KO} myoblasts is somewhat surprising and must be interpreted with care (Figure 13 B). Even though lectins are a broadly used tool in the field of glycosciences, they are prone to unspecific binding. As such, PHA-L is inhibited by α-2,6-linked sialic acids, among others (Bojar *et al.*, 2022). Hence, in Gne^{KO}

clones, where sialylation is globally reduced, an increase in PHA-L staining is most likely influenced by multiple factors. Concludingly, the PHA-L assay shows that manipulation of the sialylation status of cells can have broad effects like altered accessibility for carbohydrate-binding proteins and ligands. Again, this effect was already observed in a study using cells in which *GNE* is epigenetically silenced. Those cells showed a higher affinity for galectin-1 binding, a lectin that was also described as being important for myogenesis (Blazev *et al.*, 2021; Pham et al., 2017).

3.2 Alternative routes for the Gne substrate UDP-GlcNAc

3.2.1 *O*-GlcNAcylation

When thinking about sialylation, intracellular glycosylation is usually not the first modification to consider. However, in case of the Gne^{KO} cells, accumulation of the Gne substrate UDP-GlcNAc could have fundamental influences on cytoplasmic and nuclear glycosylation. *O*-GlcNAcylation is a master regulator of metabolic signalling in cells and often acts competitively with protein phosphorylation. The monosaccharide building block UDP-GlcNAc derives from the hexosamine biosynthetic pathway and is the only known substrate for the Gne so far. Interestingly, while *O*-GlcNAc modifications were not altered in C2C12 Gne^{KO} myoblasts, differentiated cells showed a strong tendency of increased *O*-GlcNAcylation, compared to the wild type control (Figure 13 C, D). The large error bars that come with the quantification of the western blot signals of *O*-GlcNAc reflect the dynamic nature of this PTM. In the literature, different aspects of how *O*-GlcNAcylation may modulate muscle functions have been investigated. For example, glucose metabolism has been shown to be regulated by *O*-GlcNAcylation. Increased *O*-GlcNAcylation impeded facilitated glucose transporter member 4 (GLUT4) translocation and led to insulin-resistance in rat primary adipocytes (Park et al., 2005). As insulin-resistance causes hyperglycaemia, it can eventually lead to the manifestation of diabetes type II. Interestingly, diabetic hearts showed a direct link between increased *O*-GlcNAcylation of myofilaments and contractile dysfunctions *via* modulation of their Ca^{2+}-sensitivity (Ramirez-Correa et al., 2008; Ramirez-Correa et al., 2015).

Like most established cell lines, C2C12 cells were cultured and differentiated in high-glucose medium (25 mM). These high glucose concentrations are above the physiological blood-glucose levels (~5.5 mM) and could contribute even more to alterations in *O*-GlcNAc signalling in the Gne^{KO} myotubes. Interestingly, muscle-specific glycogen phosphorylase (Pygm) was down-regulated in Gne^{KO} myotubes, along with decreased intracellular ATP levels (Figure 23, Figure 24), hinting towards impaired glucose metabolism. In fact, glycogen deposits were found

in GNE myopathy biopsies, which could be due to impaired Pygm activity (Granger *et al.*, 2022). Noteworthy, Gne^{KO} clone #26 myotubes presented equal ATP amounts as the wild type with concomitant reduction in Pygm expression. Hence, it would be interesting to decipher the differences between clone #24 and clone #26 regarding their metabolic activity. Generally, repression of Pygm expression could be a counter-mechanism in Gne^{KO} cells to prevent glucose-flux, which would ultimately lead to higher intracellular UDP-GlcNAc levels.

3.2.2 Extracellular matrix

As there was no detectable difference in *O*-GlcNAcylation in C2C12 Gne^{KO} myoblasts, it is likely that UDP-GlcNAc is used for alternative glycan structures in the proliferative state of the cells (Figure 13 A, C). Acidic glycosaminoglycans in the extracellular matrix (ECM) can be visualized by alcian blue staining, while the PAS reaction highlights neutral glycans and glycolipids in bright magenta. The combined alcian blue and PAS staining revealed striking differences between differentiated wild type and Gne^{KO} clone #24, and to a minor degree clone #26 (Figure 14). This increase in sulphated and acidic proteoglycans indicates aberrant expression of extracellular glycans. This phenomenon could be due to increased UDP-GlcNAc accumulation in the cells and alternative glycan formation, as GlcNAc is also found in glycosaminoglycans (Figure 3). Aberrant expression of extracellular proteoglycans in the Gne^{KO} myoblasts could have drastic influence on shaping the extracellular milieu that in turn provides signal cues for the differentiation process. It is also interesting that glycosaminoglycan expression seems to directly correlate with the differentiation capacity of myoblasts, as there is a clear gradient from being almost absent in wild type cells, low expression in Gne^{KO} clone #26 to strong expression in Gne^{KO} clone #24.

In the pathophysiological context of GNE myopathy, this could be a possible disease-driving mechanism of ECM remodelling during impaired muscle repair. Muscle regeneration usually requires immune cell infiltration and a balance between pro- and anti-inflammatory cytokines that trigger temporarily ECM expansion and satellite cell activation (Robertson et al., 1993). Interestingly, GNEM patients do not exhibit signs of inflammation, with some exceptions during disease-onset. Missing immune cell infiltration could hinder proper tissue regeneration, impeding myoblast differentiation. In fact, fibrosis is one of the main mechanisms that impede muscle regeneration after injury. It was further shown that transforming growth factor β-1 (TGFβ1) and fibulin 2 induce aberrant differentiation of myoblasts into myofibroblasts, enhancing fibrosis (Yang et al., 2025). Investigation of immuno-modulatory factors and cytokines in GNEM muscle tissue might lead to new insights in fibrotic events that might be exploited for therapeutic approaches regarding satellite cell differentiation.

As discussed above, GNEM patients have normal embryonic development and are healthy during childhood, therefore it seems likely that the main problem lies within impaired regenerative capacity of satellite cells.

4 Supplementation studies

4.1 Rescue of sialylation

N-acetylmannosamine (ManNAc) is the precursor of all sialic acids. Synthetically produced ManNAc was shown to enter living cells and to fuel the endogenous biosynthesis of sialic acids, even replacing natural sialic acids when modified ManNAc-derivatives were used (Keppler et al., 2001). Using human embryonic kidney cells (HEK239) that have been depleted of GNE expression, this and another study could show that ManNAc was able to rescue polysialylation, even when GNE-kinase activity is missing (Figure 15 A) (Peters et al., 2023). It is generally considered, that the GNE-kinase domain phosphorylates ManNAc under physiological conditions. However, exogenous ManNAc seemed to be phosphorylated by another enzyme, putatively the GlcNAc-kinase (NAGK) (Gorenflos Lopez *et al.*, 2023). In line with this hypothesis, NAGK expression was found to be significantly elevated in HEK293 GNE^{KO} cells and could explain the successful processing of ManNAc into Neu5Ac (Figure 15 B).

In contrast however, ManNAc supplementation had no effect on C2C12 Gne^{KO} clones under the same conditions (Figure 16). Neither Sol8 Gne^{KO} myoblasts responded to ManNAc treatment (Figure 17). Even the continuous long-term treatment during differentiation (seven days) was not sufficient to rescue sialylation in Gne^{KO} clones while Neu5Ac supplementation was (Figure 19). The more detailed metabolomic analysis revealed that ManNAc supplementation increased ManNAc-6P, Neu5Ac, and CMP-Neu5Ac levels in C2C12 wild type myotubes and to a slight degree in myoblasts. However, Gne^{KO} clones #24 and #26 did not show any response to ManNAc treatment under the observed conditions (Figure 20). Regarding ManNAc as a putative drug for enhancing sialylation in GNE myopathy patients, the results created in this study might give an explanation on why there is no approved ManNAc-based therapy so far. Even though ManNAc showed promising effects in GNEM mouse models and an open-label phase 2 study, there is still no proof that it has a significant impact on inhibiting or reversing disease progression (Malicdan et al., 2009), (Carrillo et al., 2021). Considering that GNE variants are already impaired in their enzymatic activity, applying exogenous ManNAc to GNEM subjects harbors the danger of modulating glycan structures in an unwanted way, as even endogenous substrates cannot be metabolized effectively. Furthermore, the observed increase in sialylation of serum proteins after oral ManNAc

supplementation suggests that ManNAc does not reach the muscle but is rather metabolized by the liver, potentially for elimination of excess sialic acids. Thus, additionally to serum, urine should also be analyzed to assess, whether sialic acids are cleared from the body or are distributed to distinct tissues.

Neu5Ac treatment on the other side is efficient in restoring sialylation in Gne knock out myotubes, proving for a functional salvage pathway in the absence of Gne (Figure 19, Figure 20). Nevertheless, it should be taken into account that excess Neu5Ac had a negative impact on myotube formation and gene expression in C2C12 wild type cells (Figure 19, Figure 23). Skeletal muscle is usually considered to be a tissue with low sialylation levels. Hence, modulating sialic acid contents that outreach physiological concentrations could lead to adverse side effects in a long-term setting. Intriguingly, GNEM patients have no other phenotype then the skeletal muscle atrophy and present normal cognitive functions and development. This points towards normal sialylation patterns and functions in all of the other tissues and organs and questions, whether hyposialylation is the disease-driving cause. Mutations in the allosteric site of *GNE* affect the feedback-inhibition mechanism and are the cause for another rare genetic disease termed sialuria (Ferreira et al., 1999). Patients usually present a mild phenotype including developmental delay, intellectual impairment and hepatomegaly. As they are diagnosed by excessive free sialic acids in the urine (> 1 g/d), pathologically high amounts of sialic acids seem to be simply removed from the circulation. Hence, even though artificial sialylation of biotherapeutics can improve their pharmacokinetics and bioavailability (Agatemor *et al.*, 2019), systemic administration of ManNAc or Neu5Ac to GNEM subjects will most likely result in unspecific distribution of sialic acids with no beneficial effects (Lochmuller *et al.*, 2019). Nevertheless, as another clinical study claimed significant effects of enhancing sialylation, it will be interesting to see the long-term follow-up of these patients, who received the respective therapy (Mori-Yoshimura *et al.*, 2023).

5 Functional consequences of Gne knock out in muscle cells

5.1 Transcriptomic analysis of Sol8 Gne^{KO} and GNEM patient biopsy

As mentioned above, GNEM is a monogenic disease that causes skeletal muscle atrophy. On the other side, hundreds of different genes have been identified to cause (neuro-) muscular disorders. Looking at this diverse picture of myopathies, it could be helpful to systematically analyze the interdependency of those myopathogenes to discriminate between global and specific disease mechanisms. Thus, a panel of myopathogenes was manually selected for mRNA expression analysis in the transcriptomic data set of Sol8 wild type and Sol8 Gne^{KO}

cells (Figure 21). Sol8 wild type myoblasts and myotubes showed distinct expression patterns with global increase in selected gene expression after differentiation. Hence, it could be discussed, whether impaired gene expression in the Gne^{KO} cells is due to the impaired differentiation mechanism. However, not all of the genes were differentially expressed in Gne^{KO} compared to wild type, pointing towards a more specific dysregulation. More importantly, transcriptomic analysis of affected GNEM patient muscle tissue confirmed the expression patterns of some of the selected genes (Figure 22). Like in the Sol8 model, important muscle genes like Pygm, Ryr1, Capn3, Ttn, Scn4a, and Myot were significantly down-regulated in the GNEM subject and underline the significance of these findings (for a full list see supplementary data in (Chakravorty *et al.*, 2019). Now, the mechanism of how Gne knock out affects gene transcription is one of the big remaining questions. The sections above discussed how missing sialic acids reshape the glycomic landscape of Gne^{KO} cells, influencing crucial signaling pathways like *O*-GlcNAcylation and lectin binding. It is further conceivable that aberrant sialylation of cell surface receptors and signal sensors is the trigger for dysregulated gene expression.

The following sections will discuss some of the dysregulated genes and their role in skeletal muscle in more detail.

5.2 Structural genes

Genes that were found to be strongly down-regulated in Gne^{KO} cells but were not validated independently include myotilin (Myot), titin (Ttn), nebulin (Neb), caveolin 3 (Cav3), calpain 3 (Capn3), and dysferlin (Dysf) (Figure 21). Titin is one of the largest proteins in the human proteome (~3,800 kDa) and indispensable for proper muscle function. It is associated with the thick filament in the sarcomere, spanning ~ 1 µm in length and serving as a spring, contributing to sarcomere flexibility (Figure 7). TTN variants have been linked to a subset of congenital myopathies with a broad clinical spectrum, ranging from severe early-onset cases to forms with mild muscle weakness (Oates et al., 2018). Likewise, nebulin strongly interacts with the thin filaments, acting like a molecular ruler that defines their length (Figure 7). Loss of nebulin leads to diminished contractile force and muscle weakness and is one of the causes for nemaline myopathy (Moreno et al., 2023). Calpain 3 is a muscle-specific calcium protease that is anchored to titin and is also known to interact with the ryanodine receptor (Ryr1). Its proteolytic activity is important for dynamic remodeling of the sarcomere and cytoskeleton and maintaining triad integrity (Kramerova et al., 2004). Caveolin 3 is also a structural protein that forms membrane caveolae, vesicular structures, providing membrane integrity and vesicular trafficking and is linked to a variety of myopathies (Dewulf et al., 2019). Dysferlin is a

membrane-inserted protein and has been implicated in sarcolemma stability and repair mechanisms. Upon sarcolemma disruption, dysferlin is found at the site of damage and helps to reseal the membrane. The proposed mechanism of action is *via* interaction of dysferlin with caveolin 3, by supporting vesicle-membrane fusion (Matsuda et al., 2001). Furthermore, dysferlin seems to be important for the formation and maintenance of T-tubules (Klinge et al., 2010). Myotilin is involved in actin organization and is located at the Z-disc of sarcomeres. Mutations in *MYOT* are linked to a variety of myopathic syndromes including myofibrillar myopathies. Interestingly, those myofibrillar myopathies also show characteristic cytoplasmic deposits and rimmed and non-rimmed vacuoles, with a late disease onset, similar to GNE myopathy (Olive et al., 2005).

In summary, all of those genes pose potentially interesting targets that should be investigated more closely in terms of their role in GNE myopathy. Cross-talk and interactions between the above-mentioned proteins have been proposed, highlighting the close proximity of structural proteins and the formation of tightly regulated networks within myofibers.

5.3 Excitation-contraction coupling

In contrast to cardiac muscle, skeletal muscles lack the ion channels responsible for spontaneous membrane depolarization and always require a stimulus from a nerve impulse for activation. The action potential arriving at the motor neuron terminals is amplified at the neuromuscular junction, generating an endplate potential that will eventually lead to muscle contraction. Gne^{KO} myotubes showed dysregulation of some of the highly important proteins involved in the propagation of the endplate potential and their implications in proper muscle function will be discussed below (Figure 22, Figure 23).

5.3.1 Voltage-dependent sodium channel 1.4 ($Na_V1.4$)

The $Na_V1.4$ α subunit (Scn4a) is the skeletal muscle-specific pore-forming subunit of the voltage-dependent sodium channel that associates with the β1 subunit to build a heterodimer. Its localization is enriched at the motor endplate and the traverse tubule (T-tubule) system, ensuring efficient and safe synaptic transmission of the action potential (Caldwell et al., 1986). Mutations within the *SCN4A* gene are known to cause a range of sodium channelopathies, affecting solely skeletal muscle tissue (Cannon, 2018). Interestingly, in all models, Sol8 Gne^{KO}, patient biopsy, and C2C12 Gne^{KO}, *Scn4a* mRNA expression was significantly down-regulated compared to respective controls (Figure 22, Figure 23). Several studies showed that Scn4a function, like no other voltage-gated sodium channel alpha subunit, is highly dependent on its sialylation status. Early studies already proposed the existence of poly sialic acid on the $Na_V1.4$

α subunit (James and Agnew, 1987). Another study picked up on that topic and electrophysiological studies on recombinant Scn4a in genetically engineered chines hamster ovary (CHO) cells indicated distinct roles of polysialylation and sialylation on channel function (Ahrens et al., 2011). As resting myofibers keep a negative membrane potential, the high degree of Scn4a sialylation was thought to contribute with its negative charge of the sialic acid residues (Bennett *et al.*, 1997). In fact, needle electromyography (EMG) patterns in GNE myopathy patients indicate myopathic changes that result from muscular atrophy with spontaneous activity and fibrillation potential (Liu *et al.*, 2022). This could be a direct result of subtle changes in the net charge of the sarcolemma under resting conditions, when GNE activity is impaired. A potential shift of the resting potential to a less negative value, could enable spontaneous depolarization as seen in the EMG recordings. Restoring sialylation in Gne^{KO} myotubes *via* Neu5Ac supplementation significantly increased *Scn4a* expression in C2C12 Gne^{KO} clone #24, but had only minor effects in clone #26. Interestingly, Neu5Ac had a negative impact on Scn4a expression in C2C12 wild type myotubes, as already observed during the differentiation process (Figure 23, Figure 19).

5.3.2 Voltage-gated calcium channel 1.1 ($Ca_V1.1$)

Another important part of the excitation-contraction coupling is the voltage-gated calcium channel $Ca_V1.1$, also known as dihydropyridine receptor (DHPR). $Ca_V1.1$ is an oligomeric protein complex composed of five subunits and is found in the traverse tubule system of myofibers. While $Na_V1.4$ has been extensively studied in terms of sialylation, nothing is known about the effect of sialic acids on $Ca_V1.1$. Noteworthy, the two channels show high homology in terms of their structure, suggesting similar regulatory circuits. Unlike $Na_V1.4$ function, it is not the channel function and concomitant Ca^{2+} influx that propagates the action potential, but rather a conformational change in $Ca_V1.1$ that allows the interaction with the ryanodine receptor (Ryr1). The *Cacna1s* gene encodes the α1 subunit of the DHPR, which is the subunit primarily responsible for interaction with and activation of Ryr1 (Protasi et al., 2002). Mutations in *Cacna1s* can cause malignant hyperthermia, periodic paralysis and myopathy (Dowling *et al.*, 2021). While mRNA expression of *Cacna1s* was only significantly reduced in Gne^{KO} clone #26, but not clone #24, western blot analysis confirmed the significant downregulation of Cacna1s also in clone #24 (Figure 23 D, Figure 25). Along with reduced Cacna1s protein expression, another DHPR subunit, Cacna2d1 also showed an interesting pattern in the western blot of Gne^{KO} myotubes (Figure 25). A minor reduction in the molecular weight of Cacna2d1 hints towards missing sialic acids in Gne^{KO} clones. Existence of N-glycan sites are proven by PNGase F digestion that enzymatically cleaves N-glycans from their protein backbone. In case

of Cacna2d1, a clear shift towards the theoretical molecular weight is seen in the western blot. Intriguingly, Cacna1s was detected between ~ 200 and 250 kDa, which responds to its molecular weight and the signal disappeared upon PNGase F treatment. PNGase F was added to the cell lysate that also contained a protease inhibitor cocktail (PIC), therefore, proteolytic degradation should not be the cause for the observed result. However, wild type cells showed a strong signal and a weak signal at a reduced size, possibly being a non-glycosylated form. An assumption is that the antibody preferentially recognizes the glycosylated form of Cacna1s, which would explain the missing signal upon PNGase F treatment. Unfortunately, the exact immunogen of the antibody is proprietary information and not stated in the data sheet. For future studies, it would be interesting to investigate the role of sialic acids on Cacna1s activation and conformational changes more closely. This could be done by introducing site-specific mutations of the annotated N-glycan sites or with enzymatic removal of sialic acids using neuraminidase.

5.3.3 Ryanodine receptor (Ryr1)

As already stated, DHPR turns the electrical signal received from $Na_V1.4$ into a chemical signal by activating the ryanodine receptor (Ryr1) in the terminal cisternae of the sarcoplasmic reticulum. Ryr1 is an intracellular pore-forming homo-tetrameric complex, mediating Ca^{2+} efflux into the cytoplasm, triggering contraction of the sarcomeres. Loss-of-function mutations in *RYR1* are associated with static muscle weakness and cause different types of myopathies (Dowling *et al.*, 2021). Notably, *Ryr1* was significantly reduced in the patient biopsy, in Sol8 Gne^{KO}, and in C2C12 Gne^{KO} clone #26 but not clone #24 (Figure 22, Figure 23). Generally, differences in myopathogene expression in C2C12 Gne^{KO} clones #24 and clone #26 demonstrate the heterogenic effects the depletion of one gene can have. Whether aberrant *Ryr1* expression is a Gne-specific effect is not entirely clear and should be validated by further experiments. However, the reduced *Ryr1* expression in Sol8 Gne^{KO} cells, as well as in the patient biopsy, support the relation between proper Gne function and *Ryr1* expression.

In summary, Scn4a, Cacna1s, and Ryr1 are all implemented in the propagation of the nerve-derived action potential in skeletal muscle to enable excitation-contraction cycles and have been independently verified to be dysregulated in Gne^{KO} myotubes. Based on this gene signature, Figure 26 shows a potential pathomechanism that could lead to atrophy in GNE myopathy. Subtle hyposialylation could shift the resting membrane potential to a less negative value, changing depolarization characteristics of the affected myofibers. As sialylation is known to be important for $Na_V1.4$ function, expression of Scn4a might be reduced as a direct effect to prevent incorporation of malfunctioning channels in the sarcolemma. Similarly, Cacna1s is

affected by hyposialylation and reduced Cacna1s expression leads to impaired Ryr1 activation, hence lower Ryr1 expression. Concomitantly, perturbation of glucose metabolism by aberrant Pygm expression and *O*-GlcNAc signaling alters the energy metabolism and ATP production. All those events impede sarcomere contraction, which might lead to atrophy eventually. Additionally, de-regulated expression of structural proteins like nebulin and titin should be further examined and compared to other myopathy-models.

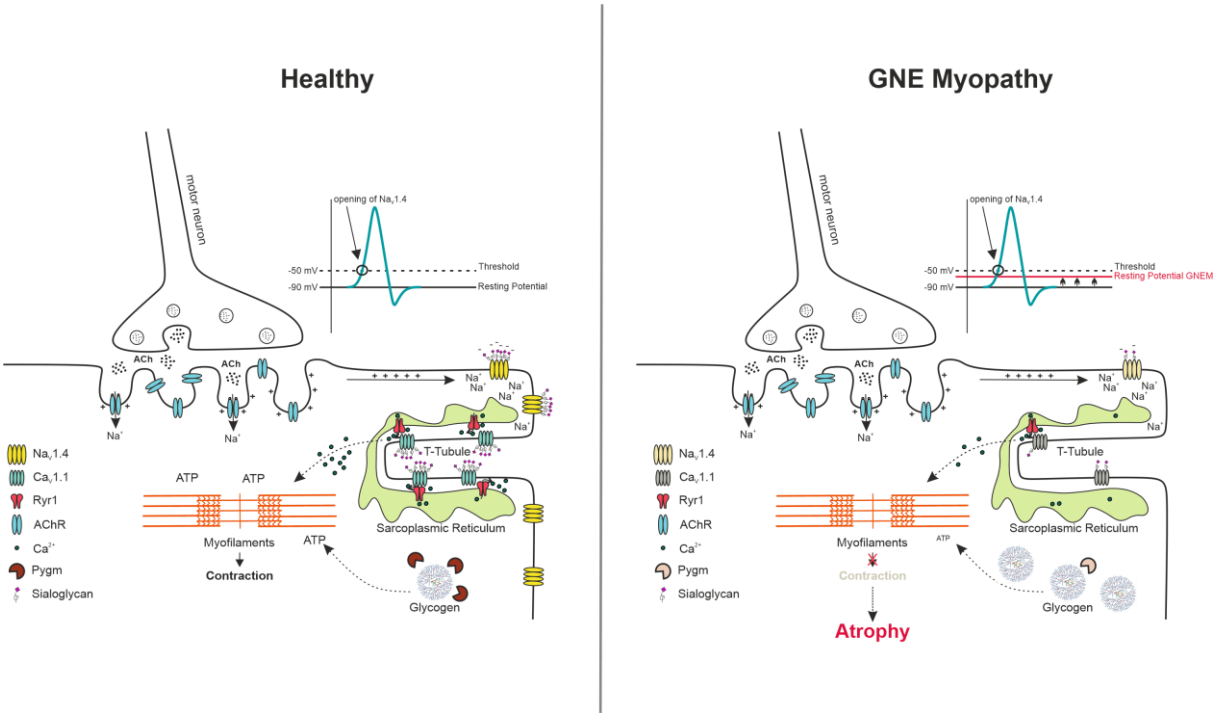

Figure 26: Possible disease mechanism of GNE myopathy.

Alterations in the membrane potential of myofibers, due to hyposialylation could cause an atrophic signaling cascade. Acetylcholine receptors at the neuromuscular junction receive the action potential from the motor neurons and pass the signal to voltage-gated sodium channel $Na_V1.4$. $Na_V1.4$ opening leads to depolarization and conformational changes in $Ca_V1.1$ that in turn activate the ryanodine receptor in the sarcoplasmic reticulum, resulting in Ca^{2+} efflux. See main text for further description. $Na_V1.4$: voltage-gated sodium channel 1.4, $Ca_V1.1$: voltage-gated calcium channel 1.1, Ryr1: ryanodine receptor 1, ACh: acetylcholine, AChR: acetylcholine receptor, Pygm: muscle-specific glycogen phosphorylase, ATP: adenosine triphosphate. Figure created in CorelDRAW.

V Conclusions and future perspectives

GNE myopathy is a rare genetic disease of which the pathomechanism remains largely elusive. As sialic acids fulfill multi-functional roles in different tissues, it is most likely that many different factors contribute to the manifestation of the disease. This work contributes to the general understanding on how sialylation influences muscle physiology by introducing a new C2C12 Gne knock out cell model.

Analysis of this model suggests that Gne expression and the sialic acid content is tightly regulated during muscle cell differentiation, as an excess of Neu5Ac impeded myotube formation in C2C12 wild type cells. On the other side, Gne knock out and reduction of sialylation negatively affected the differentiation process. These findings are in accordance with already existing results in the literature. Here, it would be interesting to investigate the role of GNE in muscle regeneration more closely and whether there are alterations within the satellite cell pool in GNE myopathy patients. Alternatively, damage-induced muscle regeneration could be studied in one of the existing GNEM mouse models. Glycomic analysis of myoblast N-glycans is only a snapshot of the glycome and revealed the existence of mouse-specific epitopes in Gne^{KO} cells. Hence, more work is needed to gain a more elaborative view on how missing sialic acids reshape the glycome. Especially glycosaminoglycans and glycoshpingolipids should be considered for future analysis. Moreover, a human-derived cell model would be more suitable in this case, as glycosylation patterns show significant alterations between different species. Thus, C2C12 as a murine cell line can give only limited knowledge that might not be transferable to the human setting.

Nevertheless, one of the major findings of this study is that unlike other cells and tissues, muscle cells that lack Gne, cannot metabolize *N*-acetylmannosamine (ManNAc) into *N*-acetylneuraminic acid (Neu5Ac). While ManNAc increased the intracellular Neu5Ac and CMP-Neu5Ac pool in C2C12 wild type cells, no such effect was observed in Gne^{KO} cells. While it has been suggested that GlcNAc kinase is the responsible enzyme for exogenous ManNAc phosphorylation, this seems not to be the case in muscle cells. To track the metabolic fate of ManNAc in Gne^{KO} myocytes, isotope-labeled ManNAc could be used for supplementation and subsequent metabolomic analysis. Furthermore, dysregulation in metabolic signaling *via O*-GlcNAcylation and aberrant Pygm expression could be the cause for decreased ATP levels in Gne^{KO} clones. It would be also interesting to investigate metabolic circuits and alterations in Gne^{KO} cells. ATP is the major energy currency of cells and muscle cells are known to have especially high ATP demands for the cross-bridge cycle. Additionally, ATP is required for

proteasomal activity and protein degradation. Hence, protein aggregations and the occurrence of rimmed vacuoles in muscle biopsies could be also due to a lack of ATP. Furthermore, disruption of Gne expression affected expression of a whole network of other (muscle-specific) genes that are known to cause muscle disease. Down-regulation of $Na_V1.4$, $Ca_V1.1$ and Ryr1 suggest a putative role of sialic acids in the excitation-contraction coupling process and the propagation of the action potential.

The results of this work are based on two mouse-derived cell lines, C2C12 and Sol8, which poses the major limitations of this project. Immortalized cell lines mimic myoblast physiology only to a certain degree and thus, primary cells should be used for further validation of the results. Moreover, any other cell types of skeletal muscle tissue and the extracellular matrix are neglected in this study, which could play important roles in the manifestation of GNE myopathy. Furthermore, the high concentrations of ManNAc and Neu5Ac used in the supplementation experiments are far above physiological ranges and are an artificial model to evaluate coarse changes in the sialylation level of Gne knock out cells, but do not serve as translational model for putative therapeutic approaches. A detailed analysis of the energy metabolism of the Gne knock out cell models was beyond the scope of this work but could lead to new insights. Generally, linking glycan structures to biological functions is an insidious work, due to the vast diversity and abundance of glycans. Hence, the observed phenotype of the C2C12 and Sol8 Gne knock out cells could have many other reasons then the ones mentioned above.

In conclusion, as symptoms of GNE myopathy appear during early-adulthood, future studies should focus on muscle repair mechanisms and satellite cell functions. Application of immuno-modulatory factors could contribute to muscle regeneration. However, early diagnosis would be fundamental for early therapeutic interventions to prevent muscle atrophy. Furthermore, transcriptomic studies on patient-derived stem cells might give valuable insight into the myopathogene-network and could lead to new insights of GNEM-specific pathways.

VI References

Aebersold, R., Agar, J.N., Amster, I.J., Baker, M.S., Bertozzi, C.R., Boja, E.S., Costello, C.E., Cravatt, B.F., Fenselau, C., Garcia, B.A., et al. (2018). How many human proteoforms are there? Nat Chem Biol *14*, 206-214. 10.1038/nchembio.2576.

Agatemor, C., Buettner, M.J., Ariss, R., Muthiah, K., Saeui, C.T., and Yarema, K.J. (2019). Exploiting metabolic glycoengineering to advance healthcare. Nat Rev Chem *3*, 605-620. 10.1038/s41570-019-0126-y.

Ahrens, J., Foadi, N., Eberhardt, A., Haeseler, G., Dengler, R., Leffler, A., Muhlenhoff, M., Gerardy-Schahn, R., and Leuwer, M. (2011). Defective polysialylation and sialylation induce opposite effects on gating of the skeletal Na+ channel NaV1.4 in Chinese hamster ovary cells. Pharmacology *87*, 311-317. 10.1159/000327389.

Angata, K., and Fukuda, M. (2003). Polysialyltransferases: major players in polysialic acid synthesis on the neural cell adhesion molecule. Biochimie *85*, 195-206. 10.1016/s0300-9084(03)00051-8.

Angata, K., Suzuki, M., and Fukuda, M. (2002). ST8Sia II and ST8Sia IV polysialyltransferases exhibit marked differences in utilizing various acceptors containing oligosialic acid and short polysialic acid. The basis for cooperative polysialylation by two enzymes. J Biol Chem *277*, 36808-36817. 10.1074/jbc.M204632200.

Argov, Z., and Yarom, R. (1984). "Rimmed vacuole myopathy" sparing the quadriceps. A unique disorder in Iranian Jews. J Neurol Sci *64*, 33-43. 10.1016/0022-510x(84)90053-4.

Arikawa-Hirasawa, E., Le, A.H., Nishino, I., Nonaka, I., Ho, N.C., Francomano, C.A., Govindraj, P., Hassell, J.R., Devaney, J.M., Spranger, J., et al. (2002). Structural and functional mutations of the perlecan gene cause Schwartz-Jampel syndrome, with myotonic myopathy and chondrodysplasia. Am J Hum Genet *70*, 1368-1375. 10.1086/340390.

Baumann, A.M., Bakkers, M.J., Buettner, F.F., Hartmann, M., Grove, M., Langereis, M.A., de Groot, R.J., and Muhlenhoff, M. (2015). 9-O-Acetylation of sialic acids is catalysed by CASD1 via a covalent acetyl-enzyme intermediate. Nat Commun *6*, 7673. 10.1038/ncomms8673.

Benarroch, L., Bonne, G., Rivier, F., and Hamroun, D. (2024a). The 2024 version of the gene table of neuromuscular disorders (nuclear genome). Neuromuscul Disord *34*, 126-170. 10.1016/j.nmd.2023.12.007.

Benarroch, L., Bonne, G., Rivier, F., Procaccio, V., and Hamroun, D. (2024b). The 2025 version of the gene table of neuromuscular disorders (nuclear genome). Neuromuscul Disord *46*, 105261. 10.1016/j.nmd.2024.105261.

Bennett, E., Urcan, M.S., Tinkle, S.S., Koszowski, A.G., and Levinson, S.R. (1997). Contribution of sialic acid to the voltage dependence of sodium channel gating. A possible electrostatic mechanism. J Gen Physiol *109*, 327-343. 10.1085/jgp.109.3.327.

Bennett, E.P., Mandel, U., Clausen, H., Gerken, T.A., Fritz, T.A., and Tabak, L.A. (2012). Control of mucin-type O-glycosylation: a classification of the polypeptide GalNAc-transferase gene family. Glycobiology *22*, 736-756. 10.1093/glycob/cwr182.

Blake, D.J., Weir, A., Newey, S.E., and Davies, K.E. (2002). Function and genetics of dystrophin and dystrophin-related proteins in muscle. Physiol Rev *82*, 291-329. 10.1152/physrev.00028.2001.

Blazev, R., Ashwood, C., Abrahams, J.L., Chung, L.H., Francis, D., Yang, P., Watt, K.I., Qian, H., Quaife-Ryan, G.A., Hudson, J.E., et al. (2021). Integrated Glycoproteomics Identifies a Role of N-Glycosylation and Galectin-1 on Myogenesis and Muscle Development. Mol Cell Proteomics *20*, 100030. 10.1074/mcp.RA120.002166.

Block, B.A., Imagawa, T., Campbell, K.P., and Franzini-Armstrong, C. (1988). Structural evidence for direct interaction between the molecular components of the transverse tubule/sarcoplasmic reticulum junction in skeletal muscle. J Cell Biol *107*, 2587-2600. 10.1083/jcb.107.6.2587.

Bojar, D., Meche, L., Meng, G., Eng, W., Smith, D.F., Cummings, R.D., and Mahal, L.K. (2022). A Useful Guide to Lectin Binding: Machine-Learning Directed Annotation of 57 Unique Lectin Specificities. ACS Chem Biol *17*, 2993-3012. 10.1021/acschembio.1c00689.

Bosch-Morato, M., Iriondo, C., Guivernau, B., Valls-Comamala, V., Vidal, N., Olive, M., Querfurth, H., and Munoz, F.J. (2016). Increased amyloid beta-peptide uptake in skeletal muscle is induced by hyposialylation and may account for apoptosis in GNE myopathy. Oncotarget *7*, 13354-13371. 10.18632/oncotarget.7997.

Broccolini, A., Gliubizzi, C., Pavoni, E., Gidaro, T., Morosetti, R., Sciandra, F., Giardina, B., Tonali, P., Ricci, E., Brancaccio, A., and Mirabella, M. (2005). alpha-Dystroglycan does not play a major pathogenic role in autosomal recessive hereditary inclusion-body myopathy. Neuromuscul Disord *15*, 177-184. 10.1016/j.nmd.2004.10.001.

Caldwell, J.H., Campbell, D.T., and Beam, K.G. (1986). Na channel distribution in vertebrate skeletal muscle. J Gen Physiol *87*, 907-932. 10.1085/jgp.87.6.907.

Cannon, S.C. (2018). Sodium Channelopathies of Skeletal Muscle. Handb Exp Pharmacol *246*, 309-330. 10.1007/164_2017_52.

Capkovic, K.L., Stevenson, S., Johnson, M.C., Thelen, J.J., and Cornelison, D.D. (2008). Neural cell adhesion molecule (NCAM) marks adult myogenic cells committed to differentiation. Exp Cell Res *314*, 1553-1565. 10.1016/j.yexcr.2008.01.021.

Carrillo, N., Malicdan, M.C., Leoyklang, P., Shrader, J.A., Joe, G., Slota, C., Perreault, J., Heiss, J.D., Class, B., Liu, C.Y., et al. (2021). Safety and efficacy of N-acetylmannosamine (ManNAc) in patients with GNE myopathy: an open-label phase 2 study. Genet Med *23*, 2067-2075. 10.1038/s41436-021-01259-x.

Celeste, F.V., Vilboux, T., Ciccone, C., de Dios, J.K., Malicdan, M.C., Leoyklang, P., McKew, J.C., Gahl, W.A., Carrillo-Carrasco, N., and Huizing, M. (2014). Mutation update for GNE gene variants associated with GNE myopathy. Hum Mutat *35*, 915-926. 10.1002/humu.22583.

Chakravorty, S., Berger, K., Arafat, D., Nallamilli, B.R.R., Subramanian, H.P., Joseph, S., Anderson, M.E., Campbell, K.P., Glass, J., Gibson, G., and Hegde, M. (2019). Clinical utility of RNA sequencing to resolve unusual GNE myopathy with a novel promoter deletion. Muscle Nerve *60*, 98-103. 10.1002/mus.26486.

Chapman, M.A., Mukund, K., Subramaniam, S., Brenner, D., and Lieber, R.L. (2017). Three distinct cell populations express extracellular matrix proteins and increase in number during skeletal muscle fibrosis. Am J Physiol Cell Physiol *312*, C131-C143. 10.1152/ajpcell.00226.2016.

Chen, X., Sun, Y., Zhang, T., Roepstorff, P., and Yang, F. (2021). Comprehensive Analysis of the Proteome and PTMomes of C2C12 Myoblasts Reveals that Sialylation Plays a Role in the Differentiation of Skeletal Muscle Cells. J Proteome Res *20*, 222-235. 10.1021/acs.jproteome.0c00353.

Cho, A., Christine, M., Malicdan, V., Miyakawa, M., Nonaka, I., Nishino, I., and Noguchi, S. (2017). Sialic acid deficiency is associated with oxidative stress leading to muscle atrophy and weakness in GNE myopathy. Hum Mol Genet *26*, 3081-3093. 10.1093/hmg/ddx192.

Comb, D.G., and Roseman, S. (1958). Enzymic synthesis of N-acetyl-D-mannosamine. Biochim Biophys Acta *29*, 653-654. 10.1016/0006-3002(58)90031-3.

Conejo, R., de Alvaro, C., Benito, M., Cuadrado, A., and Lorenzo, M. (2002). Insulin restores differentiation of Ras-transformed C2C12 myoblasts by inducing NF-kappaB through an AKT/P70S6K/p38-MAPK pathway. Oncogene *21*, 3739-3753. 10.1038/sj.onc.1205469.

Conejo, R., Valverde, A.M., Benito, M., and Lorenzo, M. (2001). Insulin produces myogenesis in C2C12 myoblasts by induction of NF-kappaB and downregulation of AP-1 activities. J Cell Physiol *186*, 82-94. 10.1002/1097-4652(200101)186:1<82::AID-JCP1001>3.0.CO;2-R.

Crowe, K.E., Zygmunt, D.A., Heller, K., Rodino-Klapac, L., Noguchi, S., Nishino, I., and Martin, P.T. (2022). Visualizing Muscle Sialic Acid Expression in the GNED207VTgGne-/-Cmah-/- Model of GNE Myopathy: A Comparison of Dietary and Gene Therapy Approaches. J Neuromuscul Dis *9*, 53-71. 10.3233/JND-200575.

Dewulf, M., Koster, D.V., Sinha, B., Viaris de Lesegno, C., Chambon, V., Bigot, A., Bensalah, M., Negroni, E., Tardif, N., Podkalicka, J., et al. (2019). Dystrophy-associated caveolin-3 mutations reveal that caveolae couple IL6/STAT3 signaling with mechanosensing in human muscle cells. Nat Commun *10*, 1974. 10.1038/s41467-019-09405-5.

Dowling, J.J., Weihl, C.C., and Spencer, M.J. (2021). Molecular and cellular basis of genetically inherited skeletal muscle disorders. Nat Rev Mol Cell Biol *22*, 713-732. 10.1038/s41580-021-00389-z.

Du, J., Shui, H., Chen, R., Dong, Y., Xiao, C., Hu, Y., and Wong, N.K. (2024). Neuraminidase-1 (NEU1): Biological Roles and Therapeutic Relevance in Human Disease. Curr Issues Mol Biol *46*, 8031-8052. 10.3390/cimb46080475.

Dube, D.H., and Bertozzi, C.R. (2003). Metabolic oligosaccharide engineering as a tool for glycobiology. Curr Opin Chem Biol *7*, 616-625. 10.1016/j.cbpa.2003.08.006.

Eckhardt, M., Muhlenhoff, M., Bethe, A., and Gerardy-Schahn, R. (1996). Expression cloning of the Golgi CMP-sialic acid transporter. Proc Natl Acad Sci U S A *93*, 7572-7576. 10.1073/pnas.93.15.7572.

Eisenberg, I., Avidan, N., Potikha, T., Hochner, H., Chen, M., Olender, T., Barash, M., Shemesh, M., Sadeh, M., Grabov-Nardini, G., et al. (2001). The UDP-N-acetylglucosamine 2-

epimerase/N-acetylmannosamine kinase gene is mutated in recessive hereditary inclusion body myopathy. Nat Genet *29*, 83-87. 10.1038/ng718.

Ferreira, H., Seppala, R., Pinto, R., Huizing, M., Martins, E., Braga, A.C., Gomes, L., Krasnewich, D.M., Sa Miranda, M.C., and Gahl, W.A. (1999). Sialuria in a Portuguese girl: clinical, biochemical, and molecular characteristics. Mol Genet Metab *67*, 131-137. 10.1006/mgme.1999.2852.

Freeze, H.H., Boyce, M., Zachara, N.E., Hart, G.W., and Schnaar, R.L. (2022). Glycosylation Precursors. In Essentials of Glycobiology, A. Varki, R.D. Cummings, J.D. Esko, P. Stanley, G.W. Hart, M. Aebi, D. Mohnen, T. Kinoshita, N.H. Packer, J.H. Prestegard, et al., eds. pp. 53-66. 10.1101/glycobiology.4e.5.

Gagiannis, D., Orthmann, A., Danssmann, I., Schwarzkopf, M., Weidemann, W., and Horstkorte, R. (2007). Reduced sialylation status in UDP-N-acetylglucosamine-2-epimerase/N-acetylmannosamine kinase (GNE)-deficient mice. Glycoconj J *24*, 125-130. 10.1007/s10719-006-9019-7.

Gehle, V.M., Walcott, E.C., Nishizaki, T., and Sumikawa, K. (1997). N-glycosylation at the conserved sites ensures the expression of properly folded functional ACh receptors. Brain Res Mol Brain Res *45*, 219-229. 10.1016/s0169-328x(96)00256-2.

Ghosh, S., and Roseman, S. (1961). Enzymatic phosphorylation of N-acetyl-D-mannosamine. Proc Natl Acad Sci U S A *47*, 955-958. 10.1073/pnas.47.7.955.

Gloster, T.M., Zandberg, W.F., Heinonen, J.E., Shen, D.L., Deng, L., and Vocadlo, D.J. (2011). Hijacking a biosynthetic pathway yields a glycosyltransferase inhibitor within cells. Nat Chem Biol *7*, 174-181. 10.1038/nchembio.520.

Go, S., Go, S., Veillon, L., Ciampa, M.G., Mauri, L., Sato, C., Kitajima, K., Prinetti, A., Sonnino, S., and Inokuchi, J.I. (2017). Altered expression of ganglioside GM3 molecular species and a potential regulatory role during myoblast differentiation. J Biol Chem *292*, 7040-7051. 10.1074/jbc.M116.771253.

Gorenflos Lopez, J.L., Schmieder, P., Kemnitz-Hassanin, K., Asikoglu, H.C., Celik, A., Stieger, C.E., Fiedler, D., Hinderlich, S., and Hackenberger, C.P.R. (2023). Real-time monitoring of the sialic acid biosynthesis pathway by NMR. Chem Sci *14*, 3482-3492. 10.1039/d2sc06986e.

Granger, A., Pinto, M.V., Milone, M., and Liewluck, T. (2022). Glycogen accumulation in GNE myopathy. Neuromuscul Disord *32*, 774-775. 10.1016/j.nmd.2022.07.396.

Griffin, M.E., and Hsieh-Wilson, L.C. (2022). Tools for mammalian glycoscience research. Cell *185*, 2657-2677. 10.1016/j.cell.2022.06.016.

Gross, H.J., and Brossmer, R. (1988). Enzymatic introduction of a fluorescent sialic acid into oligosaccharide chains of glycoproteins. Eur J Biochem *177*, 583-589. 10.1111/j.1432-1033.1988.tb14410.x.

Gross, H.J., Rose, U., Krause, J.M., Paulson, J.C., Schmid, K., Feeney, R.E., and Brossmer, R. (1989). Transfer of synthetic sialic acid analogues to N- and O-linked glycoprotein glycans using four different mammalian sialyltransferases. Biochemistry *28*, 7386-7392. 10.1021/bi00444a036.

Gu, X., and Wang, D.I. (1998). Improvement of interferon-gamma sialylation in Chinese hamster ovary cell culture by feeding of N-acetylmannosamine. Biotechnol Bioeng *58*, 642-648.

Guberman, M., and Seeberger, P.H. (2019). Automated Glycan Assembly: A Perspective. J Am Chem Soc *141*, 5581-5592. 10.1021/jacs.9b00638.

Haltiwanger, R.S., Blomberg, M.A., and Hart, G.W. (1992). Glycosylation of nuclear and cytoplasmic proteins. Purification and characterization of a uridine diphospho-N-acetylglucosamine:polypeptide beta-N-acetylglucosaminyltransferase. J Biol Chem *267*, 9005-9013.

Hart, G.W. (2019). Nutrient regulation of signaling and transcription. J Biol Chem *294*, 2211-2231. 10.1074/jbc.AW119.003226.

Hicks, M.R., and Pyle, A.D. (2023). The emergence of the stem cell niche. Trends Cell Biol *33*, 112-123. 10.1016/j.tcb.2022.07.003.

Hinderlich, S., Stasche, R., Zeitler, R., and Reutter, W. (1997). A bifunctional enzyme catalyzes the first two steps in N-acetylneuraminic acid biosynthesis of rat liver. Purification and characterization of UDP-N-acetylglucosamine 2-epimerase/N-acetylmannosamine kinase. J Biol Chem *272*, 24313-24318. 10.1074/jbc.272.39.24313.

Hinderlich, S., Weidemann, W., Yardeni, T., Horstkorte, R., and Huizing, M. (2015). UDP-GlcNAc 2-Epimerase/ManNAc Kinase (GNE): A Master Regulator of Sialic Acid Synthesis. Top Curr Chem *366*, 97-137. 10.1007/128_2013_464.

Hirata, T., Mishra, S.K., Nakamura, S., Saito, K., Motooka, D., Takada, Y., Kanzawa, N., Murakami, Y., Maeda, Y., Fujita, M., et al. (2018). Identification of a Golgi GPI-N-acetylgalactosamine transferase with tandem transmembrane regions in the catalytic domain. Nat Commun *9*, 405. 10.1038/s41467-017-02799-0.

Holdener, B.C., and Haltiwanger, R.S. (2019). Protein O-fucosylation: structure and function. Curr Opin Struct Biol *56*, 78-86. 10.1016/j.sbi.2018.12.005.

Honke, K., and Taniguchi, N. (2002). Sulfotransferases and sulfated oligosaccharides. Med Res Rev *22*, 637-654. 10.1002/med.10020.

Horstkorte, R., Nohring, S., Danker, K., Effertz, K., Reutter, W., and Lucka, L. (2000). Protein kinase C phosphorylates and regulates UDP-N-acetylglucosamine-2-epimerase/N-acetylmannosamine kinase. FEBS Lett *470*, 315-318. 10.1016/s0014-5793(00)01331-4.

Horstkorte, R., Nohring, S., Wiechens, N., Schwarzkopf, M., Danker, K., Reutter, W., and Lucka, L. (1999). Tissue expression and amino acid sequence of murine UDP-N-acetylglucosamine-2-epimerase/N-acetylmannosamine kinase. Eur J Biochem *260*, 923-927. 10.1046/j.1432-1327.1999.00253.x.

Horstkorte, R., Rau, K., Laabs, S., Danker, K., and Reutter, W. (2004). Biochemical engineering of the N-acyl side chain of sialic acid leads to increased calcium influx from intracellular compartments and promotes differentiation of HL60 cells. FEBS Lett *571*, 99-102. 10.1016/j.febslet.2004.06.067.

Huai, G., Qi, P., Yang, H., and Wang, Y. (2016). Characteristics of alpha-Gal epitope, anti-Gal antibody, alpha1,3 galactosyltransferase and its clinical exploitation (Review). Int J Mol Med *37*, 11-20. 10.3892/ijmm.2015.2397.

Huizing, M., Rakocevic, G., Sparks, S.E., Mamali, I., Shatunov, A., Goldfarb, L., Krasnewich, D., Gahl, W.A., and Dalakas, M.C. (2004). Hypoglycosylation of alpha-dystroglycan in patients with hereditary IBM due to GNE mutations. Mol Genet Metab *81*, 196-202. 10.1016/j.ymgme.2003.11.012.

Humphrey, J.D., Dufresne, E.R., and Schwartz, M.A. (2014). Mechanotransduction and extracellular matrix homeostasis. Nat Rev Mol Cell Biol *15*, 802-812. 10.1038/nrm3896.

Ilouz, N., Harazi, A., Guttman, M., Daya, A., Ruppo, S., Yakovlev, L., and Mitrani-Rosenbaum, S. (2022). In vivo and in vitro genome editing to explore GNE functions. Front Genome Ed *4*, 930110. 10.3389/fgeed.2022.930110.

James, W.M., and Agnew, W.S. (1987). Multiple oligosaccharide chains in the voltage-sensitive Na channel from electrophorus electricus: evidence for alpha-2,8-linked polysialic acid. Biochem Biophys Res Commun *148*, 817-826. 10.1016/0006-291x(87)90949-1.

Jang-Lee, J., North, S.J., Sutton-Smith, M., Goldberg, D., Panico, M., Morris, H., Haslam, S., and Dell, A. (2006). Glycomic profiling of cells and tissues by mass spectrometry: fingerprinting and sequencing methodologies. Methods Enzymol *415*, 59-86. 10.1016/S0076-6879(06)15005-3.

Janot, M., Audfray, A., Loriol, C., Germot, A., Maftah, A., and Dupuy, F. (2009). Glycogenome expression dynamics during mouse C2C12 myoblast differentiation suggests a sequential reorganization of membrane glycoconjugates. BMC Genomics *10*, 483. 10.1186/1471-2164-10-483.

Jiang, H., Lopez-Aguilar, A., Meng, L., Gao, Z., Liu, Y., Tian, X., Yu, G., Ovryn, B., Moremen, K.W., and Wu, P. (2018). Modulating Cell-Surface Receptor Signaling and Ion Channel Functions by In Situ Glycan Editing. Angew Chem Int Ed Engl *57*, 967-971. 10.1002/anie.201706535.

Jourdian, G.W., Swanson, A.L., Watson, D., and Roseman, S. (1964). Isolation of Sialic Acid 9-Phosphatase from Human Erythrocytes. J Biol Chem *239*, PC2714-2716.

Kayser, H., Zeitler, R., Kannicht, C., Grunow, D., Nuck, R., and Reutter, W. (1992). Biosynthesis of a nonphysiological sialic acid in different rat organs, using N-propanoyl-D-hexosamines as precursors. J Biol Chem *267*, 16934-16938.

Keppler, O.T., Hinderlich, S., Langner, J., Schwartz-Albiez, R., Reutter, W., and Pawlita, M. (1999). UDP-GlcNAc 2-epimerase: a regulator of cell surface sialylation. Science *284*, 1372-1376. 10.1126/science.284.5418.1372.

Keppler, O.T., Horstkorte, R., Pawlita, M., Schmidt, C., and Reutter, W. (2001). Biochemical engineering of the N-acyl side chain of sialic acid: biological implications. Glycobiology *11*, 11R-18R. 10.1093/glycob/11.2.11r.

Klinge, L., Harris, J., Sewry, C., Charlton, R., Anderson, L., Laval, S., Chiu, Y.H., Hornsey, M., Straub, V., Barresi, R., et al. (2010). Dysferlin associates with the developing T-tubule system in rodent and human skeletal muscle. Muscle Nerve *41*, 166-173. 10.1002/mus.21166.

Kornfeld, R., and Kornfeld, S. (1985). Assembly of asparagine-linked oligosaccharides. Annu Rev Biochem *54*, 631-664. 10.1146/annurev.bi.54.070185.003215.

Kornfeld, S., Kornfeld, R., Neufeld, E.F., and O'Brien, P.J. (1964). The Feedback Control of Sugar Nucleotide Biosynthesis in Liver. Proc Natl Acad Sci U S A *52*, 371-379. 10.1073/pnas.52.2.371.

Kramerova, I., Kudryashova, E., Tidball, J.G., and Spencer, M.J. (2004). Null mutation of calpain 3 (p94) in mice causes abnormal sarcomere formation in vivo and in vitro. Hum Mol Genet *13*, 1373-1388. 10.1093/hmg/ddh153.

Krause, S., Schlotter-Weigel, B., Walter, M.C., Najmabadi, H., Wiendl, H., Muller-Hocker, J., Muller-Felber, W., Pongratz, D., and Lochmuller, H. (2003). A novel homozygous missense mutation in the GNE gene of a patient with quadriceps-sparing hereditary inclusion body myopathy associated with muscle inflammation. Neuromuscul Disord *13*, 830-834. 10.1016/s0960-8966(03)00140-8.

Larsen, I.S.B., Narimatsu, Y., Joshi, H.J., Siukstaite, L., Harrison, O.J., Brasch, J., Goodman, K.M., Hansen, L., Shapiro, L., Honig, B., et al. (2017). Discovery of an O-mannosylation pathway selectively serving cadherins and protocadherins. Proc Natl Acad Sci U S A *114*, 11163-11168. 10.1073/pnas.1708319114.

Lemieux, G.A., Yarema, K.J., Jacobs, C.L., and Bertozzi, C.R. (1999). Exploiting differences in sialoside expression for selective targeting of MRI contrast reagents. Journal of the American Chemical Society *121*, 4278-4279. DOI 10.1021/ja984228m.

Lewis, A.L., Chen, X., Schnaar, R.L., and Varki, A. (2022). Sialic Acids and Other Nonulosonic Acids. In Essentials of Glycobiology, A. Varki, R.D. Cummings, J.D. Esko, P. Stanley, G.W. Hart, M. Aebi, D. Mohnen, T. Kinoshita, N.H. Packer, J.H. Prestegard, et al., eds. pp. 185-204. 10.1101/glycobiology.4e.15.

Lilja, K.C., Zhang, N., Magli, A., Gunduz, V., Bowman, C.J., Arpke, R.W., Darabi, R., Kyba, M., Perlingeiro, R., and Dynlacht, B.D. (2017). Pax7 remodels the chromatin landscape in skeletal muscle stem cells. PLoS One *12*, e0176190. 10.1371/journal.pone.0176190.

Liu, X., Zhang, Y., Zhang, S., Sun, A., Zheng, D., Fan, D., and Liu, X. (2022). Different electrophysiology patterns in GNE myopathy. Orphanet J Rare Dis *17*, 206. 10.1186/s13023-022-02355-0.

Lochmuller, H., Behin, A., Caraco, Y., Lau, H., Mirabella, M., Tournev, I., Tarnopolsky, M., Pogoryelova, O., Woods, C., Lai, A., et al. (2019). A phase 3 randomized study evaluating sialic acid extended-release for GNE myopathy. Neurology *92*, e2109-e2117. 10.1212/WNL.0000000000006932.

Machado, L., Esteves de Lima, J., Fabre, O., Proux, C., Legendre, R., Szegedi, A., Varet, H., Ingerslev, L.R., Barres, R., Relaix, F., and Mourikis, P. (2017). In Situ Fixation Redefines Quiescence and Early Activation of Skeletal Muscle Stem Cells. Cell Rep *21*, 1982-1993. 10.1016/j.celrep.2017.10.080.

Malicdan, M.C., Noguchi, S., Hayashi, Y.K., and Nishino, I. (2008). Muscle weakness correlates with muscle atrophy and precedes the development of inclusion body or rimmed vacuoles in the mouse model of DMRV/hIBM. Physiol Genomics *35*, 106-115. 10.1152/physiolgenomics.90219.2008.

Malicdan, M.C., Noguchi, S., Hayashi, Y.K., Nonaka, I., and Nishino, I. (2009). Prophylactic treatment with sialic acid metabolites precludes the development of the myopathic phenotype in the DMRV-hIBM mouse model. Nat Med *15*, 690-695. 10.1038/nm.1956.

Malicdan, M.C., Noguchi, S., Nonaka, I., Hayashi, Y.K., and Nishino, I. (2007). A Gne knockout mouse expressing human GNE D176V mutation develops features similar to distal myopathy with rimmed vacuoles or hereditary inclusion body myopathy. Hum Mol Genet *16*, 2669-2682. 10.1093/hmg/ddm220.

Malicdan, M.C., Noguchi, S., Tokutomi, T., Goto, Y., Nonaka, I., Hayashi, Y.K., and Nishino, I. (2012). Peracetylated N-acetylmannosamine, a synthetic sugar molecule, efficiently rescues muscle phenotype and biochemical defects in mouse model of sialic acid-deficient myopathy. J Biol Chem *287*, 2689-2705. 10.1074/jbc.M111.297051.

Maliekal, P., Vertommen, D., Delpierre, G., and Van Schaftingen, E. (2006). Identification of the sequence encoding N-acetylneuraminate-9-phosphate phosphatase. Glycobiology *16*, 165-172. 10.1093/glycob/cwj050.

Manis, C., Casula, M., Roos, A., Hentschel, A., Vorgerd, M., Pogoryelova, O., Derksen, A., Spendiff, S., Lochmuller, H., and Caboni, P. (2024). Ion Mobility QTOF-MS Untargeted Lipidomics of Human Serum Reveals a Metabolic Fingerprint for GNE Myopathy. Molecules *29*. 10.3390/molecules29215211.

Mann, C.J., Perdiguero, E., Kharraz, Y., Aguilar, S., Pessina, P., Serrano, A.L., and Munoz-Canoves, P. (2011). Aberrant repair and fibrosis development in skeletal muscle. Skelet Muscle *1*, 21. 10.1186/2044-5040-1-21.

Matsuda, C., Hayashi, Y.K., Ogawa, M., Aoki, M., Murayama, K., Nishino, I., Nonaka, I., Arahata, K., and Brown, R.H., Jr. (2001). The sarcolemmal proteins dysferlin and caveolin-3 interact in skeletal muscle. Hum Mol Genet *10*, 1761-1766. 10.1093/hmg/10.17.1761.

McKinnell, I.W., Ishibashi, J., Le Grand, F., Punch, V.G., Addicks, G.C., Greenblatt, J.F., Dilworth, F.J., and Rudnicki, M.A. (2008). Pax7 activates myogenic genes by recruitment of a histone methyltransferase complex. Nat Cell Biol *10*, 77-84. 10.1038/ncb1671.

Meyer, R.A., Sweeney, H.L., and Kushmerick, M.J. (1984). A simple analysis of the "phosphocreatine shuttle". Am J Physiol *246*, C365-377. 10.1152/ajpcell.1984.246.5.C365.

Mitrani-Rosenbaum, S., Yakovlev, L., Becker Cohen, M., Argov, Z., Fellig, Y., and Harazi, A. (2022). Pre Clinical Assessment of AAVrh74.MCK.GNE Viral Vector Therapeutic Potential: Robust Activity Despite Lack of Consistent Animal Model for GNE Myopathy. J Neuromuscul Dis *9*, 179-192. 10.3233/JND-210755.

Moremen, K.W., Tiemeyer, M., and Nairn, A.V. (2012). Vertebrate protein glycosylation: diversity, synthesis and function. Nat Rev Mol Cell Biol *13*, 448-462. 10.1038/nrm3383.

Moreno, C.A.M., Artilheiro, M.C., Fonseca, A., Camelo, C.G., de Medeiros, G.C., Sassi, F.C., de Andrade, C.R.F., Donkervoort, S., Silva, A.M.S., Dalfior-Junior, L., et al. (2023). Clinical Manifestation of Nebulin-Associated Nemaline Myopathy. Neurol Genet *9*, e200056. 10.1212/NXG.0000000000200056.

Mori-Yoshimura, M., Suzuki, N., Katsuno, M., Takahashi, M.P., Yamashita, S., Oya, Y., Hashizume, A., Yamada, S., Nakamori, M., Izumi, R., et al. (2023). Efficacy confirmation study

of aceneuramic acid administration for GNE myopathy in Japan. Orphanet J Rare Dis *18*, 241. 10.1186/s13023-023-02850-y.

Morin, P., Sagne, C., and Gasnier, B. (2004). Functional characterization of wild-type and mutant human sialin. EMBO J *23*, 4560-4570. 10.1038/sj.emboj.7600464.

Morozzi, C., Sedlakova, J., Serpi, M., Avigliano, M., Carbajo, R., Sandoval, L., Valles-Ayoub, Y., Crutcher, P., Thomas, S., and Pertusati, F. (2019). Targeting GNE Myopathy: A Dual Prodrug Approach for the Delivery of N-Acetylmannosamine 6-Phosphate. J Med Chem *62*, 8178-8193. 10.1021/acs.jmedchem.9b00833.

Mukund, K., and Subramaniam, S. (2020). Skeletal muscle: A review of molecular structure and function, in health and disease. Wiley Interdiscip Rev Syst Biol Med *12*, e1462. 10.1002/wsbm.1462.

Munster-Kuhnel, A.K., Tiralongo, J., Krapp, S., Weinhold, B., Ritz-Sedlacek, V., Jacob, U., and Gerardy-Schahn, R. (2004). Structure and function of vertebrate CMP-sialic acid synthetases. Glycobiology *14*, 43R-51R. 10.1093/glycob/cwh113.

Nairn, A.V., York, W.S., Harris, K., Hall, E.M., Pierce, J.M., and Moremen, K.W. (2008). Regulation of glycan structures in animal tissues: transcript profiling of glycan-related genes. J Biol Chem *283*, 17298-17313. 10.1074/jbc.M801964200.

Nakamura, K., Tsukamoto, Y., Hijiya, N., Higuchi, Y., Yano, S., Yokoyama, S., Kumamoto, T., and Moriyama, M. (2010). Induction of GNE in myofibers after muscle injury. Pathobiology *77*, 191-199. 10.1159/000292652.

Narimatsu, Y., Joshi, H.J., Nason, R., Van Coillie, J., Karlsson, R., Sun, L., Ye, Z., Chen, Y.H., Schjoldager, K.T., Steentoft, C., et al. (2019). An Atlas of Human Glycosylation Pathways Enables Display of the Human Glycome by Gene Engineered Cells. Mol Cell *75*, 394-407 e395. 10.1016/j.molcel.2019.05.017.

Neu, C.T., Weilepp, L., Bork, K., Gesper, A., and Horstkorte, R. (2024). GNE deficiency impairs Myogenesis in C2C12 cells and cannot be rescued by ManNAc supplementation. Glycobiology *34*. 10.1093/glycob/cwae004.

Noguchi, S., Keira, Y., Murayama, K., Ogawa, M., Fujita, M., Kawahara, G., Oya, Y., Imazawa, M., Goto, Y., Hayashi, Y.K., et al. (2004). Reduction of UDP-N-acetylglucosamine 2-epimerase/N-acetylmannosamine kinase activity and sialylation in distal myopathy with rimmed vacuoles. J Biol Chem *279*, 11402-11407. 10.1074/jbc.M313171200.

North, S.J., Hitchen, P.G., Haslam, S.M., and Dell, A. (2009). Mass spectrometry in the analysis of N-linked and O-linked glycans. Curr Opin Struct Biol *19*, 498-506. 10.1016/j.sbi.2009.05.005.

Oates, E.C., Jones, K.J., Donkervoort, S., Charlton, A., Brammah, S., Smith, J.E., 3rd, Ware, J.S., Yau, K.S., Swanson, L.C., Whiffin, N., et al. (2018). Congenital Titinopathy: Comprehensive characterization and pathogenic insights. Ann Neurol *83*, 1105-1124. 10.1002/ana.25241.

Olive, M., Goldfarb, L.G., Shatunov, A., Fischer, D., and Ferrer, I. (2005). Myotilinopathy: refining the clinical and myopathological phenotype. Brain *128*, 2315-2326. 10.1093/brain/awh576.

Ortiz-Meoz, R.F., Jiang, J., Lazarus, M.B., Orman, M., Janetzko, J., Fan, C., Duveau, D.Y., Tan, Z.W., Thomas, C.J., and Walker, S. (2015). A small molecule that inhibits OGT activity in cells. ACS Chem Biol *10*, 1392-1397. 10.1021/acschembio.5b00004.

Paccalet, T., Coulombe, Z., and Tremblay, J.P. (2010). Ganglioside GM3 levels are altered in a mouse model of HIBM: GM3 as a cellular marker of the disease. PLoS One *5*, e10055. 10.1371/journal.pone.0010055.

Park, S.Y., Ryu, J., and Lee, W. (2005). O-GlcNAc modification on IRS-1 and Akt2 by PUGNAc inhibits their phosphorylation and induces insulin resistance in rat primary adipocytes. Exp Mol Med *37*, 220-229. 10.1038/emm.2005.30.

Park, Y.E., Park, E., Choi, J., Go, H., Park, D.B., Kim, M.Y., Sung, N.J., Kim, L., and Shin, J.H. (2023). Pharmacokinetics and clinical efficacy of 6'-sialyllactose in patients with GNE myopathy: Randomized pilot trial. Biomed Pharmacother *168*, 115689. 10.1016/j.biopha.2023.115689.

Patzel, K.A., Yardeni, T., Le Poec-Celic, E., Leoyklang, P., Dorward, H., Alonzi, D.S., Kukushkin, N.V., Xu, B., Zhang, Y., Sollogoub, M., et al. (2014). Non-specific accumulation of glycosphingolipids in GNE myopathy. J Inherit Metab Dis *37*, 297-308. 10.1007/s10545-013-9655-6.

Paulson, J.C., and Colley, K.J. (1989). Glycosyltransferases. Structure, localization, and control of cell type-specific glycosylation. J Biol Chem *264*, 17615-17618.

Penner, J., Mantey, L.R., Elgavish, S., Ghaderi, D., Cirak, S., Berger, M., Krause, S., Lucka, L., Voit, T., Mitrani-Rosenbaum, S., and Hinderlich, S. (2006). Influence of UDP-GlcNAc 2-epimerase/ManNAc kinase mutant proteins on hereditary inclusion body myopathy. Biochemistry *45*, 2968-2977. 10.1021/bi0522504.

Periasamy, M., and Kalyanasundaram, A. (2007). SERCA pump isoforms: their role in calcium transport and disease. Muscle Nerve *35*, 430-442. 10.1002/mus.20745.

Peters, E., Selke, P., Bork, K., Horstkorte, R., and Gesper, A. (2023). Evaluation of N-Acetylmannosamine Administration to Restore Sialylation in GNE-Deficient Human Embryonal Kidney Cells. Front Biosci (Landmark Ed) *28*, 300. 10.31083/j.fbl2811300.

Pham, N.D., Pang, P.C., Krishnamurthy, S., Wands, A.M., Grassi, P., Dell, A., Haslam, S.M., and Kohler, J.J. (2017). Effects of altered sialic acid biosynthesis on N-linked glycan branching and cell surface interactions. J Biol Chem *292*, 9637-9651. 10.1074/jbc.M116.764597.

Pietrobono, S., and Stecca, B. (2021). Aberrant Sialylation in Cancer: Biomarker and Potential Target for Therapeutic Intervention? Cancers (Basel) *13*. 10.3390/cancers13092014.

Praissman, J.L., Willer, T., Sheikh, M.O., Toi, A., Chitayat, D., Lin, Y.Y., Lee, H., Stalnaker, S.H., Wang, S., Prabhakar, P.K., et al. (2016). The functional O-mannose glycan on alpha-dystroglycan contains a phospho-ribitol primed for matriglycan addition. Elife *5*. 10.7554/eLife.14473.

Protasi, F., Paolini, C., Nakai, J., Beam, K.G., Franzini-Armstrong, C., and Allen, P.D. (2002). Multiple regions of RyR1 mediate functional and structural interactions with alpha(1S)-dihydropyridine receptors in skeletal muscle. Biophys J *83*, 3230-3244. 10.1016/S0006-3495(02)75325-3.

Rabouille, C., Hui, N., Hunte, F., Kieckbusch, R., Berger, E.G., Warren, G., and Nilsson, T. (1995). Mapping the distribution of Golgi enzymes involved in the construction of complex oligosaccharides. J Cell Sci *108 (Pt 4)*, 1617-1627. 10.1242/jcs.108.4.1617.

Ramirez-Correa, G.A., Jin, W., Wang, Z., Zhong, X., Gao, W.D., Dias, W.B., Vecoli, C., Hart, G.W., and Murphy, A.M. (2008). O-linked GlcNAc modification of cardiac myofilament proteins: a novel regulator of myocardial contractile function. Circ Res *103*, 1354-1358. 10.1161/CIRCRESAHA.108.184978.

Ramirez-Correa, G.A., Ma, J., Slawson, C., Zeidan, Q., Lugo-Fagundo, N.S., Xu, M., Shen, X., Gao, W.D., Caceres, V., Chakir, K., et al. (2015). Removal of Abnormal Myofilament O-GlcNAcylation Restores Ca2+ Sensitivity in Diabetic Cardiac Muscle. Diabetes *64*, 3573-3587. 10.2337/db14-1107.

Rillahan, C.D., Antonopoulos, A., Lefort, C.T., Sonon, R., Azadi, P., Ley, K., Dell, A., Haslam, S.M., and Paulson, J.C. (2012). Global metabolic inhibitors of sialyl- and fucosyltransferases remodel the glycome. Nat Chem Biol *8*, 661-668. 10.1038/nchembio.999.

Robertson, T.A., Maley, M.A., Grounds, M.D., and Papadimitriou, J.M. (1993). The role of macrophages in skeletal muscle regeneration with particular reference to chemotaxis. Exp Cell Res *207*, 321-331. 10.1006/excr.1993.1199.

Roseman, S., Jourdian, G.W., Watson, D., and Rood, R. (1961). Enzymatic synthesis of sialic acid 9-phosphates. Proc Natl Acad Sci U S A *47*, 958-961. 10.1073/pnas.47.7.958.

Rothman, J.E., and Lodish, H.F. (1977). Synchronised transmembrane insertion and glycosylation of a nascent membrane protein. Nature *269*, 775-780. 10.1038/269775a0.

Rutishauser, U., and Landmesser, L. (1996). Polysialic acid in the vertebrate nervous system: a promoter of plasticity in cell-cell interactions. Trends Neurosci *19*, 422-427. 10.1016/0166-2236(96)10041-2.

Saito, F., Tomimitsu, H., Arai, K., Nakai, S., Kanda, T., Shimizu, T., Mizusawa, H., and Matsumura, K. (2004). A Japanese patient with distal myopathy with rimmed vacuoles: missense mutations in the epimerase domain of the UDP-N-acetylglucosamine 2-epimerase/N-acetylmannosamine kinase (GNE) gene accompanied by hyposialylation of skeletal muscle glycoproteins. Neuromuscul Disord *14*, 158-161. 10.1016/j.nmd.2003.09.006.

Sakaidani, Y., Ichiyanagi, N., Saito, C., Nomura, T., Ito, M., Nishio, Y., Nadano, D., Matsuda, T., Furukawa, K., and Okajima, T. (2012). O-linked-N-acetylglucosamine modification of mammalian Notch receptors by an atypical O-GlcNAc transferase Eogt1. Biochem Biophys Res Commun *419*, 14-19. 10.1016/j.bbrc.2012.01.098.

Samandari, M., Quint, J., Rodriguez-delaRosa, A., Sinha, I., Pourquie, O., and Tamayol, A. (2022). Bioinks and Bioprinting Strategies for Skeletal Muscle Tissue Engineering. Adv Mater *34*, e2105883. 10.1002/adma.202105883.

Saxon, E., and Bertozzi, C.R. (2000). Cell surface engineering by a modified Staudinger reaction. Science *287*, 2007-2010. 10.1126/science.287.5460.2007.

Schauer, R., and Kamerling, J.P. (2018). Exploration of the Sialic Acid World. Adv Carbohydr Chem Biochem *75*, 1-213. 10.1016/bs.accb.2018.09.001.

Schauer, R., and Wember, M. (1996). Isolation and characterization of sialate lyase from pig kidney. Biol Chem Hoppe Seyler *377*, 293-299. 10.1515/bchm3.1996.377.5.293.

Schjoldager, K.T., Narimatsu, Y., Joshi, H.J., and Clausen, H. (2020). Global view of human protein glycosylation pathways and functions. Nat Rev Mol Cell Biol *21*, 729-749. 10.1038/s41580-020-00294-x.

Schmitt, R.E., Smith, D.Y.t., Cho, D.S., Kirkeby, L.A., Resch, Z.T., Liewluck, T., Niu, Z., Milone, M., and Doles, J.D. (2022). Myogenesis defects in a patient-derived iPSC model of hereditary GNE myopathy. NPJ Regen Med *7*, 48. 10.1038/s41536-022-00238-3.

Schwarzkopf, M., Knobeloch, K.P., Rohde, E., Hinderlich, S., Wiechens, N., Lucka, L., Horak, I., Reutter, W., and Horstkorte, R. (2002). Sialylation is essential for early development in mice. Proc Natl Acad Sci U S A *99*, 5267-5270. 10.1073/pnas.072066199.

Sela, I., Goss, V., Becker-Cohen, M., Dell, A., Haslam, S.M., and Mitrani-Rosenbaum, S. (2020). The glycomic sialylation profile of GNE Myopathy muscle cells does not point to consistent hyposialylation of individual glycoconjugates. Neuromuscul Disord *30*, 621-630. 10.1016/j.nmd.2020.05.008.

Sela, I., Yakovlev, L., Becker Cohen, M., Elbaz, M., Yanay, N., Ben Shlomo, U., Yotvat, H., Fellig, Y., Argov, Z., and Mitrani-Rosenbaum, S. (2013). Variable phenotypes of knockin mice carrying the M712T Gne mutation. Neuromolecular Med *15*, 180-191. 10.1007/s12017-012-8209-7.

Shcherbakova, A., Tiemann, B., Buettner, F.F., and Bakker, H. (2017). Distinct C-mannosylation of netrin receptor thrombospondin type 1 repeats by mammalian DPY19L1 and DPY19L3. Proc Natl Acad Sci U S A *114*, 2574-2579. 10.1073/pnas.1613165114.

Sommar, K.M., and Ellis, D.B. (1972). Uridine diphosphate N-acetyl-D-glucosamine-2-epimerase from rat liver. I. Catalytic and regulatory properties. Biochim Biophys Acta *268*, 581-589. 10.1016/0005-2744(72)90355-5.

Sparks, S., Rakocevic, G., Joe, G., Manoli, I., Shrader, J., Harris-Love, M., Sonies, B., Ciccone, C., Dorward, H., Krasnewich, D., et al. (2007). Intravenous immune globulin in hereditary inclusion body myopathy: a pilot study. BMC Neurol *7*, 3. 10.1186/1471-2377-7-3.

Stanley, P. (2011). Golgi glycosylation. Cold Spring Harb Perspect Biol *3*. 10.1101/cshperspect.a005199.

Sterner, E., Flanagan, N., and Gildersleeve, J.C. (2016). Perspectives on Anti-Glycan Antibodies Gleaned from Development of a Community Resource Database. ACS Chem Biol *11*, 1773-1783. 10.1021/acschembio.6b00244.

Suzuki, M., Angata, K., Nakayama, J., and Fukuda, M. (2003). Polysialic acid and mucin type o-glycans on the neural cell adhesion molecule differentially regulate myoblast fusion. J Biol Chem *278*, 49459-49468. 10.1074/jbc.M308316200.

Takeuchi, H., Schneider, M., Williamson, D.B., Ito, A., Takeuchi, M., Handford, P.A., and Haltiwanger, R.S. (2018). Two novel protein O-glucosyltransferases that modify sites distinct from POGLUT1 and affect Notch trafficking and signaling. Proc Natl Acad Sci U S A *115*, E8395-E8402. 10.1073/pnas.1804005115.

Varki, A., Cummings, R.D., Aebi, M., Packer, N.H., Seeberger, P.H., Esko, J.D., Stanley, P., Hart, G., Darvill, A., Kinoshita, T., et al. (2015). Symbol Nomenclature for Graphical Representations of Glycans. Glycobiology *25*, 1323-1324. 10.1093/glycob/cwv091.

Voermans, N.C., Guillard, M., Doedee, R., Lammens, M., Huizing, M., Padberg, G.W., Wevers, R.A., van Engelen, B.G., and Lefeber, D.J. (2010). Clinical features, lectin staining, and a novel GNE frameshift mutation in hereditary inclusion body myopathy. Clin Neuropathol *29*, 71-77.

Wang, P., Dong, S., Shieh, J.H., Peguero, E., Hendrickson, R., Moore, M.A.S., and Danishefsky, S.J. (2013). Erythropoietin derived by chemical synthesis. Science *342*, 1357-1360. 10.1126/science.1245095.

Wild, R., Kowal, J., Eyring, J., Ngwa, E.M., Aebi, M., and Locher, K.P. (2018). Structure of the yeast oligosaccharyltransferase complex gives insight into eukaryotic N-glycosylation. Science *359*, 545-550. 10.1126/science.aar5140.

Wong, N.S., Wati, L., Nissom, P.M., Feng, H.T., Lee, M.M., and Yap, M.G. (2010). An investigation of intracellular glycosylation activities in CHO cells: effects of nucleotide sugar precursor feeding. Biotechnol Bioeng *107*, 321-336. 10.1002/bit.22812.

Wratil, P.R., Horstkorte, R., and Reutter, W. (2016). Metabolic Glycoengineering with N-Acyl Side Chain Modified Mannosamines. Angew Chem Int Ed Engl *55*, 9482-9512. 10.1002/anie.201601123.

Wuhrer, M. (2013). Glycomics using mass spectrometry. Glycoconj J *30*, 11-22. 10.1007/s10719-012-9376-3.

Xu, Y., Masuko, S., Takieddin, M., Xu, H., Liu, R., Jing, J., Mousa, S.A., Linhardt, R.J., and Liu, J. (2011). Chemoenzymatic synthesis of homogeneous ultralow molecular weight heparins. Science *334*, 498-501. 10.1126/science.1207478.

Yamashita, T., Hashiramoto, A., Haluzik, M., Mizukami, H., Beck, S., Norton, A., Kono, M., Tsuji, S., Daniotti, J.L., Werth, N., et al. (2003). Enhanced insulin sensitivity in mice lacking ganglioside GM3. Proc Natl Acad Sci U S A *100*, 3445-3449. 10.1073/pnas.0635898100.

Yang, Y., Li, L., Fei, J., and Li, Z. (2025). C2C12 myoblasts differentiate into myofibroblasts via the TGF-beta1 signaling pathway mediated by Fibulin2. Gene *936*, 149048. 10.1016/j.gene.2024.149048.

Yonekawa, T., Malicdan, M.C., Cho, A., Hayashi, Y.K., Nonaka, I., Mine, T., Yamamoto, T., Nishino, I., and Noguchi, S. (2014). Sialyllactose ameliorates myopathic phenotypes in symptomatic GNE myopathy model mice. Brain *137*, 2670-2679. 10.1093/brain/awu210.

Yoshida-Moriguchi, T., Willer, T., Anderson, M.E., Venzke, D., Whyte, T., Muntoni, F., Lee, H., Nelson, S.F., Yu, L., and Campbell, K.P. (2013). SGK196 is a glycosylation-specific O-mannose kinase required for dystroglycan function. Science *341*, 896-899. 10.1126/science.1239951.

Curriculum Vitae

Personal Details

Name:	Carolin Tanja Neu
Date of birth, birthplace:	**Aus Datenschutzgründen entfernt**
Address:	**Aus Datenschutzgründen entfernt**
Nationality:	German

Education

Sep 2000 – Jul 2005	Freie Waldorfschule Wernstein
Sep 2005 – Jul 2010	Staatliche Realschule Burgkunstadt
Aug 2010 – Jun 2011	Hanford High School, Richland, WA, USA
Sep 2011 – Jun 2014:	Meranier-Gymnasium Lichtenfels – Abitur

Scientific Education

Oct 2014 – Jan 2018:	University of Greifswald
	B. Sc. Biology
Oct 2017 – Sep 2019:	University of Greifswald
	M. Sc. Molecular Biology and Physiology
Oct 2019 – Mar 2022:	Martin-Luther-University Halle-Wittenberg
	Research assistant (Group of Prof. Dr. M. Hämmerle)
Jun 2022 – May 2025	Institute for Physiological Chemistry, MLU Halle-Wittenberg
	PhD Thesis (Group of Prof. Dr. Rüdiger Horstkorte)
Nov 2023 – Feb 2024	Life Science Department, Imperial College London, UK
	Visiting PhD student (Group of Prof. A. Dell and Prof. S. Haslam)

List of Publications and Presentations

Parts of the results presented in this work were published in:

Neu CT, Weilepp L, Bork K, Gesper A, Horstkorte R. GNE deficiency impairs Myogenesis in C2C12 cells and cannot be rescued by ManNAc supplementation. Glycobiology. 2024 Apr 1;34(3):cwae004. doi: 10.1093/glycob/cwae004.

Other Publications:

Hagenhaus V, Gorenflos López JL, Rosenstengel R, **Neu C**, Hackenberger CPR, Celik A, Weinert K, Nguyen MB, Bork K, Horstkorte R, Gesper A. Glycation Interferes with the Activity of the Bi-Functional UDP-*N*-Acetylglucosamine 2-Epimerase/*N*-Acetyl-mannosamine Kinase (GNE). Biomolecules. 2023 Feb 23;13(3):422. doi: 10.3390/biom13030422.

Poster and oral presentations

Aug 2023 Glyco26, Taipei, Taiwan

Oral Presentation: "Ac3ManNAc-6-phosphoramidate Prodrugs as Potential New Treatment for GNE Myopathy"

Poster: "The Role of GNE and Sialylation in GNE Myopathy"

Oct 2023 Sialoglycans in Immunity and Development, Hannover, Germany

Poster: "Role of Sialic Acids in Skeletal Muscle Physiology and Pathophysiology"

Apr 2024 International ProDGNE Meeting, Cagliari, Italy

Oral Presentation: "Lessons learned from a C2C12 Gne^{KO} model"

Apr 2024 ProMoAge Annual Retreat, Gotha, Germany

Oral Presentation: "Structural Analysis of Glycans in Skeletal Muscle Tissue"

Jun 2024 SialoGlyco2024, Lille, France

Poster: "The Role of GNE and Sialylation in GNE Myopathy"

Sep 2024 Joint Glycobiology Meeting Hannover, Germany

Oral Presentation: "The Role of GNE and Sialylation in GNE Myopathy"

Acknowledgments

Aus Datenschutzgründen entfernt.

Eidesstattliche Erklärung

Hiermit erkläre ich, dass ich meine Dissertationsschrift selbständig und ohne fremde Hilfe verfasst habe. Ich habe keine anderen als die von mir angegebenen Quellen und Hilfsmittel benutzt. Die aus den benutzten Werken wörtlich oder inhaltlich entnommenen Stellen habe ich als solche kenntlich gemacht. Die eingereichte schriftliche Fassung der Arbeit entspricht der auf dem elektronischen Speichermedium. Weiterhin versichere ich, dass die vorliegende Arbeit noch nicht als Abschlussarbeit an anderer Stelle eingereicht wurde. Zudem versichere ich, dass diesem Promotionsverfahren keine gescheiterten Promotionsverfahren vorrausgegangen sind.

_____

Datum, Unterschrift